Roughness with thickness about equal to the thickness of the boundary layer has drastically reduced the synchronization range of cylinder oscillations (Fig. 7.3). Chang (2011) also reported that roughness height as low as 1/3 of the thickness of the boundary layer can cause transition from VIV to galloping.

In Fig. 7.4, for all roughness cases (P60, P120 and P180), response frequency registers an overall increase with increasing reduced velocity but with a sudden dip at the beginning of the desynchronization range. Also, the cylinder oscillations are faster (higher frequency) in these cases compared to smooth cylinder response. Especially for P60, the cylinder motion was suppressed very well and a dominant oscillation frequency was not found ($8.5<U^*<10.0$).

T7 rougher cylinders also have a tendency to "hard VIV" or "hard excitation". That is, a minimum threshold static displacement is required to trigger VIV at $U^*=5.5$; otherwise, VIV will start at $U^*=6.5$ for P60.

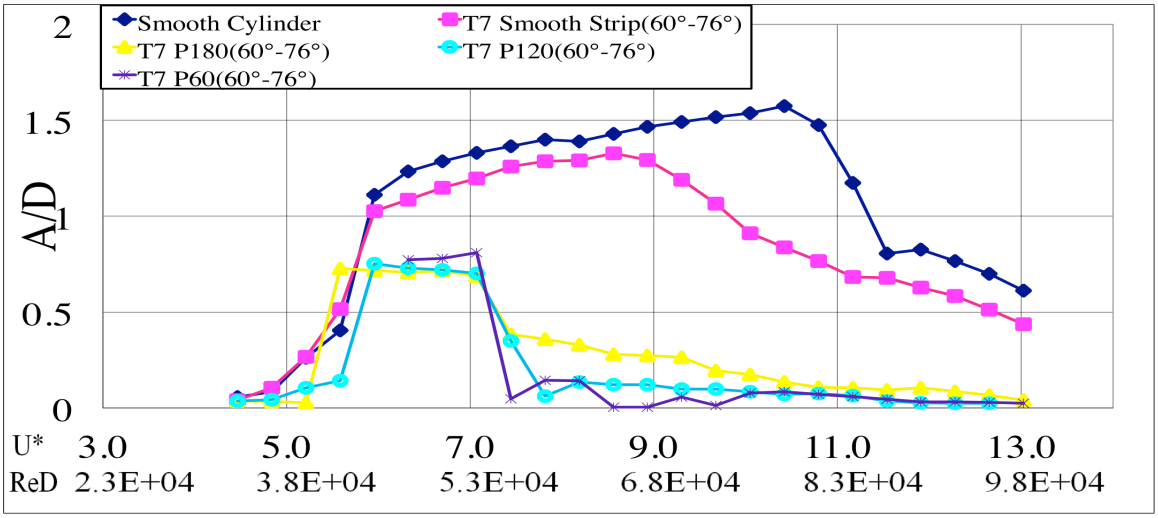

Fig. 7.3. Effect of surface roughness on the cylinder amplitude response

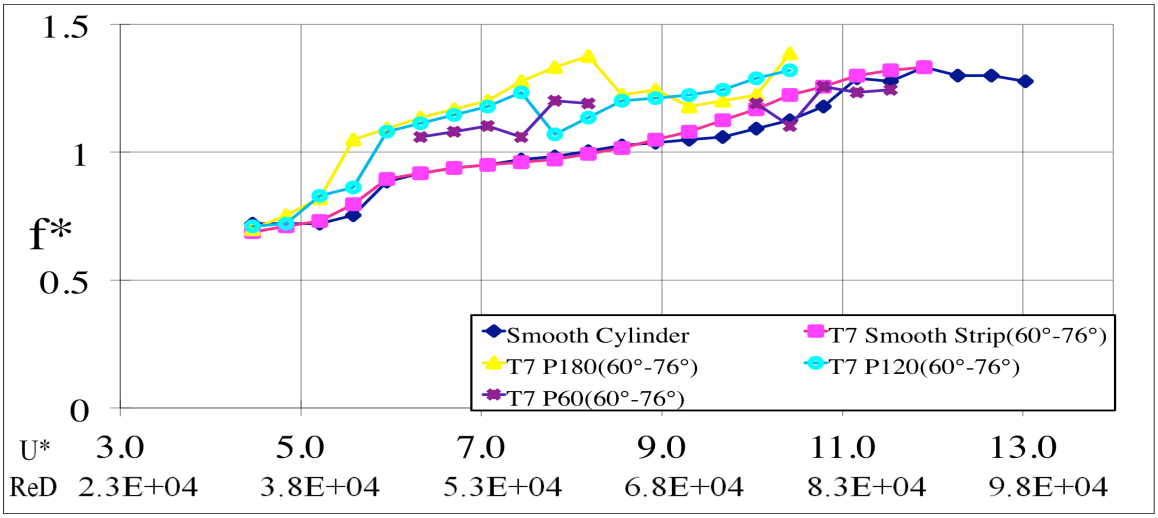

Fig. 7.4. Effect of surface roughness on the cylinder frequency response

7.2.3. Effect of location

To study the effect of strip location, strips are placed at various locations in the range 60°-80° and the results are plotted in Figs. 7.5 and 7.6. All cases pertain to configuration T7 with strips of half-inch width. Out of many cases studied (Fig. 7.5), except for the case with strip location at 90°, all the other cases exhibit very similar amplitude profiles though finer differences could be observed between them. For strip configuration T7: 90°-106°, amplitude trend is very similar to that of the smooth cylinder but with significantly subdued amplitude values. The response branches are quite similar to those of the smooth cylinder with nearly the same synchronization range in both cases. This is in agreement with the PTC-to-FIM map presented in Chapter 6. At other locations, the general response is characterized by much shortened range of synchronization with oscillatory amplitudes severely curbed for U^*>7.0. The effect of location on excitation amplitude is highly nonlinear as evidenced in Fig. 7.5. There is a general tendency that,

for strip angles ≤80°, as strip position angle increases (farther away from the front stagnation point), the synchronization range decreases but with higher amplitudes for U^*>7.0. At high U^* values (≅13.0), amplitudes are brought to negligible levels by the application of roughness. The aforementioned non-linearity could be seen in the trend of response frequency also in Fig. 7.6. Overall, the oscillatory frequency reduces with increasing strip angle for lower reduced velocities (U^*<8.0) and thereafter, this trend reverses, i.e., smaller strip angles favor lower oscillation frequency. Except for configuration T7:90°-106°, all other roughness configurations induce oscillation frequency higher than that of the smooth cylinder as could be seen in Fig. 7.6.

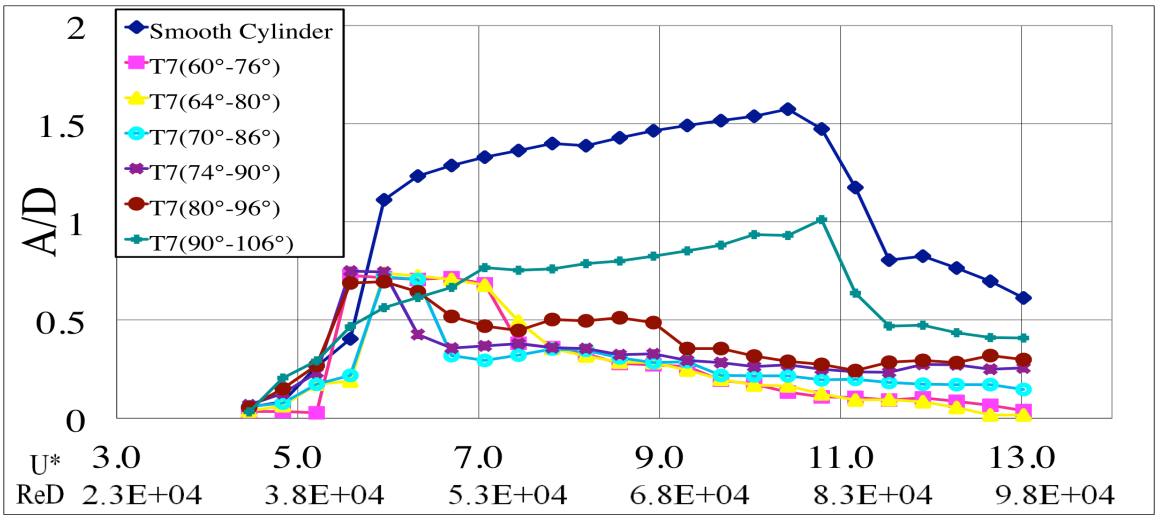

Fig. 7.5. Effect of strip location on the cylinder amplitude response

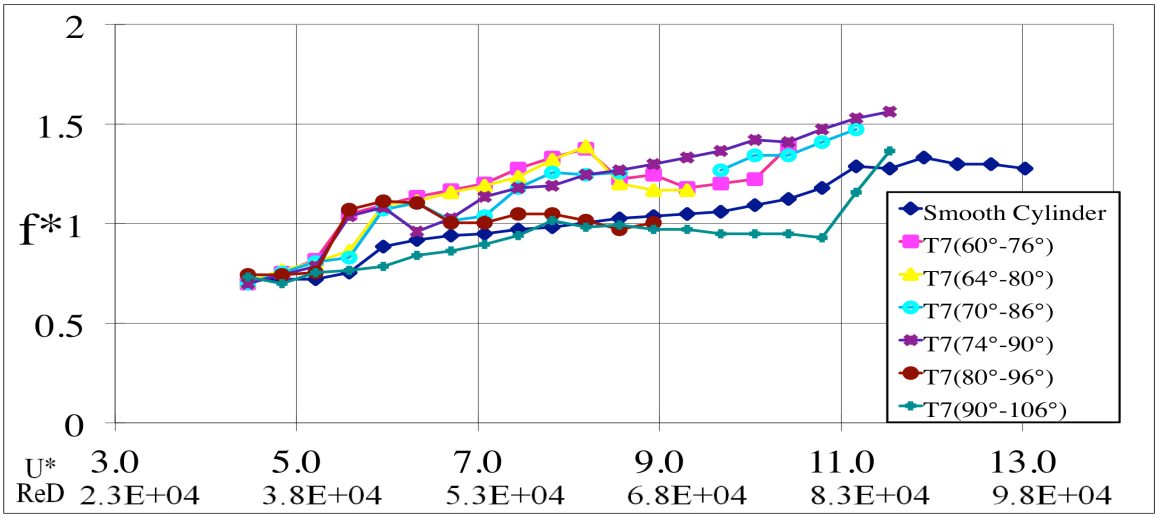

Fig. 7.6. Effect of strip location on the cylinder frequency response

7.2.4. Effect of roughness strip orientation

As part of this investigation, the effect of orientation of the PTC with 1.27cm width is studied. Each of the three strips on each side of configuration T7, has from left to right a starting-point and an end-point along the cylinder. The leading edge of the end-point is located at 60° (upstream edge of the strip is at an angle of 60° from the front stagnation point). The leading edge of the starting-point is located at 76°, 86° and 96°. Results are presented in Fig. 7.7 showing that amplitude A^* is substantially reduced in cases of PTC coverage compared to that of the smooth cylinder. The maximum amplitude is about 45% of that of the smooth cylinder. Furthermore, the greater the coverage, the shorter is the synchronization range but with the maximum amplitude nearly the same in all cases. For $U^*>8.5$, broader area coverage gives rise to higher amplitude of oscillation, though in general, the excitation amplitudes are significantly reduced in all cases. In the range $6.0 \leq U^* \leq 8.5$, a reverse trend is observed, i.e., broader area coverage results in lower

amplitudes of excitation. The corresponding oscillation frequency trends are shown in Fig. 7.8. More or less, similar trends could be observed for oscillation frequency also. That is, in the range $6.0 \leq U^* \leq 8.5$, higher is the oscillation frequency for lower strip angles and for $U^* > 8.5$, this trend is reversed. Response frequency trends exhibit a non-linear behavior with respect to U^*.

Results presented in Figs. 7.3-7.8, show that for the T7 configuration, in the lower range of reduced velocity ($U^* \leq 7.5$), cylinder undergoes vibrations with $A^* \cong 0.75$ suppressed by a factor of 2. Beyond $U^* \cong 7.5$, vibrations are severely suppressed up to a factor of 6. Figs. 7.3-7.8 also show that selective application of roughness is very effective in significantly reducing the cylinder oscillations, partially over a portion of the synchronization range and totally over the rest. To recall, in all these cases, the strip angle is varied from 60° to 106°. This range of suppression closely matches with the strong suppression zone (SS) of the PTC-to-FIM map developed in Fig. 6.1.

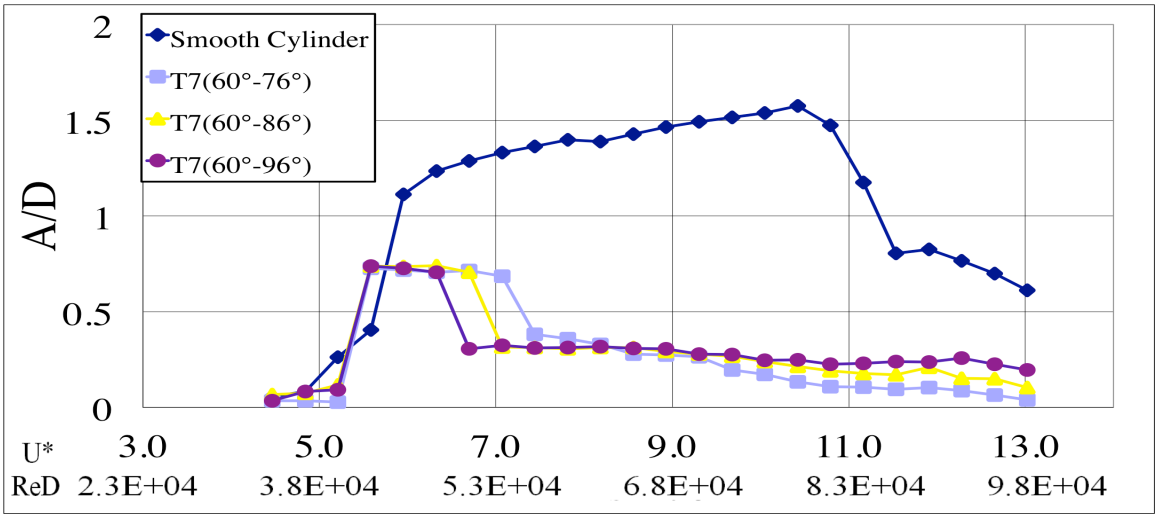

Fig. 7.7. Effect of strip area coverage on the cylinder amplitude response

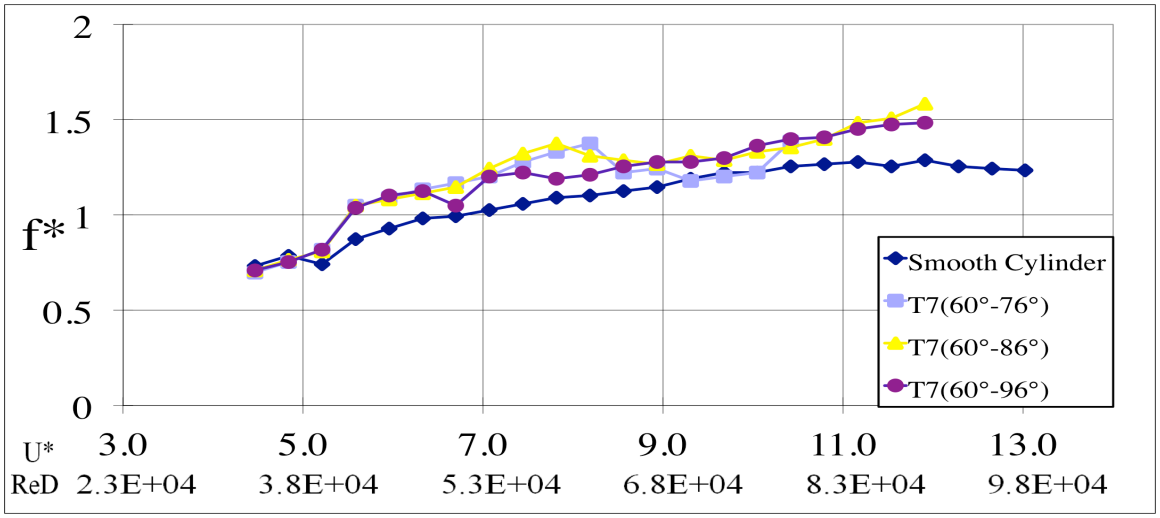

Fig. 7.8. Strip area coverage on the cylinder frequency response

The PTC-to-FIM map in Fig. 6.1 was developed based on experimental tests performed with straight roughness strips with half-inch width attached to the cylinder surface parallel to the cylinder axis unlike in the present study where the strips are attached inclined to the cylinder axis for T7 configuration. The range of the zone assures robustness, a feature that is particularly useful in using PTC in design for suppression or enhancement. The compliance of the present suppression results with the PTC-to-FIM map indicate that the zonal coverage of roughness is the key factor deciding the suppression response and not the design of roughness application, though the style of strip application has proved to influence the response features to a certain extent. To reiterate, strip position is most important in FIM suppression. Basically, the effective geometry of the section is altered with strip placement at various circumferential locations giving rise to various forms of FIM including suppression.

7.2.5. Wake vortex structure

From the flow visualization experiments conducted as part of the present study, the wake structure undergoes drastic changes when PTC is introduced on the cylinder surface. For a typical case (T7:60°-76°), where the flow is suppressed to a considerable extent, two typical wake structures are presented in Figs 7.9 (a) & (b). It is found that for the T7 configuration, the vortices shed are much weaker (less circulation) compared to those shed from a smooth cylinder at the same reduced velocity. From visualization, poor roll up of shear layers is evident giving rise to weaker (less circulation) vortices.

For PTC cylinder with roughness, for $5.5<U^*<7.5$ maximum amplitude is about 0.75 and vortex size to body size ratio is reduced to about 0.65. For $7.5<U^*<9$, wake structure becomes disorganized and amplitude reduces to less than 0.3. Frequently, the shedding process loses consistency; sometimes regular alternate shedding is observed behind the cylinder and other times, vortices are shed nearly simultaneously from the top and bottom shear layers (Fig. 7.9 (a)). Both these facts, that is poor roll up of shear layers leading to weaker (less circulation) vortices and near-simultaneous generation of vortices from the top and bottom shear layers contribute to low lift and consequently to low amplitudes of excitation as reflected in Figs 7.3, 7.5, and 7.7. It is contemplated that, roughness induces turbulence in the separating boundary layers, which diffuses the resulting vorticity generation giving rise to weaker (less circulation) vortices. For the shedding mechanism suggested by Gerrard (1966) to operate in the wake, the formed vortex (on one side of the body, Side-A) should be of sufficient strength to pull the shear layer from the opposite side (Side-B) enabling the oppositely-signed vorticity (from Side-B) to cut the vorticity supply of Side-A and shed the vortex on Side-A. Once the formation and roll up of shear

layer is adversely affected due to roughness, obviously Gerrard's mechanism cannot successfully operate thereby leading to weaker and irregular shedding process, with varying shedding cycle timings. As pointed out, this could possibly be a direct consequence of the roughness-induced changes in the boundary layer of the cylinder.

At higher reduced velocities (U^*>9), wake structures become still more vague characterized by the absence of stable vortex shedding. Most of the times, the wake shows either partially rolled up extremely weak (less circulation) vortices or very small (in core size), irregular, turbulent eddies depicted in Fig. 7.9(b). Additionally, the wake becomes narrower compared to smooth cylinder. Correspondingly, only negligible amplitudes are observed at higher reduced velocities as shown in Figs. 7.3, 7.5, and 7.7.

Though visualization is carried out systematically for one case of T7 configuration, similar wake vortex structures are observed at identical amplitudes of vibration for other configurations as well, including T6. It should be noted that flow visualization analysis is carried out and the wake structures are obtained at a particular span-wise location of the cylinder. At other span-wise locations of the cylinder, wake structures might vary but not significantly. Another salient feature of T6 and T7 PTC is that they possibly break the span-wise correlation of vortex shedding which is not conducive for strengthening VIV since lose of shedding correlation essentially reduces the total fluid dynamic lift force acting on the cylinder Bernitsas et al. (2008b). Also, the higher the excitation amplitude, the higher is the span-wise correlation of vortex shedding Bearman (1984). In other words, span-wise correlation of shedding becomes weaker at lower amplitudes of vibration. Hence, lower amplitudes resulting out of weaker vortex shedding due to roughness would be further subdued due to lose of span-wise correlation of shedding.

The major advantage of the T6 (helical) configuration is that it is omni-directional and hence not affected by the flow direction. On the other hand, T6 exhibits longer synchronization range compared to the T7 configuration.

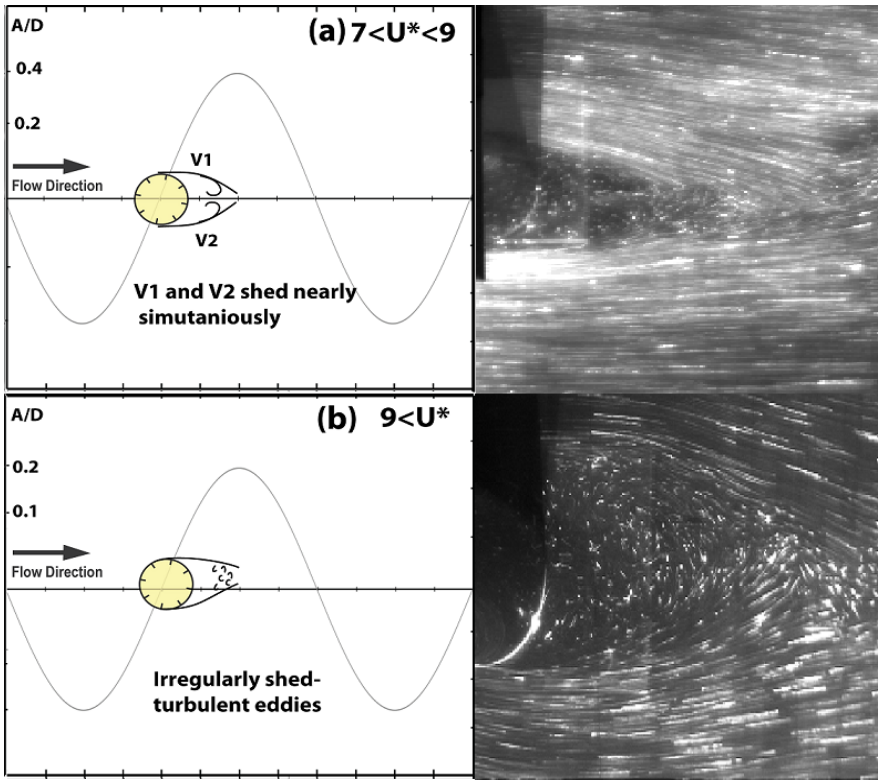

Fig. 7.9 Typical wake structures behind the cylinder with PTC configurationT7

7.3 MAIN FINDING

From the results presented in Chapter 7 we can draw the following conclusions:

(i) Passive Turbulence Control in the form of roughness strips with thickness close to that of the boundary layer was applied in the high-lift, TrSL3 flow regime and tested experimentally. PTC has major impact on the cylinder FIM in spite of the minimal geometric change implemented.

(ii) Response of cylinders with PTC configuration T7 exhibits a narrow range peak near the system natural frequency with A^* about half the corresponding A^* of the smooth cylinder in VIV. Past this peak, amplitude A^* is reduced by as much as a factor of 6 compared to A^* of the smooth cylinder.

(iii) Beyond the peak $U^*>7.5$, a high suppression branch is achieved. This is not in nature similar to the lower branch of VIV as confirmed by visualization showing that the wake is disorganized not exhibiting the typical 2P structure of the lower branch.

(iv) Wake structures indicate that roughness markedly influences the characteristics of shear layer roll up and consequent vortex shedding. Compared to smooth cylinder, shedding becomes substantially weaker, consequently giving rise to significantly lower amplitudes of vibration. Vortex shedding becomes irregular with sharp changes in the shedding timing apart from becoming disorganized and weakly rolled up.

(v) For $U^*>7.5$, visualization further shows two new wake structures which are compatible with the lift reduction notion. The first wake structure shows two weaker (less circulation) vortices shedding almost simultaneously rather than periodically alternating resulting in total circulation reduction. According to the Kutta-Joukowski theorem, this total circulation reduction results in proportional drop in the lift force. The second wake structure shows the cylinder near-wake confined between two flow lines forming a foil-like hydrodynamic tail with small eddies escaping into a narrow wake.

CHAPTER 8

MULTI-ZONE PTC

8.1. INTRODUCTION

From the results presented in Chapters 6 and 7, the map of PTC-to-FIM is very robust and different configuration applied on the cylinder show only minor changes. However, at the boundaries of zones, the response is very sensitive to PTC width because PTC may then cover multiple zones. In this Chapter 8, multi-zone coverage effect on the cylinder response is presented using staggered PTC configuration. To verify multi-zone effects, the PTC zone coverage is increased by one additional zone at a time from the WS1 zone to the WS2 zone. After PTC has covered all zones, the process is reversed and one zone is removed at a time starting with WS1. Using the results of the process of progressively covering and uncovering zones, suppression devices are design and tested which are independent of the flow direction.

8.2. RESULTS, OBSERVATIONS, AND DISCUSSION

The results of progressive zone coverage and un-coverage are discussed in Sections 8.2.1 and 8.2.2, respectively. In Section 8.2.3, the results of flow direction independent suppression devices are presented.

8.2.1. Progressive zone coverage

For progressive roughness coverage, T8 (staggered) PTC configuration is used and a zone is added in the order of a clockwise direction in the map of PTC-to-FIM shown in Fig. 6.1 starting from WS1. Fig. 8.1 shows the amplitude response of the progressive coverage. In the legend, the coverage angles show which zones are included and the final effect of cylinder response is also shown next to the zone coverage. For example, T8:0°-56° indicates that the T8 configuration covers 0°-56° and that means that WS1, HG1, and SG zones are covered by the T8 configuration and the final cylinder response is soft galloping.

For the T8:0°-8° configuration covering only the WS1 zone, the PTC-cylinder response is weak suppression with some amplitude modulation. This small increase is due to nonlinear property of VIV. Roughness may modify the spanwise relation, correlation length, and so on and these change cause slight amplitude modulation. For T8:0°-24° configuration wrapping WS1 and HG1 zones, the final roughness cylinder response is hard galloping and the general trend is almost the same as in the HG1 case introduced in Chapter 4. However, this configuration also shows slight amplitude increase in VIV region ($5.5<U^*<11$) same as T8:0°-8° configuration compared to HG of T7. Before the onset of galloping, at $U^* \cong 14.5$, the roughness cylinder exhibits a small

oscillation which is exactly the same for HG1 and the PTC-cylinder oscillation suddenly jumps to $A^* \cong 3$ when given a threshold displacement of about $1 \bullet D$. For the T8:0°-56° and T8:0°-72° configurations, the rough-cylinder response is soft galloping and the initial branches start at $U^* \cong 5$. When the HG2 zone is included (T8:0°-72° configuration), the amplitudes between $5.5 < U^* < 12$ (VIV region and VIV-galloping transition region) are slightly decreased compared to those of the T8:0°-56° configuration. Regardless of amplitude magnitude, the onset of the synchronization and the VIV-galloping transition regions are identical. For the T8:0°-104° and T8:0°-180° configurations, strong suppression results are observed and the rough-cylinder oscillations are dramatically reduced compared to those of the smooth cylinder. T8:0°-104° configuration which covers the WS1, HG1, SG, HG2, and SS zones, has slightly higher amplitude at $5 < U^* < 10$ than that of the T8:0°-180° configuration, which covers the WS1, HG1, SG, HG2, SS, and, WS2 zones, and maximum amplitudes of both cases are reduced more than 50% compared to that of the smooth cylinder. Especially, the maximum amplitude of the T8:0°-180° configuration is reduced up to 60% of the maximum amplitude of the smooth cylinder. After $U^* > 10$, the cylinder oscillations are negligible for both cases and totally suppressed at high reduced velocity.

The correlation length is measured as the length along the cylinder span where vortex shedding occurs within a small phase difference. Theoretically, the higher the correlation length is, the higher the average fluctuating lift force and the amplitude of oscillation are. T8 configuration that has unequally distributed roughness along cylinder spanwise would theoretically break the correlation length of vortex shedding. As shown in Fig. 8.1, however, the T8 configurations initiate galloping at high reduced velocity. This may

appear as a contradiction to the correlation length notion. It should be kept in mind however, that the cause of galloping is not vortex shedding but system instability.

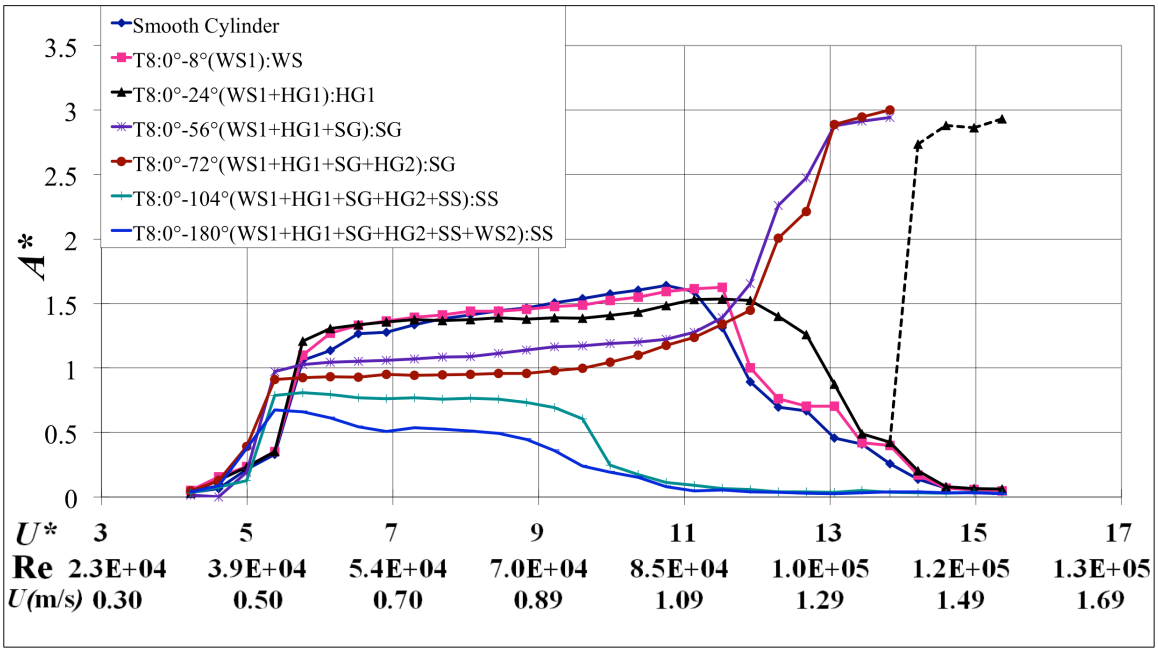

Fig. 8.1. Amplitude response for progressive coverage

As shown in Fig. 8.2, the frequency ratio for the rough cylinders is generally higher than that of the smooth cylinder similarly to other PTC-cylinder cases studied in this dissertation. The T8:0°-8° configuration has very similar frequency ratio to that of the smooth cylinder for $4<U^*<7.5$ and $U^*>7.5$. For the T8:0°-24° configuration - enfolding zones WS1 and HG1 – the frequency ratio follows that of the smooth cylinder at $4<U^*<7.5$ and deviate from that of the smooth cylinder at $U^*>8$. At $11<U^*<13$, the frequency ratio becomes constant. As the reduced velocity increases, the cylinder oscillation becomes negligible and no dominant frequency is present. Given a threshold amplitude, a dominant frequency reappears and the frequency ratio becomes close to unity in the fully developed galloping region. For the T8:0°-56° and T8:0°-72°

configurations, the frequency ratio is higher than that of the smooth cylinder in the VIV region ($4<U^*<10$). Beginning with the VIV-galloping transition region, the frequency ratio starts decreasing and reaches near unity in the fully developed galloping region. For the T8:0°-104° and T8:0°-180° configurations, overall the frequency ratio is very high compared to that of the smooth cylinder. A high frequency ratio is characteristic of strong suppression. The maximum frequency ratio of 1.7 is observed at $U^* \cong 12.5$.

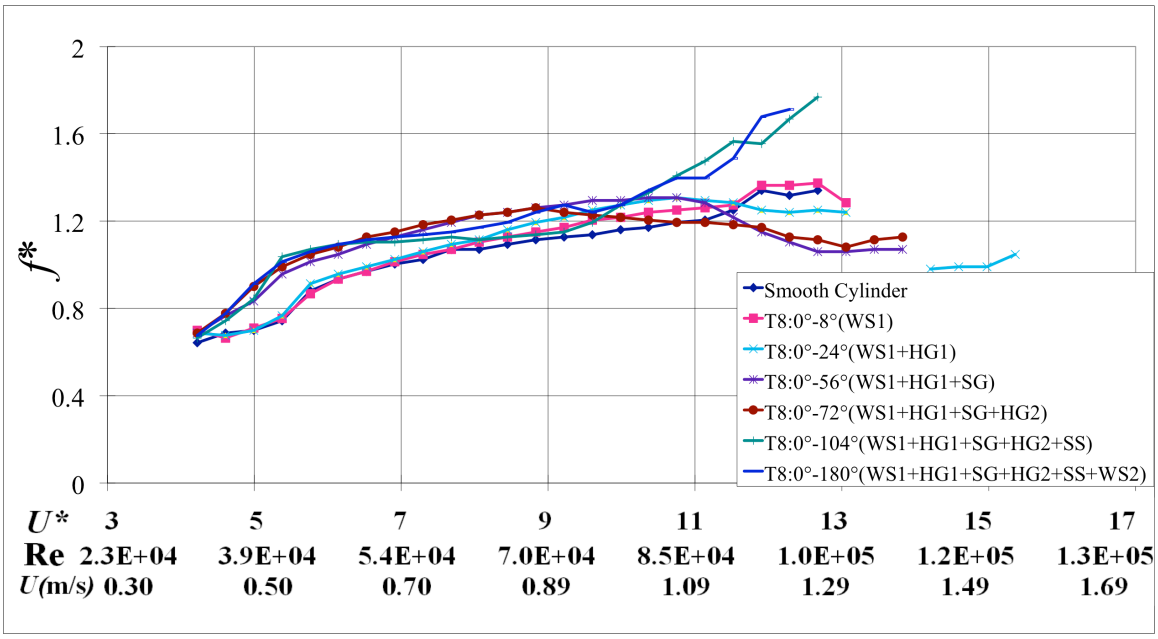

Fig. 8.2. Frequency ratio for progressive coverage

From the progressive zones tests, the following conclusions can be drawn.

(a) The SS zone is the most dominant zone in the Map of PTC-to-FIM. When the SS zone is covered by the PTC, the amplitude response of rough cylinders is always strong suppression.

(b) The SG zone has stronger effect than the WS1, HG1, and HG2 zones. If four zones (WS1, HG1, HG2, and SG) were covered by roughness, soft galloping is manifested.

(c) The HG1 zone is more effective than the WS1 zone. If both are covered by roughness, the resulting FIM is hard galloping.

(d) Covering all zones with the T8 configuration is a better suppression means than a cylinder with all zones except WS2 covered. Even though WS2 has similar response with a smooth cylinder and roughness is located mostly behind the cylinder, it may create more three-dimensional flow over the whole cylinder and interrupt the already formed vortices.

8.2.2. Progressive zone uncoverage

In this section, a zone is eliminated in the order of a clockwise direction in the Map of PTC-to-FIM from the last progressive zone coverage model covering up the WS1, HG1, SG, HG2, SS, and WS2 zones. In other words, the experiment is started from the T8:0°-180° configuration and the legends in Figs. 8.3 and 8.4 also show the final results of the rough cylinder response.

As seen in Fig. 8.3, the T8:8°-180° configuration which covers the HG1, SG, HG2, SS, and WS2 zones has maximum amplitude of $A^* \cong 0.7$ at $U^* \cong 5.2$ and the cylinder amplitude is negligible at $U^* > 11$. Amplitude response of the T8:8°-180° configuration is almost identical to the T8:0°-180° configuration. Excluding slight amplitude dissimilarity at the initial branch, both configurations have similar amplitude response at the same reduced velocities – same maximum amplitude point, identically the same initial, upper, and lower branch ranges in terms of reduced velocity. It is believed that WS1 has minor effect on reducing the amplitude. For the T8:24°-180° configuration removing the WS1

and HG1 zones, amplitude gradually decreases from the maximum amplitude ($A^*\cong 0.7$) at $U^*\cong 5.5$ to $A^*\cong 0.55$ at $U^*\cong 9.3$ and is negligible for $U^*>12$. For the T8:56°-180° configuration covering the HG2, SS, and WS2 zones, the maximum amplitude of $A^*\cong 0.65$ is obtained at $U^*\cong 6.0$ and the rough cylinder displacement is negligible for $U^*>14$. High amplitude region (upper branch) ($5.5<U^*<6.5$) is significantly reduced compared to previous T8 configurations. The rough cylinder, however, still has a small amplitude of $A^*\cong 0.2$ at high reduced velocities and this amplitude is higher than that of the T8:0°-180°, T8:8°-180°, and T8:24°-180° configurations. This "trade off" is also seen in T8:72°-180° configuration. For T8:72°-180° configuration covering only the SS and WS2 zones, the least maximum amplitude of $A^*\cong 0.45$ is observed with a significant change in the upper and lower branch range. The upper and lower branches are extended to $U^*\cong 9.5$ and $U^*\cong 14$, respectively. At high reduced velocities, there is also "trade off" between cylinder amplitude and response range. The rough cylinder still reaches $A^*\cong 0.3$ of amplitude up to $U^*\cong 14$. From progressive un-coverage tests, covering only SS and WS2 is a very effective means to minimize the maximum cylinder amplitude. However, it increases the upper branch range and keeps small amplitude at high reduced velocity. The T8:104°-180° configuration, which covers only the WS2 zone has maximum amplitude $A^*\cong 1.1$ and the frequency increases for all reduced velocity values. This is typical WS2 response discussed in Chapter 5 and the staggered configuration does not change the FIM type. As shown in Chapter 5, depending on a certain sandpaper location in WS2, a rough cylinder response could be very close to that of the smooth cylinder. Therefore, this zone was defined as WS in Chapter 5. From the results so far, all the

rough cylinders have less amplitude in the VIV synchronization regions when compared to the smooth cylinder. It is believed that roughness protrusions could enhance boundary layer mixing and affect the resultant vortices to be more diffused and weaker (less circulation).

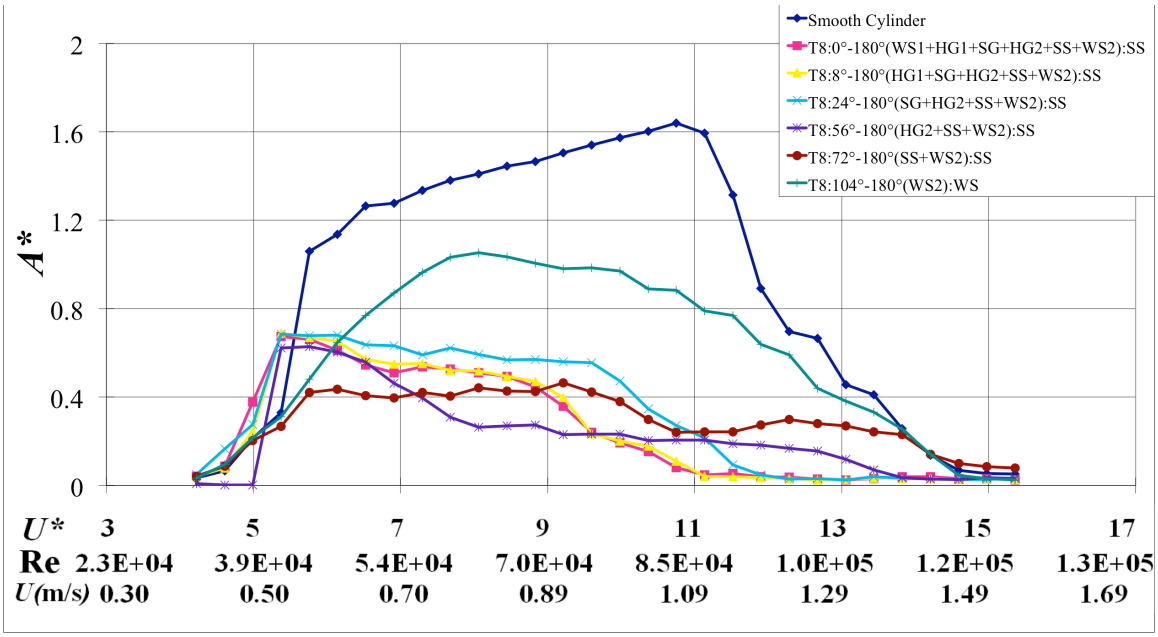

Fig. 8.3. Amplitude response for progressive un-coverage

As shown in Fig. 8.3, all roughness cylinder responses except for the T8:104°-180° configuration are classified as SS cases. For a typical strong suppression frequency ratio graph as discussed in Chapter 5, either the frequency ratio keeps increasing and very high frequency ratio is observed at high reduced velocities or the frequency ratio is only observed in a very short range of U^*. As shown in Fig. 8.4, as proof of strong suppression, for all PTC cylinders but the T8:72°-180° configuration which shows weak suppression, frequency ratio keeps increasing and reaches high values between 1.6 and 1.8 at $U^* \cong 12$. The frequency ratio of the T8:72°-180° configuration is lower than that of

the smooth cylinder in the upper branch region ($5<U^*<9$) and then increases slightly after $U^* \cong 9$. Same as in previous results in Chapter 5, WS1 (0°-8° configuration in Figs. 5.3 and 8.2) has slightly higher frequency ratio and WS2 (104°-180° configuration in Figs. 5.3 and 8.4) has generally lower frequency ratio than that of a smooth cylinder.

From progressive coverage and un-coverage results in Figs. 8.1 and 8.3, hysteresis is not observed from the initial branch to the upper branch. All rough cylinders jump to the upper branch earlier when compared to the smooth cylinder case. It is worthy to note that Hover et al. (2001) studied tripping wire on an oscillating circular cylinder and they found that frequency lock-in of the cylinder with tripping wire shifts to earlier reduced velocity. As seen in Figs. 8.2 and 8.4, all roughness configurations except for the two WS zones (0°-8° and 104°-180°) have earlier frequency lock-in as observed by Hover et al. (2001). In the present study, vivid premature lock-in is observed not only in frequency response but also in amplitude response. Sandpaper used in this study has enough total thickness (roughness height plus paper thickness) to disturb the flow around the cylinder and this disturbance causes earlier synchronization in the rough cylinders. Thus, sharp edge and proper thickness of the sandpaper roughness might play same role as tripping wire and cause disturbance in the boundary layer.

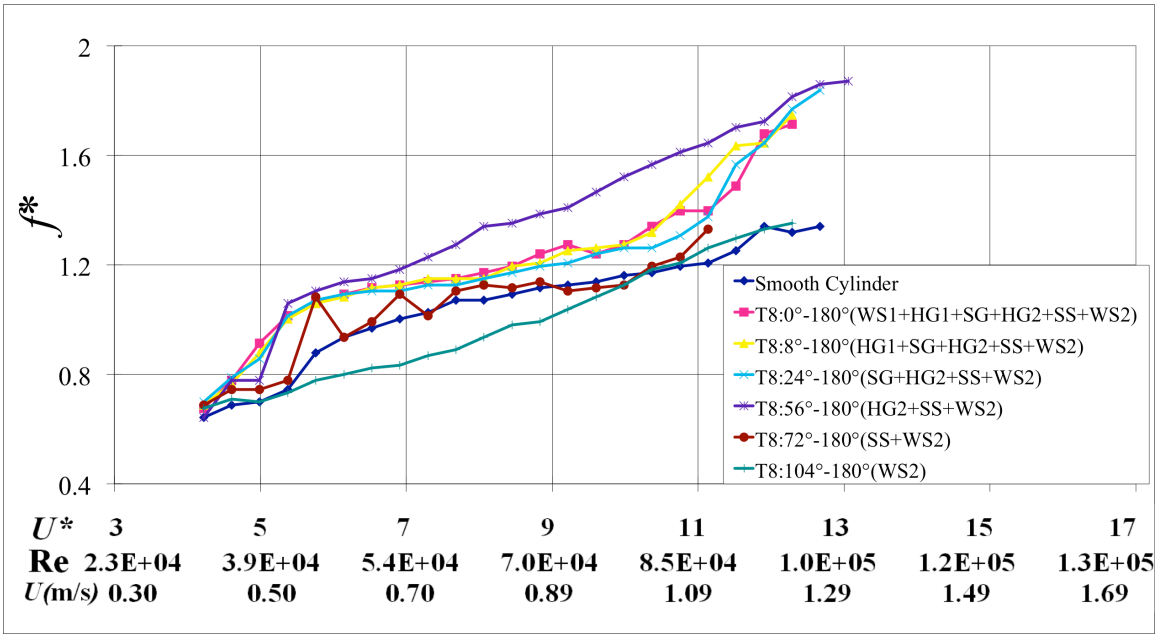

Fig. 8.4. Frequency ratio for progressive un-coverage

From progressive un-coverage results, the following conclusions are drawn and reconfirmed.

(a) When the SS zone is covered, the influence of the SS zone is the most powerful among zones and the SS zone dominates the response of the roughness cylinder.

(b) Perfect suppression means is not found in all ranges of U^* and there is "trade off" between the cylinder suppression and reduced velocity range. The T8:72°-180° configuration has a least maximum amplitude of $A^* \cong 0.45$ (at $U^* \cong 6$) among T8 configurations but is not perfectly suppressed at $11<U^*<14$. In other hands, the T8:8°-180° configuration has negligible amplitude at high reduced velocity but has the maximum amplitude of $A^* \cong 0.7$ at $U^* \cong 5.5$. Our results are similar to Bearman & Brankovic (2004) who tested straked and bumpy cylinders. Both prototypes had lower maximum amplitude than a plain cylinder. Bumpy cylinder has higher upper

branch region than the straked one but at $U^* \cong 12$ the two amplitude graphs cross each other so that the straked cylinder reached higher amplitude at $U^* > 12$.

(c) Removing the HG1 and SG zones increases the cylinder amplitude in the upper branch but reduces the amplitude at high reduced velocities.

8.2.3. Omni directional flow suppression devices

In Chapters 4 to 6, sandpaper strips were attached at a specific angle of cylinder surface and the configurations are not symmetric to relative change of a flow direction. Hence, the configurations introduced in Chapters 4 to 6 are flow direction dependent suppression devices, that is, they are effective only for unidirectional flow. In this section, three roughness configurations are studied by wrapping roughness around circular cylinders in symmetric patterns regardless of the flow direction. Thus, these configurations are omni-directional suppression devices and they are applicable to all flow directions.

First, a full roughness model is a roughness cylinder covered fully with uniformly distributed roughness. This model is different from the T8 staggered and T6 helically applied configurations in which roughness is selectively placed on the cylinder.

Second, the T8 configuration used in this section is the same model as the T8:0°-180° configuration which was introduced in Sections 8.2.1 and 8.2.2. Consequently, the T8 configuration in this section is covered full angles in symmetric pattern by roughness and the model is a flow direction independent suppression device.

Third, the T6 model consists of four strips, equally spaced circumferentially. They are wound around the cylinder in a helical fashion like helical strakes that are a very good suppression device in industry.

Fig. 8.5 shows the amplitude response of flow direction independent devices and all three are effective on VIV suppression. For all three roughness models, the onset of VIV shifts to lower reduced velocity compared to that of the smooth cylinder and hysteresis is not observed unlike hysteresis occurring when covering only the SS zone. Moreover, long flat branches observed in T7 and T8 results in Figs. 7.1, 8.1, and 8.3 are not distinctive in omni-directional suppression devices. For the full roughness model, the roughness cylinder maintains almost a constant oscillation at $6<U^*<13$ and maximum amplitude of the roughness cylinder is reduced by about 50% of that of the smooth cylinder. At $U^*>13$, desynchronization begins and the amplitude becomes trivial. The main reason is because roughness induces premature transition to turbulence in lower Reynolds number. Transition to a turbulent boundary layer provides more energy to the flow retarding separation and the shift of separation points instigates narrow wakes behind the roughness cylinder. This results in lower lift forces and oscillation in the fully-covered roughness cylinder. This full roughness model is the same configuration used by Kiu et al. (2011) with similar grit size. They reported that the amplitude of the roughness was around $A^* \cong 0.5\text{-}0.7$ and on-set of roughness cylinder response was delayed when compared to their smooth cylinder. These differences may be attributed to the fact that their Reynolds number (8.3×10^4) is lower than the one used in the study (1.2×10^5) and their mass ratio ($m^*=2.36$) is higher than this study as well ($m^*=1.725$). For the T8 model, the rough cylinder oscillation starts slightly earlier than those of other rough

cylinders. At $U^*\cong5.5$, the maximum amplitude of $A^*\cong0.7$ is achieved and the amplitude begins to drop off slowly between $5.5<U^*<9$. After $U^*\cong9$, the oscillation amplitude drops rapidly and becomes negligible. In the overall range of reduced velocity, the T8 configuration is the best suppression device even though it has slightly higher maximum amplitude than that of rough cylinders. The T6 configuration has the least maximum amplitude of $A^*\cong0.6$ than any other rough cylinder. However, an amplitude of $A^*\cong0.5$ persists until $U^*\cong11$. Beyond $U^*\cong11$, the amplitude starts to drop and the cylinder oscillations become negligible.

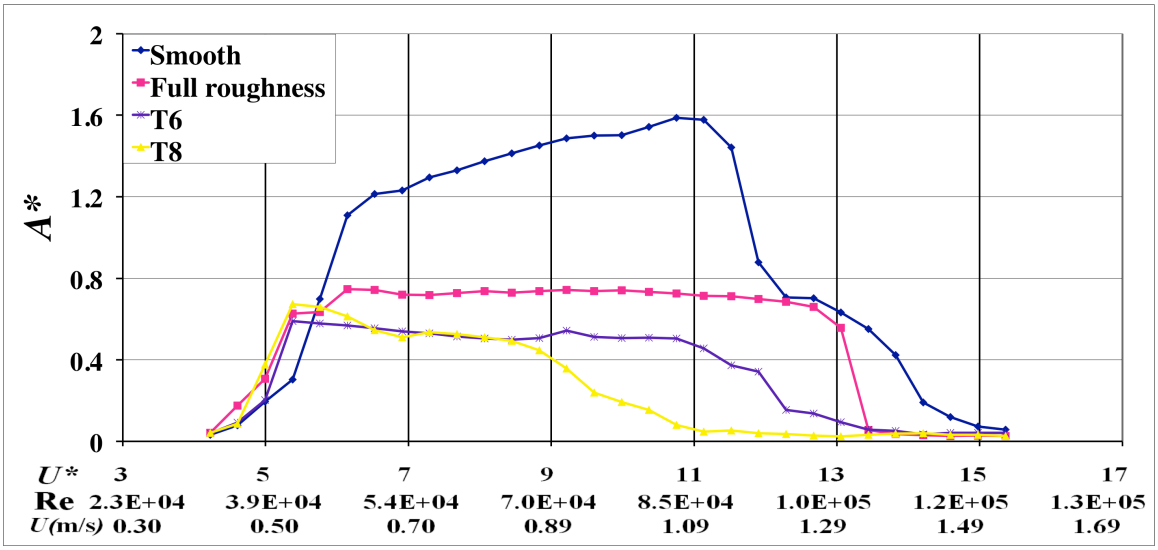

Fig. 8.5. Amplitude response for flow independent suppression devices

The T6 and T8 configurations are very effective in VIV suppression as they cause three-dimensional vortex shedding. Since the rough cylinder is moving, the separation point is altered due to the roughness. The latter also influences the local forces on the cross section. Moreover, three-dimensional effects caused by roughness alters the correlation of vortex shedding along the span of the cylinder.

Fig. 8.6 shows frequency ratios of flow direction independent suppression devices. Similarly to previous strong suppression results (Figs. 5.5, 7.2, 8.2, and 8.4), all three have generally higher frequency ratio than that of the smooth cylinder. T8 configurations have similar frequency trend to fully-covered roughness models with slight higher frequency ratio. For T8 and fully-covered roughness cylinders, the frequency ratios jump at $U^* \cong 5.0$ and slowly increase until $U^* \cong 13$. Frequency ratios of the T8 configuration have the highest frequency ratio among the three suppression models at $4<U^*<5$. From $U^* \cong 5$, the frequency ratio increases slowly until $U^* \cong 11.0$. After $U^* \cong 9$, modulation is observed until $U^* \cong 11$. This modulation is considered to be due to the effect of the lower branch and desynchronization regions. Hysteresis from the initial branch to upper branch for the SS zone is not noticed for flow direction independent suppression devices.

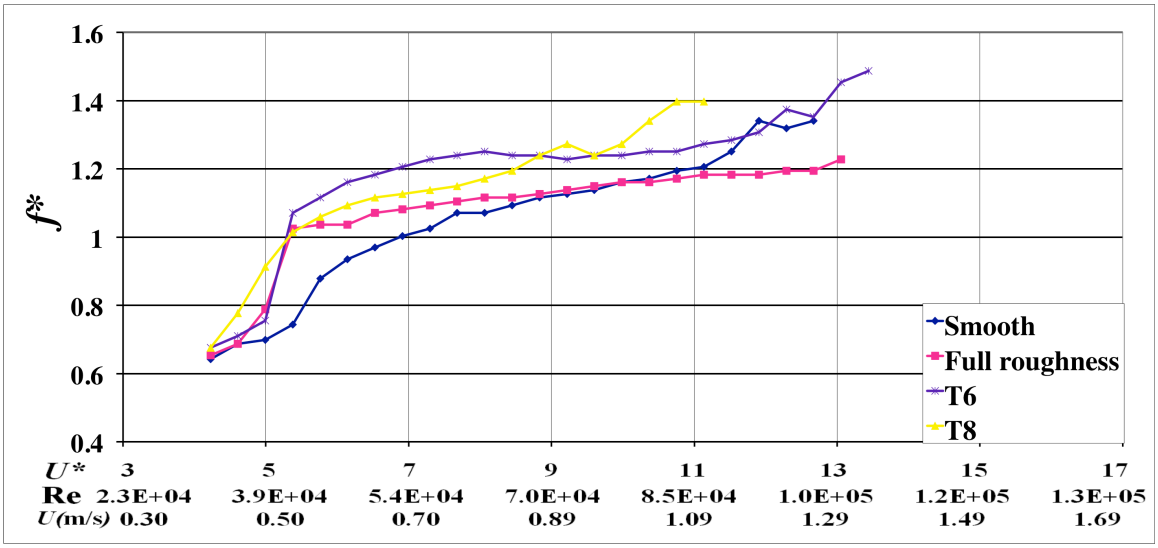

Fig. 8.6. Frequency response for flow independent suppression devices

8.3. MAIN FINDINGS

From the results presented in Chapter 8 we can draw the following conclusions:

(i) From multi-zone tests (progressive zone coverage and un-coverage), the SS zone is the most dominant zone. When the SS zone is covered in multi-zone coverage, the cylinder response is always strong suppression.

(ii) From multi-zone tests, a configuration covering all zones in a staggered T8 form is an effective suppression device. The upper branch region is shorter with maximum amplitude by 56% of that of the smooth cylinder. Also the desycnhronization region starts at lower U^* compared to the smooth cylinder.

(iii) For suppression devices, trade off between amplitude and response range are important. The T8:72°-180° configuration has the least maximum amplitude of $A^* \cong 0.45$ (at $U^* \cong 6$) among T8 configurations but is not perfectly suppressed at $11 < U^* < 14$. On the other hand, the T8:8°-180° configuration has negligible amplitude at high reduced velocity but has maximum amplitude of $A^* \cong 0.7$ at $U^* \cong 5.5$.

(iv) For the flow-direction independent configurations T6 and T8, amplitude A^* is reduced by as much as a factor of 3 compared to A^* of the smooth cylinder.

CHAPTER 9

SUPPRESSION OF MULTIPLE CYLINDER FIM

9.1. LITERATURE REVIEW

A single cylinder has been studied widely but in practice arrays of multiple cylinders are used more frequently, such as in heat exchangers, offshore structures, buildings, chimneys just to name a few. Flow around multiple cylinders is much complicated than that around a single cylinder because of interactions between shear layers, shedding processes, vortices, wake and Karman vortex streets (Sumner 2010). As Reynolds number is an important variable for a single cylinder, new parameters significantly influence the flow around multiple cylinders. For the multiple cylinders, the center-to-center distance (L'/D, T/D, and P/D) between the cylinders shown in Fig. 9.1, the angle (α') of the orientation of the cylinders in the x-y plane, and the Reynolds number are important parameters (Sumner 2010; Bearman 2011). Multiple cylinder configurations most commonly used in application are tandem configuration, side-by-side configuration, and staggered configuration. Fig. 9.1 shows three configurations of two circular cylinders in cross flow.

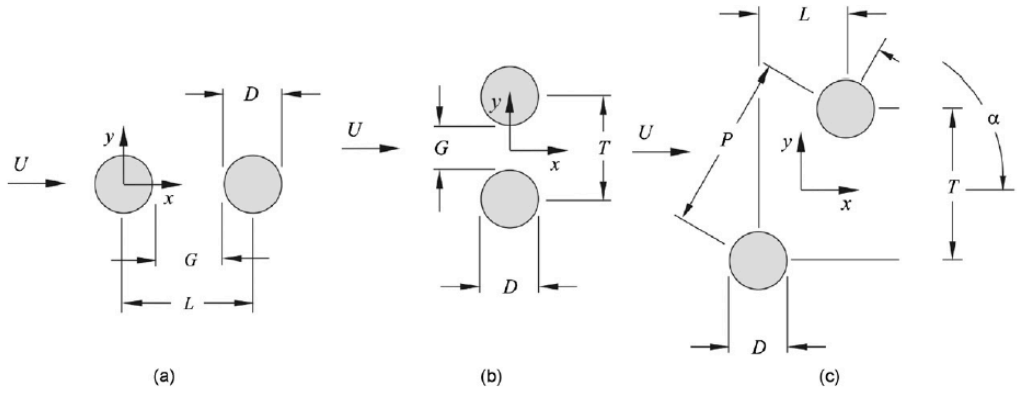

Fig. 9.1. Two circular cylinders of equal diameter in cross-flow: (a) tandem configuration; (b) side-by-side configuration; and (c) staggered configuration (Sumner 2010)

When two stationary cylinders arranged in tandem, side-by-side, or staggered in close proximity, two types of interference may occur (Zdravkovich 1977, 1985, 1987, 1988).

(i) When a downstream cylinder is submerged fully or partially in the wake of an upstream cylinder, wake interference occurs.

(ii) When two cylinders are located close enough but not in the wake of each other proximity interference is occurred.

As shown in Fig. 9.2, Zdravkovich (1985) studied the interference regions for various cylinder arrangements as a function of center-to-center distances. A schematic drawing of the corresponding flow interference regions is also shown in Fig. 9.3. The scope of the present study is the response of the two oscillating cylinders in tandem configuration. So, only the relevant literature for only two cylinders in tandem and staggered configuration is reviewed.

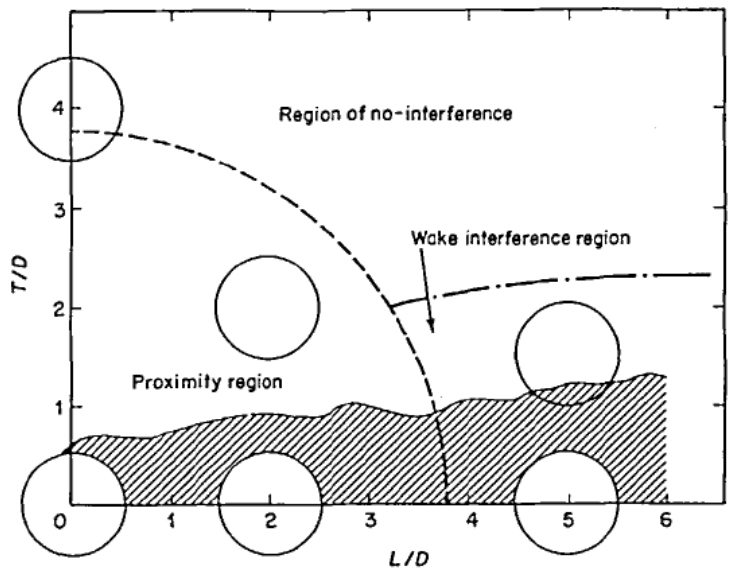

Fig. 9.2. Classification of interference regions (Zdravkovich 1985)

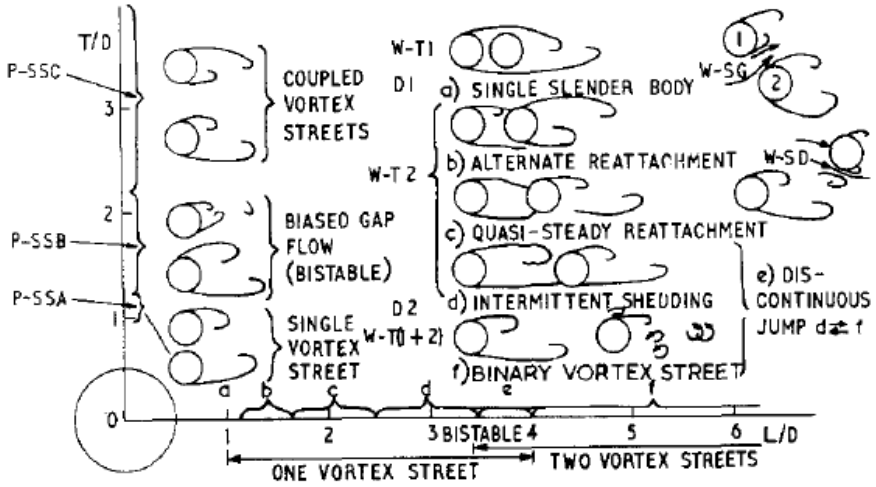

Fig. 9.3. Flow interference regions (Zdravkovich 1985)

(a) Two cylinders in tandem configuration

When two cylinders with equal diameter are placed in tandem, the wake of the upstream cylinder induces unsteady flow to the downstream cylinder. In addition, the

presence of the downstream cylinder modifies the vortex formation process and wake dynamics of the upstream cylinder. According to Zdravkovich (1987), the flow pattern around two cylinders can be divided into three regions depending on center-to-center distance.

(i) Single bluff-body behavior: For small L'/D ($1<L'/D<1.2$-1.8), which slightly varies with Reynolds number, the shear layers from the upstream cylinder are elongated compared to a single cylinder and wrap around the downstream cylinder without reattachment to the surface of the downstream cylinder. Since the downstream cylinder is positioned inside of the vortex formation region of the upstream cylinder, vortex roll up starts behind the downstream cylinder. Hence, two cylinders behave like a single cylinder as seen in Fig. 9.4 (pattern A) and Fig. 9.5(a) and (b).

(ii) Shear layer reattachment behavior: For intermediate L'/D (1.2-$1.8<L'/D<3.4$-3.8), which slightly varies with Reynolds number, the separated two shear layer in the upstream cylinder continuously reattach to the surface of the downstream cylinder as shown in Fig. 9.4 (Pattern B, C, D, and E) and Fig. 9.5 (c) and (f) (Igarashi 1981, 1984; Ljungkrona 1992). Reattached shear layers interact with boundary layer development and separation of the downstream cylinder. In the gap region between the two cylinders, eddies form and shed.

(iii) Kármán vortex shedding from each cylinder: For large L'/D ($L'/D>3.4$-3.8), which slightly varies with Reynolds number, each cylinder has its own vortex shedding. Since the downstream cylinder is located outside of the vortex formation region of the upstream cylinder, shed vortices from the upstream cylinder interfere with vortices of

the downstream cylinder and influence the vortex size (Ishigai et al. 1972; Zhou & Yiu 2006).

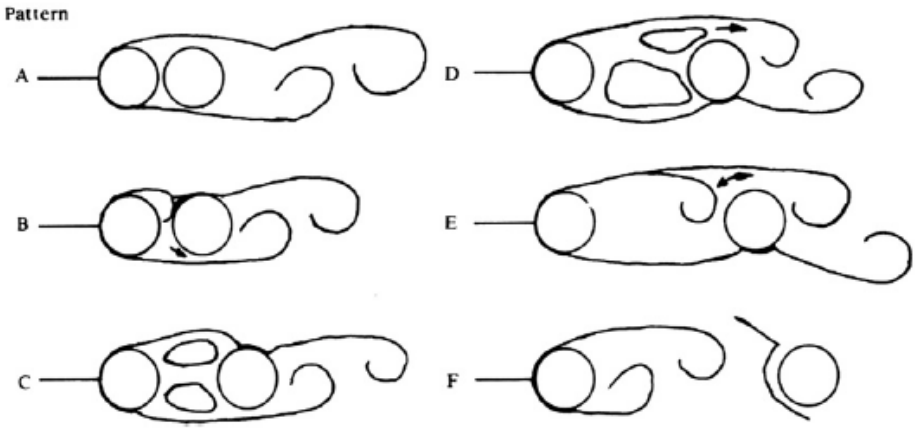

Fig. 9.4. Classification of flow patterns for two tandem cylinders (Igarashi 1981; Ljungkrona et al. 1991; Sumner 2010)

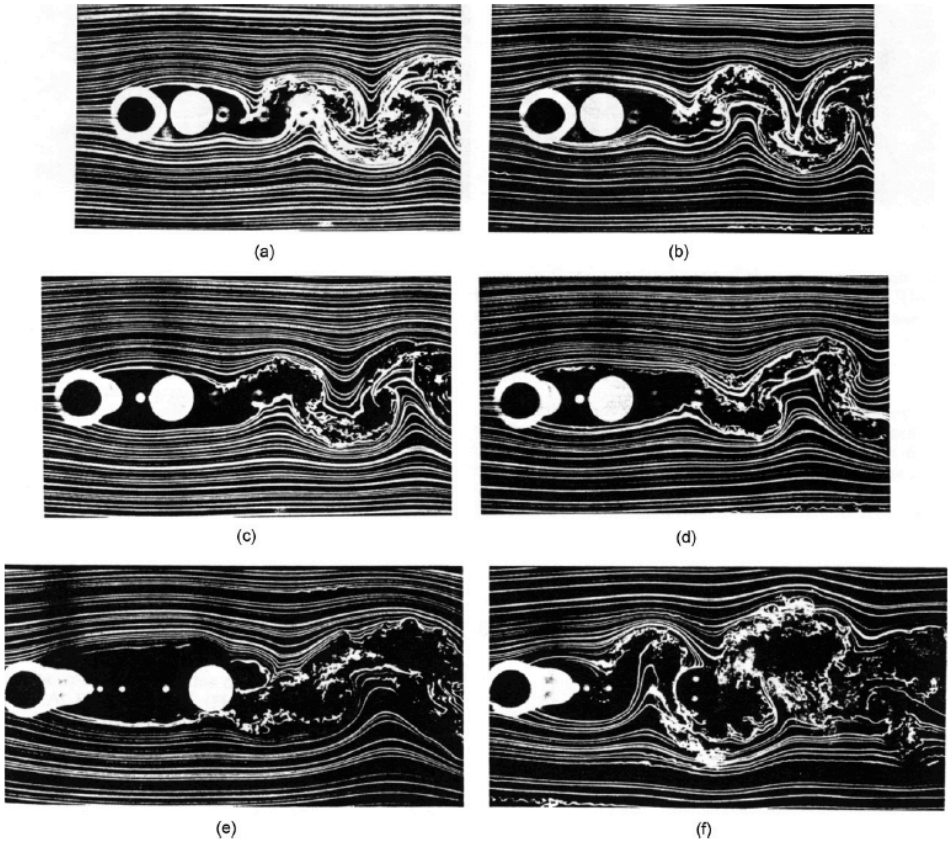

Fig. 9.5. Flow past two tandem circular cylinders. Single bluff body behavior: (a) L'/D=1.25, Re=1×10^4; (b) L'/D=1.25, Re=1.2×10^4; Shear layer reattachment: (c) L'/D=2,

Re=1×10^4; (d) L'/D=2, Re=1.2×10^4; (e) L'/D=4, Re=1×10^4; Kármán vortex shedding from each cylinder: (f) L'/D=4, Re=1.2×10^4 (Ljungkrona & Sundén 1993; Sumner 2011)

(b) Two cylinders in staggered configuration

For two cylinders in a staggered configuration, flow patterns are more complicated than those around two cylinders in tandem since the downstream cylinder can be exposed to wake interference and/or proximity interference. Gu & Sun (1999) investigated two cylinders in a staggered configuration and found three interference patterns – interference of wake, shear layer, and neighborhood as shown in Fig. 9.6.

Later, Sumner et al. (2005) extended their study and found that flow patterns around two cylinders in staggered arrangement are influenced by interaction of four separated free shear layers, two Kármán vortex formation and shedding process, and interactions between the two Kármán vortex streets. Depending on these interactions, they sorted flow patterns around a staggered arrangement as three patterns.

(i) Single bluff body flow pattern: For small pitch ratios (P/D=1-1.25), two cylinders behave like a single bluff body. Only a single vortex street occurs with vortex shedding from the outer shear layer.

(ii) Small incidence angle flow patterns: For pitch ratios (P/D=1.125-4) with small incidence angles (0°-30°), a shear layer of the upstream cylinder can be reattached to the downstream cylinder (Fig. 9.7(d)) or deflected through the gap between the cylinders (Fig. 9.7(e)). Even for a larger longitudinal distance between two cylinders, the downstream cylinder can be exposed to impingement from the vortices shed by the upstream cylinder (Fig. 9.7(f)).

(iii) Large incidence angle flow patterns: For pitch ratios (*P/D*=1.25-5) with large incidence angles (15°-90°), similar to a tandem configuration, vortex shedding occurs in each cylinder with enveloping of the vortex (Fig. 9.7(g)-(h)) or synchronized vortex shedding (Fig. 9.7(i)).

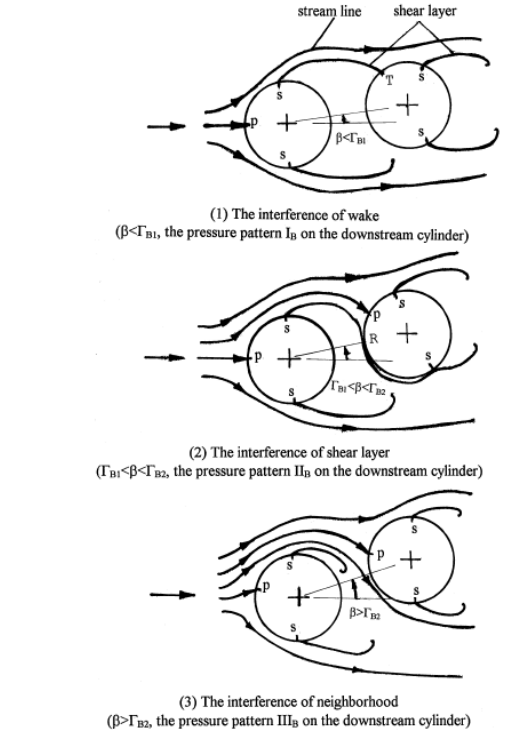

Fig. 6. Sketches of the classification of three flow patterns of two circular cylinders in staggered arrangements (S: separation point; P: stagnation point; R: reattachment point; T: shear layer touch point).

Fig. 9.6. Three flow patterns of two cylinders in staggered configuration (Gu & Sun 1999)

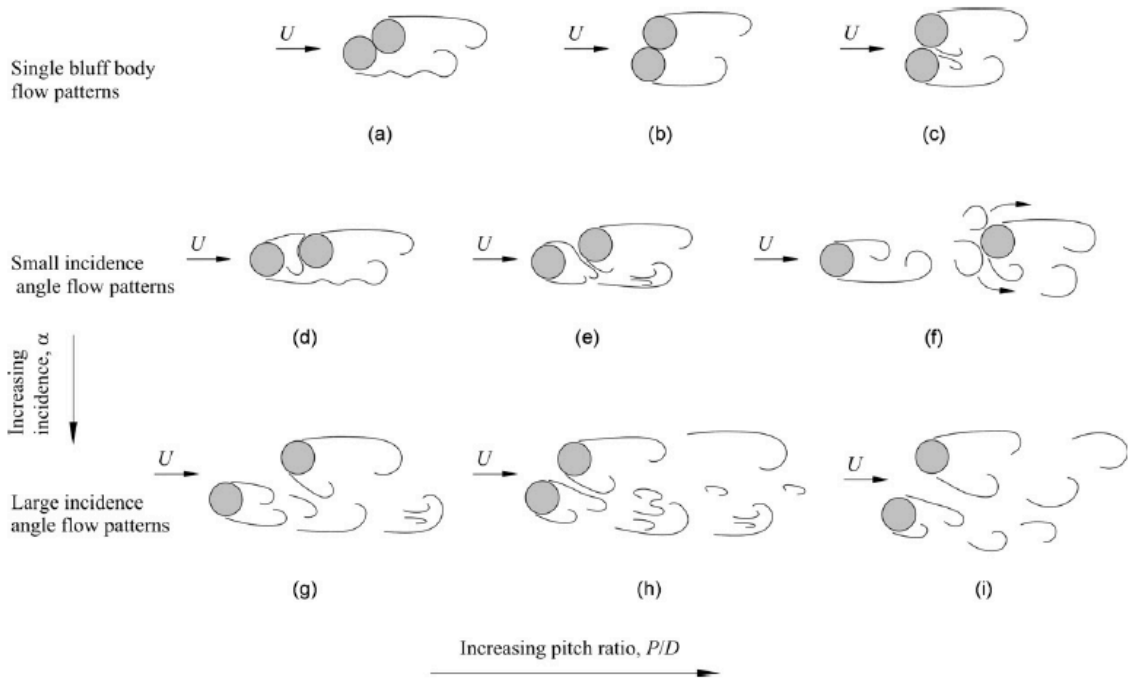

Fig. 9.7. Flow patterns around two cylinders in staggered configuration. G: gap, R: reattachment (Sumner et al. 2005; Sumner 2010)

(c) Oscillating cylinder in a tandem configuration

Since multiple cylinder motions are significantly more complex than a single cylinder motion, both oscillating cylinders have not been researched extensively. A lot of research published in the literature restrict parameters by fixing either the upstream or the downstream cylinder. When two cylinders are placed close enough and either the upstream or the downstream cylinder is moving, vortex shedding may be hindered and/or suppressed. Hence lift force due to vortex shedding is decreased or suppressed. Rather than VIV, as shown in Fig. 9.8, similar to galloping response may be observed in the moving cylinder.

Bokaian & Geoola (1984a, 1984b) investigated two cases.

(i) The upstream cylinder was free to oscillate and the downstream cylinder was fixed. In this case, the proximity of cylinders creates asymmetry in the flow and thus, produces lift forces. This vibration is called as proximity-induced galloping.

(ii) The upstream cylinder was fixed and the downstream cylinder was elastically mounted. In this case, downstream cylinder is exposed to wake of upstream cylinder. These vibrations are called wake-induced galloping or wake-induced vibrations. For these two cases, VIV and galloping can occur simultaneously in the moving cylinder.

It should be noted that the term galloping used in proximity and wake galloping has different mechanism from the definition used for the cross sectional-shape of the body (Bearman 2011). For the cross-sectional shape of the body such as a square cylinder, the hydrodynamic damping from the relative fluid motion induces instability to the system and the body motion of the structure even increases the amplitude of vibration by generating additional force (Den Hartog 1956; Blevins 2001). For tandem cylinders, when the downstream cylinder is placed in transverse direction from the x axis defined in Fig. 9.1, the hydrodynamic restoring force acts to return the rear cylinder in the original position (Assi 2009; Bearman 2011). Assi et al. (2010) found that the restoring transverse force on the downstream cylinder came from vortex interactions between vortices shed from the upstream and downstream cylinders. As shown in Fig. 9.10, Assi et al. (2010) also investigated that shed vortices from the upstream and downstream cylinders interacted and could enhance or reduce the transverse force of the downstream cylinder. Especially for the downstream cylinder, VIV and wake-induced vibrations caused by interactions of the shed vortices from both cylinders occurred.

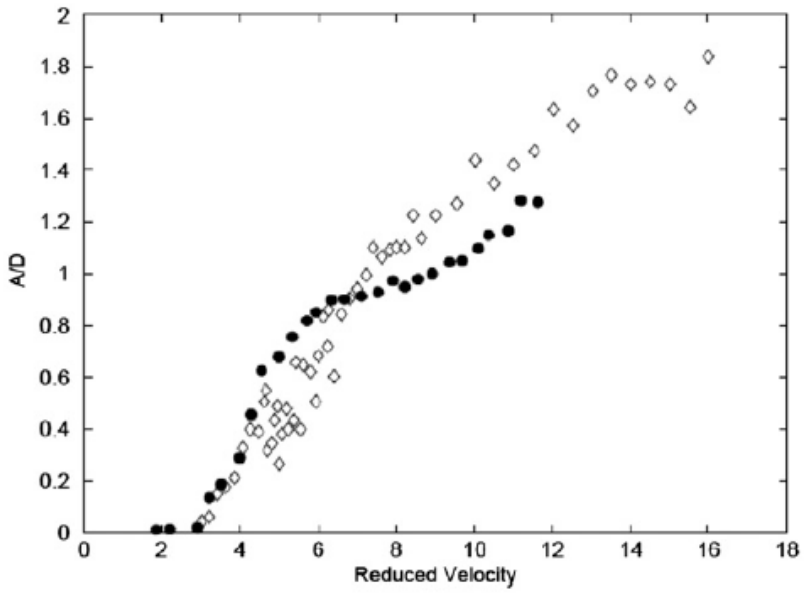

Fig. 9.8. Transverse response amplitude versus reduced velocity for the downstream circular cylinder of a pair of cylinders in a tandem arrangement: ●, L'/D=4 (Assi et al. 2006); ◇, L'/D=4.75 (Hover & Triantafyllou 2001); Reproduced from Bearman (2011).

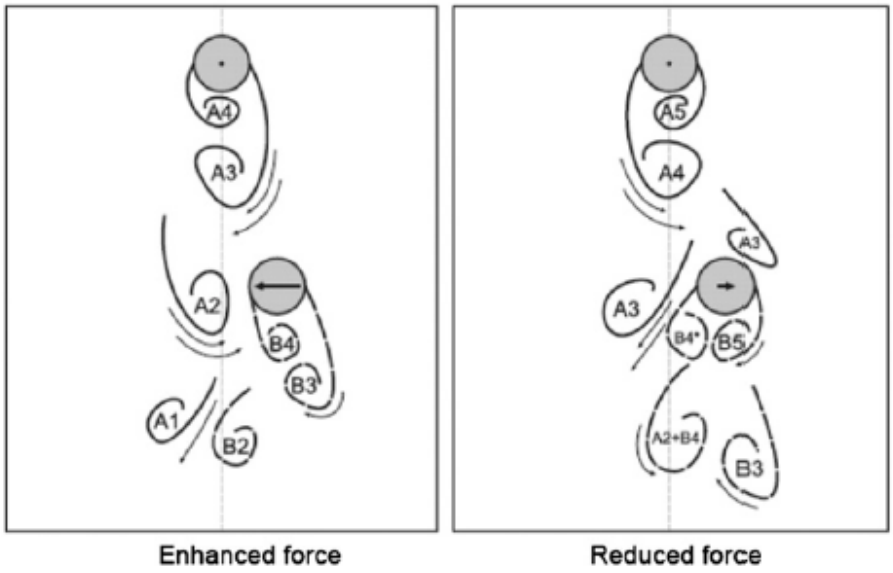

Fig. 9.9. Sketches showing the generation of an unsteady transverse force on the downstream cylinder for a reduced velocity above vortex resonance (Assi et al., 2010)

Thorough reviews of multiple cylinder interaction and response were published by Zdravkovich (1977, 1987, 1993, 2003), Nishimura (1986), Chen (1987), and Sumner (2010). In the current study, only two cylinders mounted on linear springs in a tandem configuration are studied. Since amplitude response of the cylinder does not increase like galloping, proximity-galloping or wake-induced galloping is not observed.

9.2. RESULTS, OBSERVATIONS, AND DISCUSSION

In this chapter, two flow-direction independent suppression models (T6 and T8) suggested in Chapter 8 are studied. The results of two cylinders with PTC suppression means in a tandem arrangement are presented along with the results of the two smooth cylinders. The lowest available center-to-center distance (L'/D) in the present study is 2.5 and the highest one is 5.0. As defined earlier, this L'/D range is either the shear layer reattachment region or the region of the Kármán vortex shedding from each cylinder. Because of the limited view of the laser sheet, flow patterns around cylinders are not presented.

9.2.1. Amplitude and frequency response

(a) Two smooth cylinders in tandem configuration

Figs. 9.10-9.15 show amplitude response of two T6 in a tandem configuration with varying center-to-center distance. For an upstream smooth cylinder at L'/D=2.5, the upper and lower branches are wider with slight amplitude difference than that of the single

smooth cylinder as shown in Fig. 9.10. As L'/D increases from 2.5 to 4.0, the synchronization region decreases and the amplitude response of the upstream smooth cylinder at L'/D=4.0 is close to the amplitude response of the single smooth cylinder. That is, proximity interference from the downstream cylinder is reduced. Further increase of L'/D as shown in Figs. 9.14 and 9.15, results in amplitude response of the upstream cylinder similar to that of the single smooth cylinder with delayed onset of the upper branch.

For the downstream smooth cylinder, the following observations are made regardless of L'/D:

(i) Gradual amplitude increase in the initial branch

(ii) Amplitude modulation in the upper branch

(iii) Lower amplitude in the upper branch and higher amplitude in the lower branch than that of the smooth cylinder. As L'/D increases from 2.5 to 5.0, proximity interference from the upstream cylinder is reduced and the amplitude modulation is gradually decreased.

Frequency response is shown in Fig. 9.16–9.21 and the oscillation frequency for both cylinders is normalized by the natural frequency of the upstream device. The frequency ratios for the upstream and the downstream cylinders at L'/D=2.5 (Fig. 9.16) are lower compared to the single smooth cylinder. As L'/D increases from 2.5, the frequency ratio of the upstream cylinder approaches to the values of the single smooth cylinder and becomes close to that of the single smooth cylinder after $L'/D \geq 3.5$. For the downstream cylinder, the frequency response in the upper and lower branches is lower than that of the single smooth cylinder and f^* in the lower branch is almost constant regardless of L'/D

values. It is worthy to note that oscillation frequency synchronization is observed at some range of U^* in the tandem arrangement. This will be discussed in Section 9.2.2.

(b) Two T6 cylinders in tandem configuration

Figs. 9.10-9.15 also show the amplitude response of two T6 cylinders (helically applied roughness strip) in a tandem arrangement. For the upstream T6 cylinder, because of proximity interference the onset of the upper branch is delayed more than that of single T6 cylinder. The amplitude of upstream T6 cylinder is higher than that of the single T6 cylinder over all U^* range. As L'/D increases from 2.5 to 5.0, the amplitude of T6 reduces and the response becomes close to the single T6 cylinder. General amplitude response of the downstream T6 is the same regardless of L'/D and the amplitude is increased compared to the single T6 in the entire U^* range. As L'/D increases, the amplitude in the upper branch is decreased slightly and the upper branch range is becomes slightly shorter. This shows that for the downstream T6 cylinder, wake interference has significant effect on the amplitude response and proximity interference effect is minor. It should be noted that for all L'/D, as the amplitude response of the upstream cylinder approaches desynchronization, the downstream cylinder amplitude is decreased and the downstream cylinder response becomes the lower branch. This is clearly an effect of the upstream cylinder and the upstream cylinder influences the amplitude response range of the downstream cylinder.

Regarding the frequency response, both T6 cylinders in the tandem configuration have lower values than that of the single T6 cylinder. Interestingly, as shown in Figs. 9.16-9.20, the frequencies of the upstream and the downstream T6 cylinders are

synchronized for a broad range of U^*. For side-by-side arrangement of stationary cylinders, synchronization of vortex shedding frequency or phase was observed (Sumner 2010). According to Zdravkovich (1987), synchronization between the vortex shedding processes and vortex streets of the upstream and downstream cylinder may happen at L'/D<6-8. But the synchronization of the body oscillation frequency is not reported in literature.

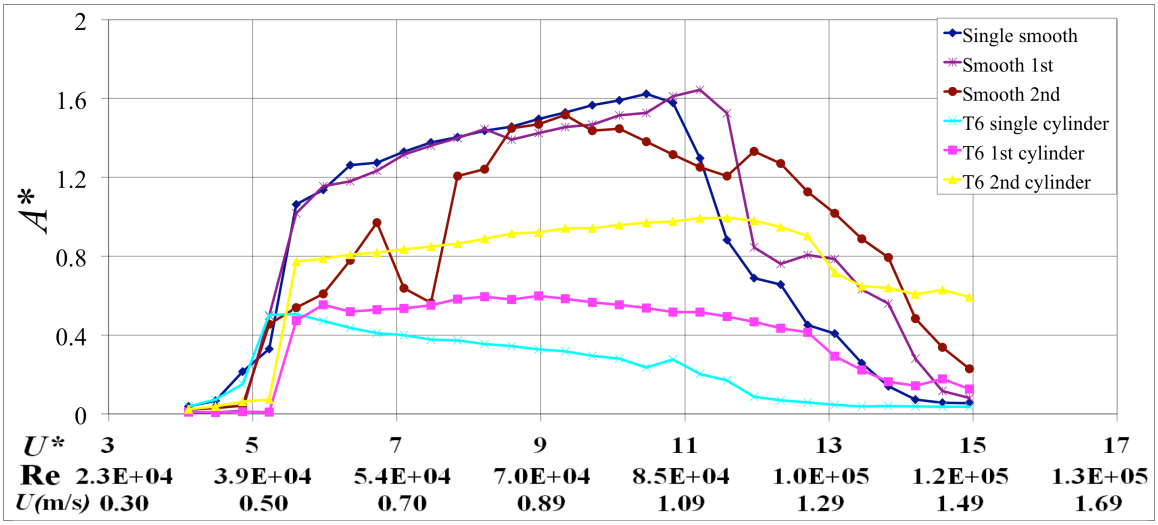

Fig. 9.10. Amplitude response of two smooth cylinders and two T6 cylinders in tandem arrangement at L'/D=2.5

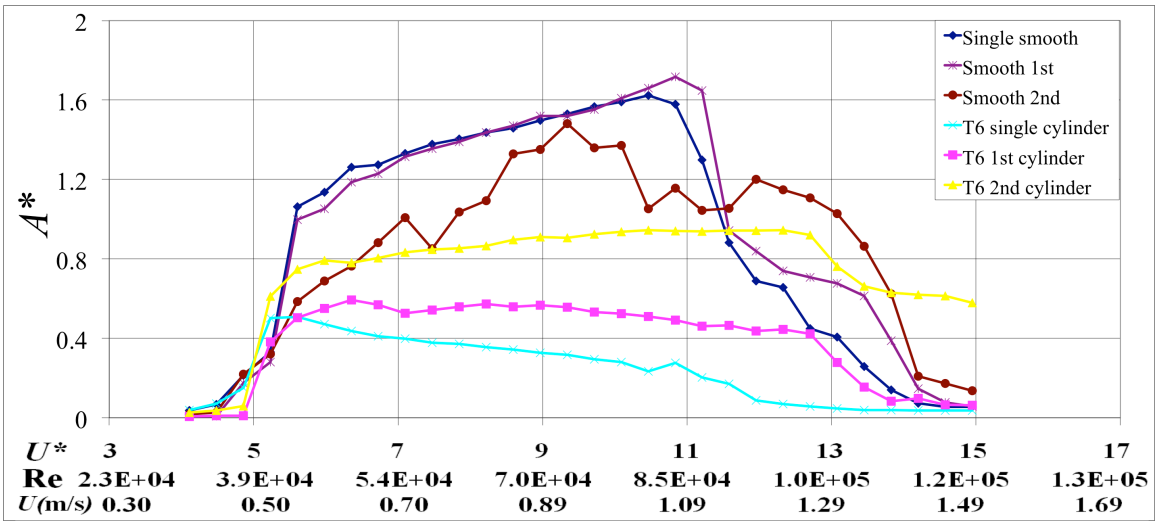

Fig. 9.11. Amplitude response of two smooth cylinders and two T6 cylinders in tandem arrangement at L'/D=3.0

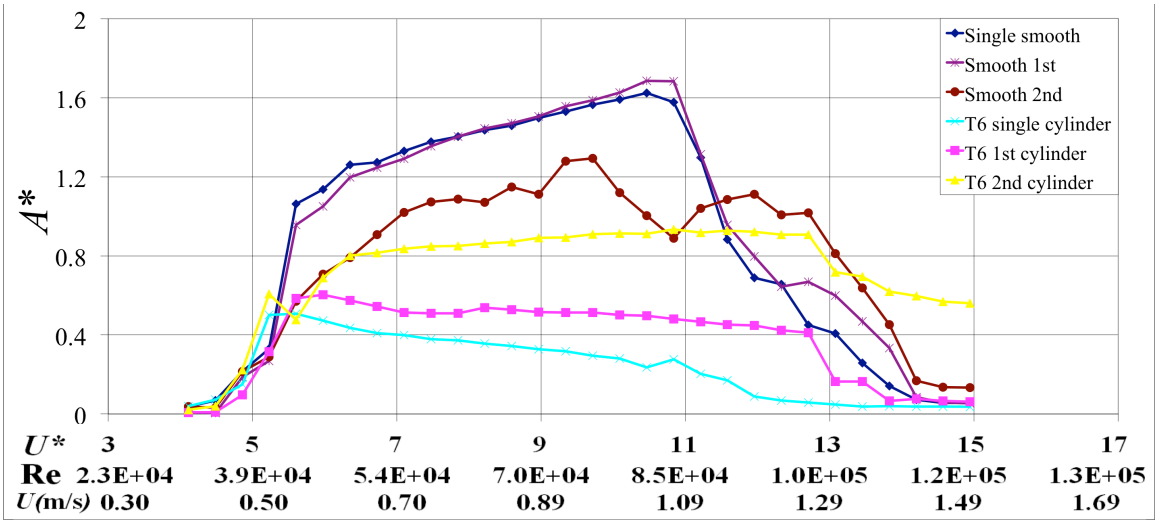

Fig. 9.12. Amplitude response of two smooth cylinders and two T6 cylinders in tandem arrangement at L'/D=3.5

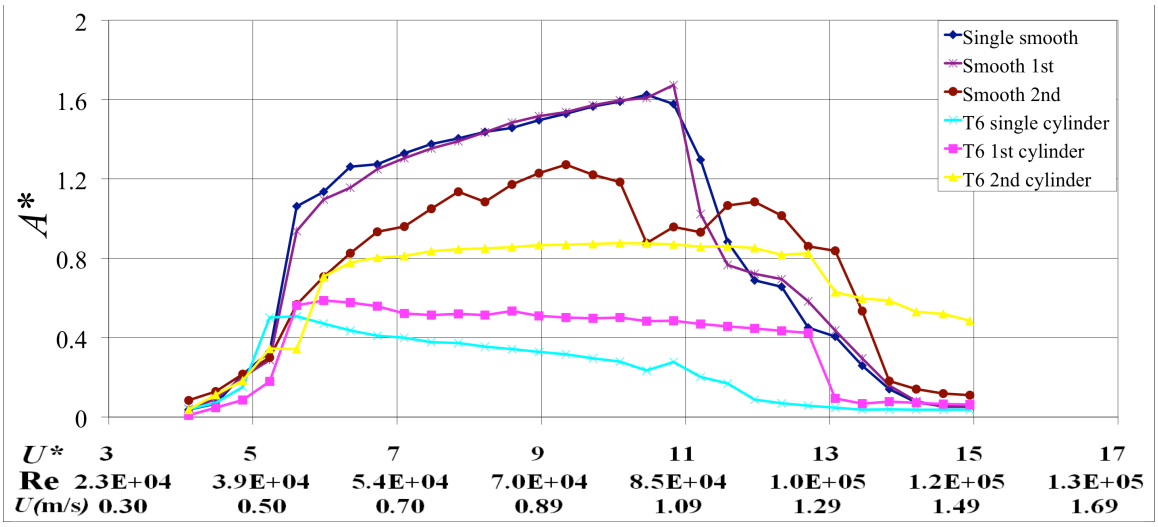

Fig. 9.13. Amplitude response of two smooth and two T6 cylinders in tandem arrangement at L'/D=4.0

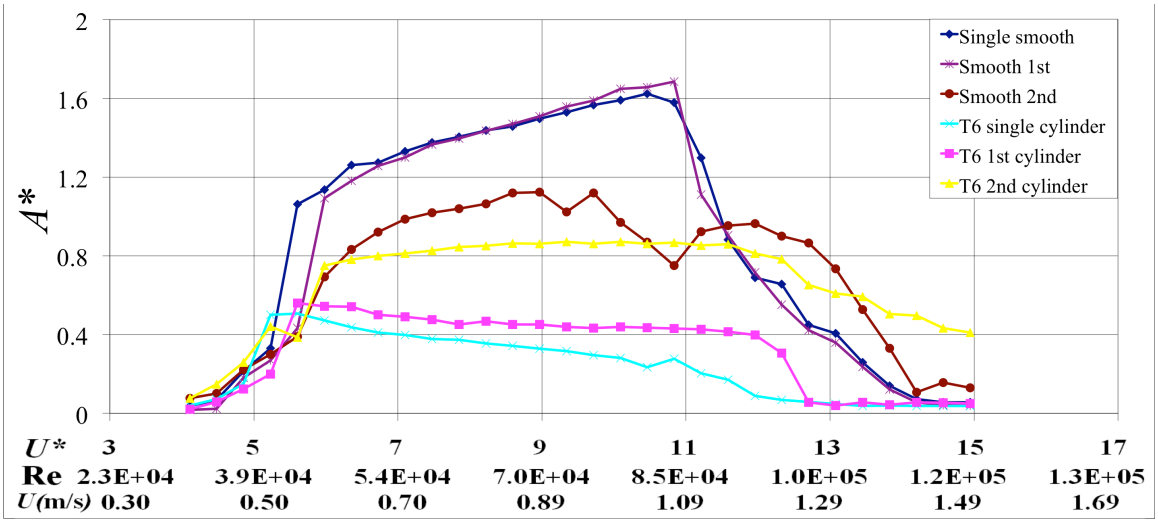

Fig. 9.14. Amplitude response of two smooth cylinders and two T6 cylinders in tandem arrangement at L'/D=4.5

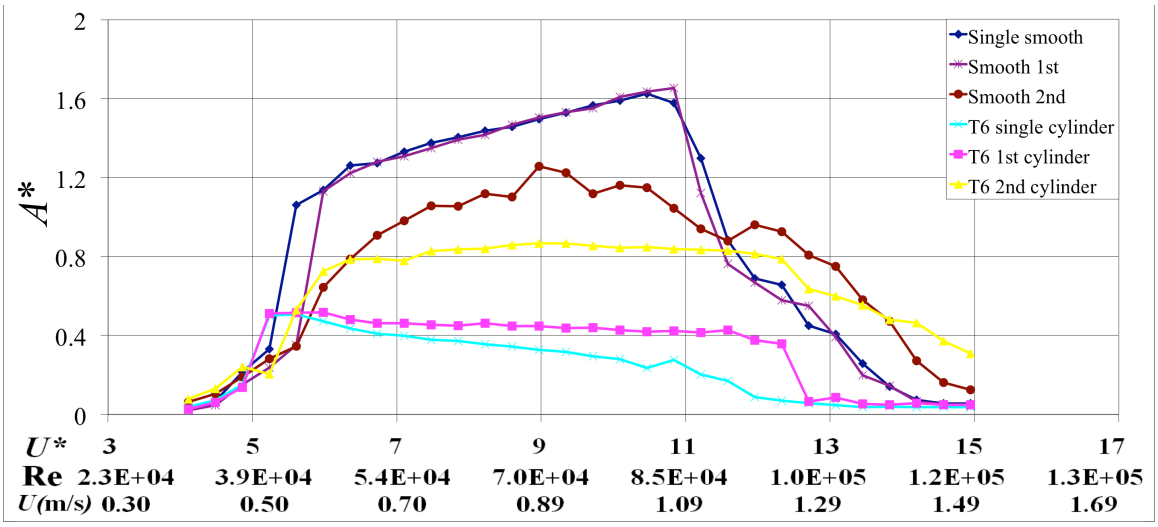

Fig. 9.15. Amplitude response of two smooth cylinders and two T6 cylinders in tandem arrangement at L'/D=5.0

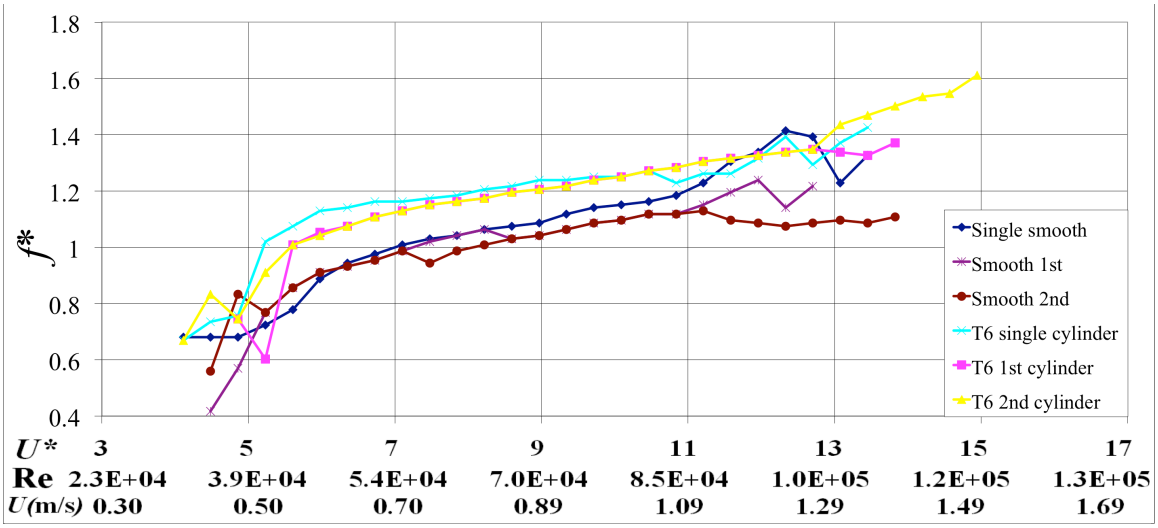

Fig. 9.16. Frequency response of two smooth cylinders and two T6 cylinders in tandem arrangement at L'/D=2.5

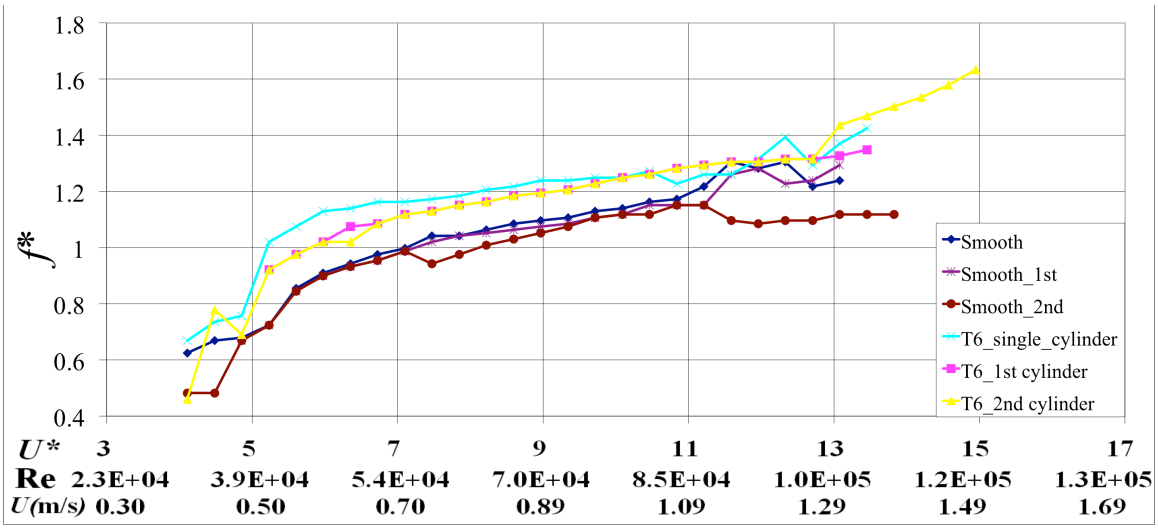

Fig. 9.17. Frequency response of two smooth cylinders and two T6 cylinders in tandem arrangement at L'/D=3.0

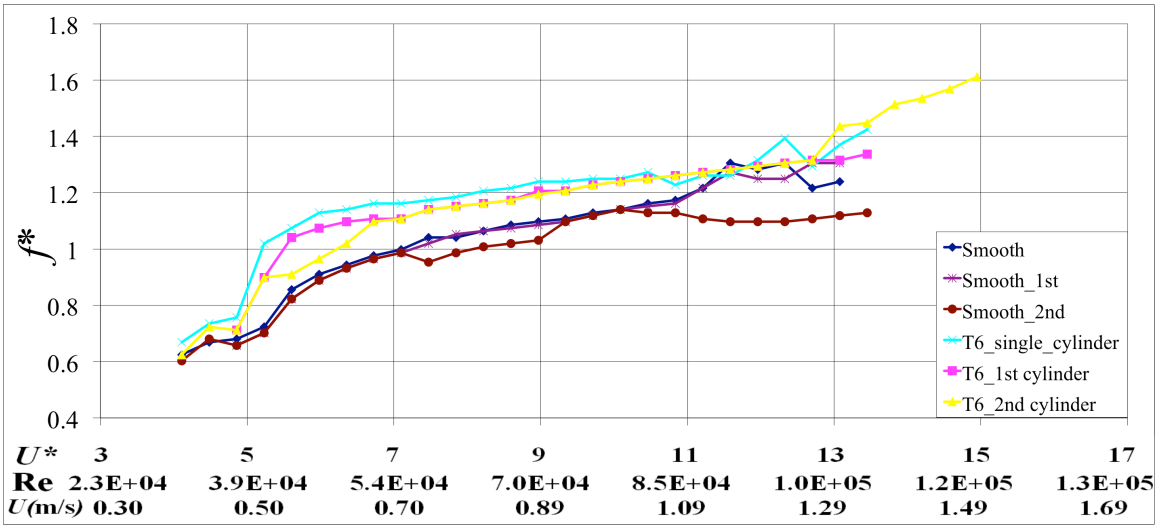

Fig. 9.18. Frequency response of two smooth cylinders and two T6 cylinders in tandem arrangement at L'/D=3.5

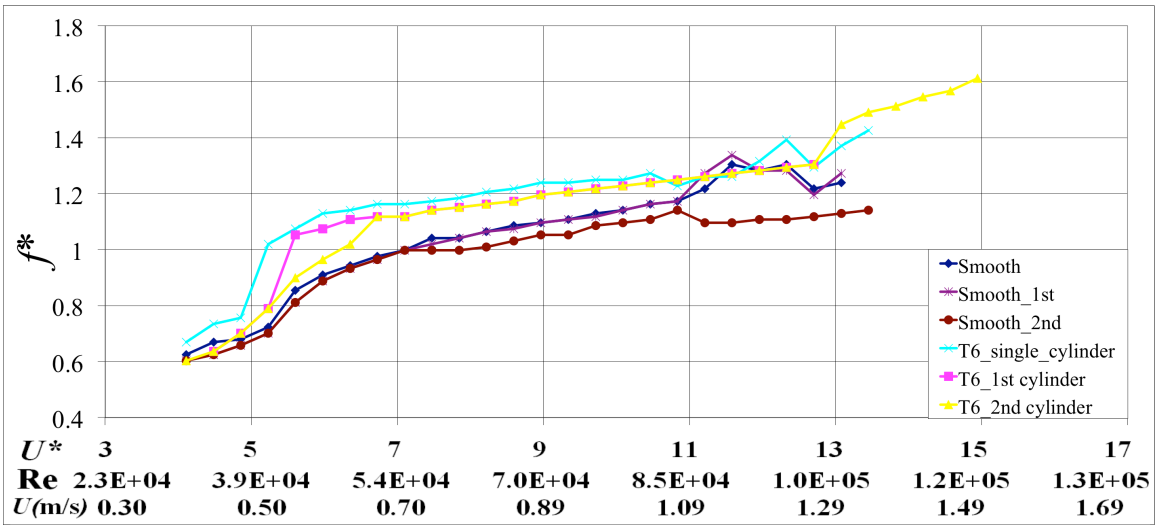

Fig. 9.19. Frequency response of two smooth cylinders and two T6 cylinders in tandem arrangement at L'/D=4.0

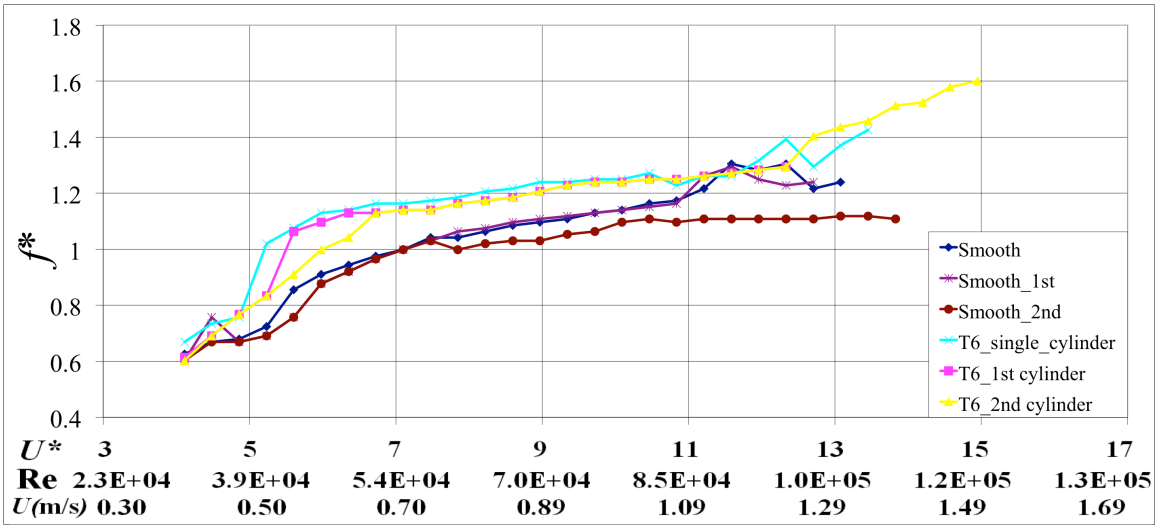

Fig. 9.20. Frequency response of two smooth cylinders and two T6 cylinders in tandem arrangement at L'/D=4.5

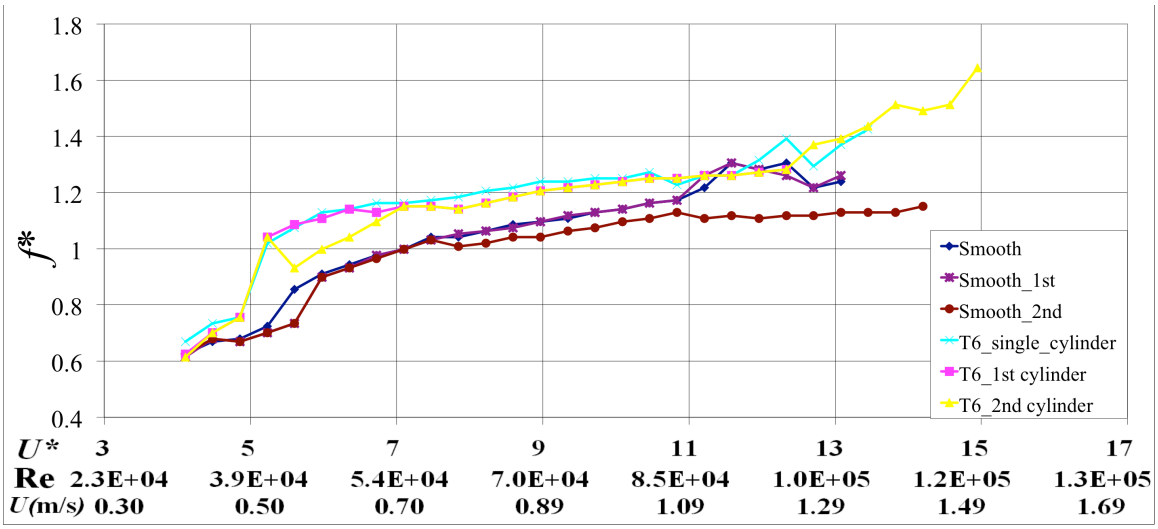

Fig. 9.21. Frequency response of two smooth cylinders and two T6 cylinders in tandem arrangement at L'/D=5.0

(c) Two T8 cylinders in tandem configuration

Figs. 9.22-9.27 show amplitude response of T8 cylinders. Similarly to the T6 cylinders upstream, the synchronization region and the amplitude response of the upstream T8 cylinder decreases as L'/D increases from 2.5 to 5.0. For the T8 cylinder upstream for all L'/D spacing values, the onset of the upper branch is delayed compared to a single T8 response. Same as the T6 cylinder downstream, the T8 cylinder downstream has higher amplitude at $5<U^*<15$ and broader upper branch than that of the single T8 cylinder. As L'/D increases (less proximity interference), the upper branch range and the amplitude in the upper branch are slightly decreased. For the downstream cylinders (T6 and T8) with suppression means, wake interference dominates the cylinder response. For both T6 and T8 cylinders downstream, the amplitude at high U^* is much higher than that of the smooth cylinder downstream. From visualization results, the upstream cylinder with PTC suppression means has narrower and twice longer wake region than that of the smooth cylinder while wake of the upstream smooth cylinder is

short and diffused very quickly. Thus, a PTC cylinder downstream is exposed more to the wake regions at the same center-to-center distance compared to the smooth cylinder and this wake interference causes more amplitude vibration in the cylinder with PTC suppression means. Vickery & Watkins (1964) also noticed that helical strakes used on the upstream cylinder were not effective in suppression of amplitude in downstream cylinders. Zdravkovich (1981) also noticed that for suppression devices, vortices do not vanish but merely occur further downstream.

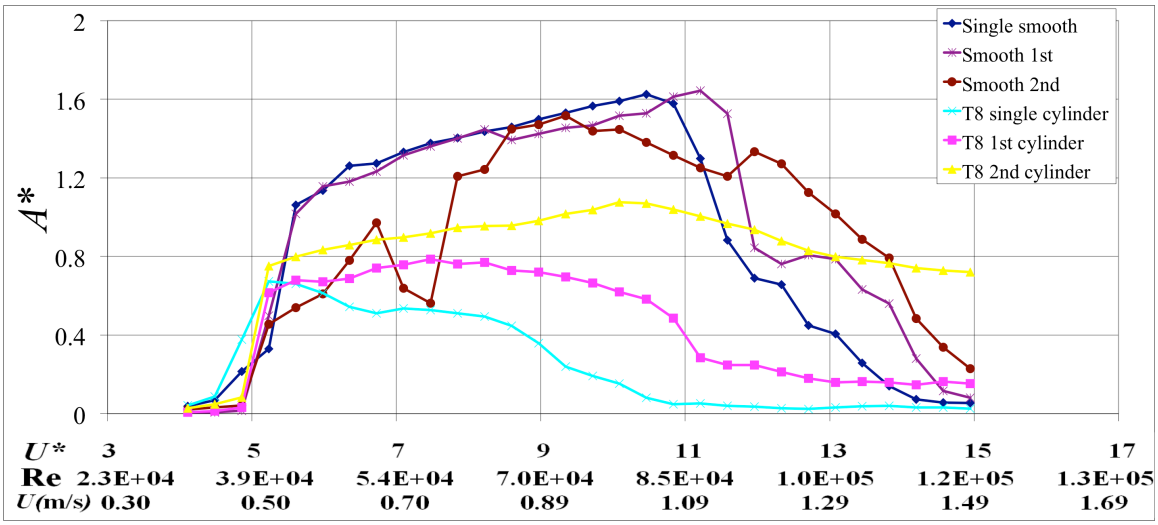

Fig. 9.22. Amplitude response of two T8 cylinders in tandem arrangement at L'/D=2.5

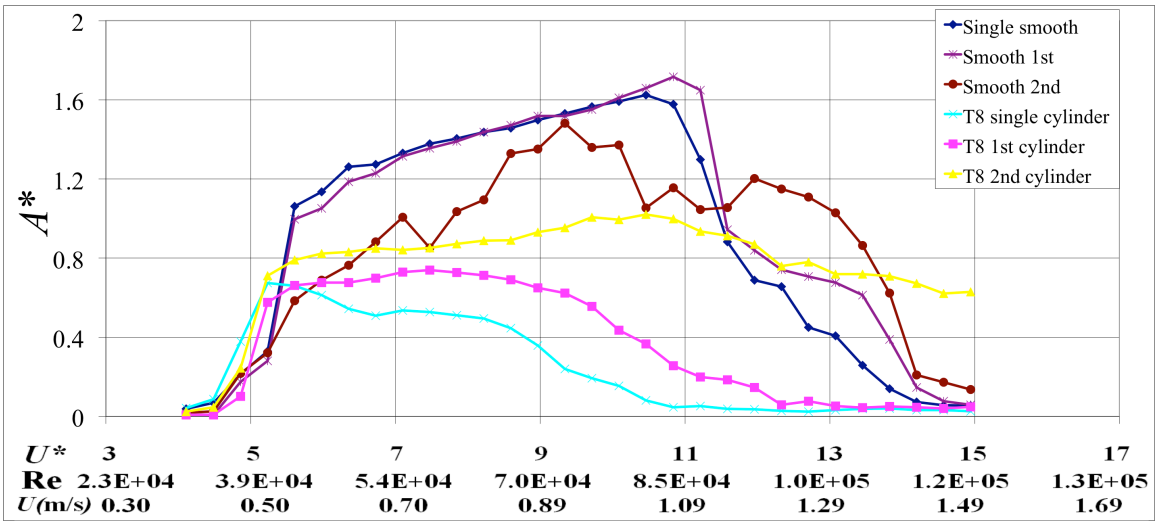

Fig. 9.23. Amplitude response of two T8 cylinders in tandem arrangement at L'/D=3.0

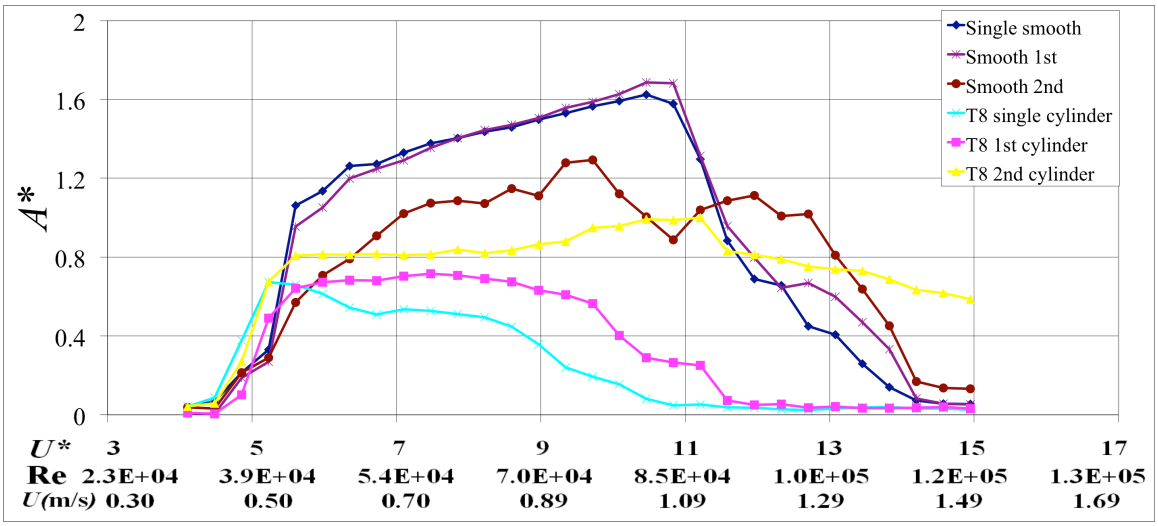

Fig. 9.24. Amplitude response of two T8 cylinders in tandem arrangement at L'/D=3.5

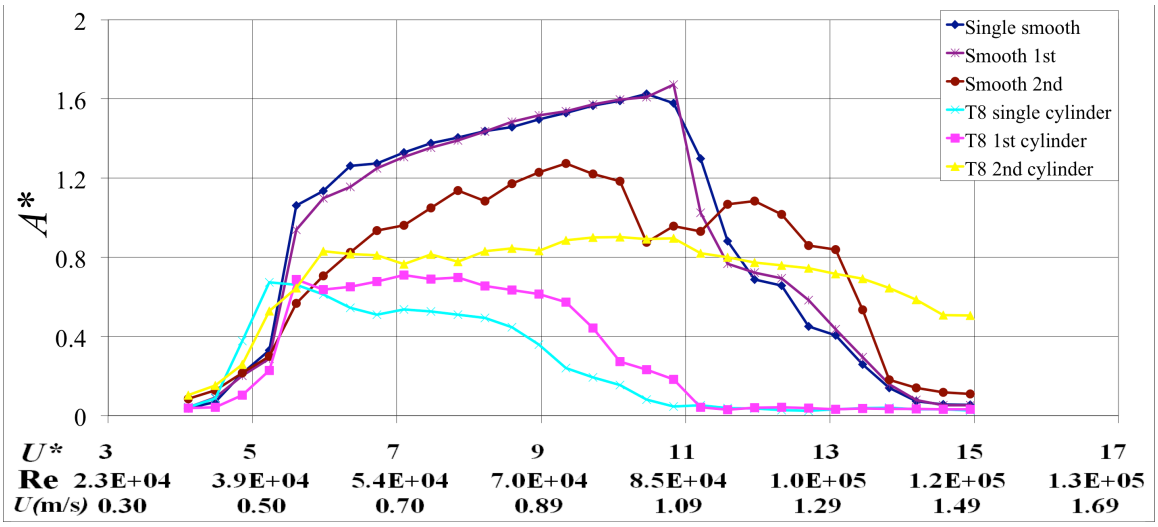

Fig. 9.25. Amplitude response of two T8 in tandem arrangement at L'/D=4.0

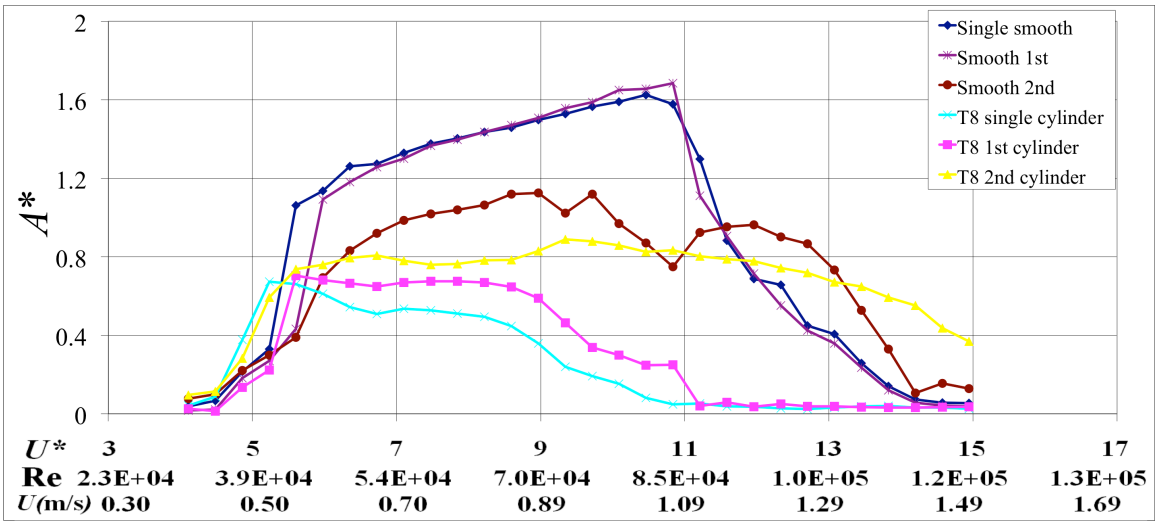

Fig. 9.26. Amplitude response of two T8 cylinders in tandem arrangement at L'/D=4.5

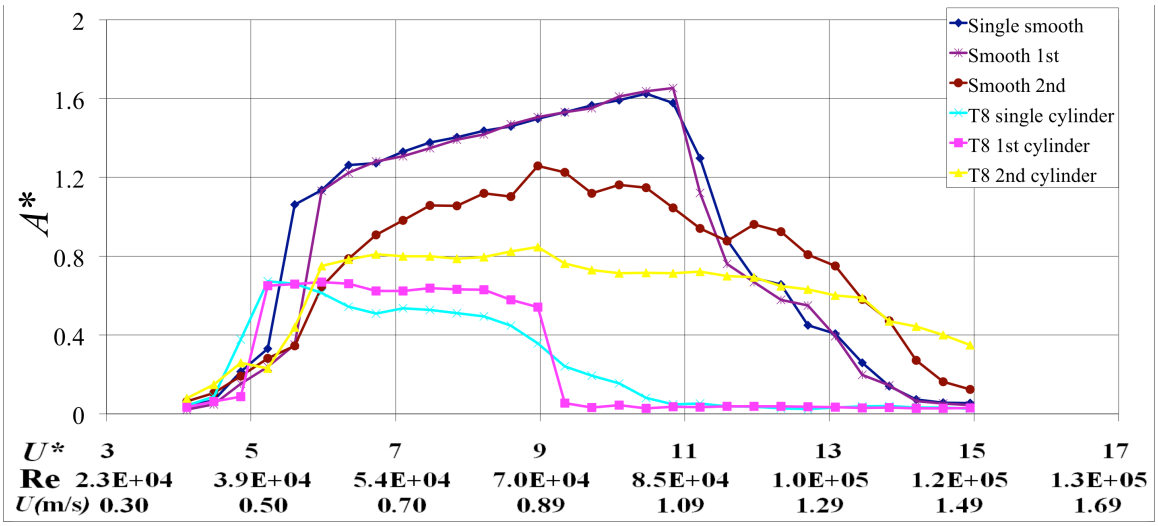

Fig. 9.27. Amplitude response of two T8 cylinders in tandem arrangement at L'/D=5.0

As seen in Figs. 9.28-9.33, The synchronization of the two-body oscillation frequencies is even more severe in the T8 cylinders. At $2.5 \leq L'/D \leq 3.5$ (Figs. 9.28-9.30), the oscillation frequencies of the upstream and downstream cylinders lock in together almost through the entire range of U^*. As L'/D increases from 4.0 to 4.5 (Figs. 9.31 and 9.32), the two frequency ratios separate from each other and variation of frequency ratio between the two T8 cylinders is observed at $11.0 \leq U^* \leq 15.0$. At L'/D=5.0 (Fig. 9.33), the frequency ratio of the upstream T8 cylinder is close to that of the single T8 cylinder and more frequency variation between two T8 cylinders is found. When PTC was located in the soft galloping zone for the two tandem cylinders, the frequency synchronization was not observed (Kim et al. 2011). Hence, two cylinders with PTC in the SG zone are like two independent systems and two cylinders with PTC suppression means are more or less two dependent systems. Two smooth cylinders can be considered as two intermediate systems. Coupled oscillators are often found in nonlinear systems and Huygens

(Blekhman 1988; Benett 2001) first found frequency synchronization of pendulum clocks with 180° out of phase.

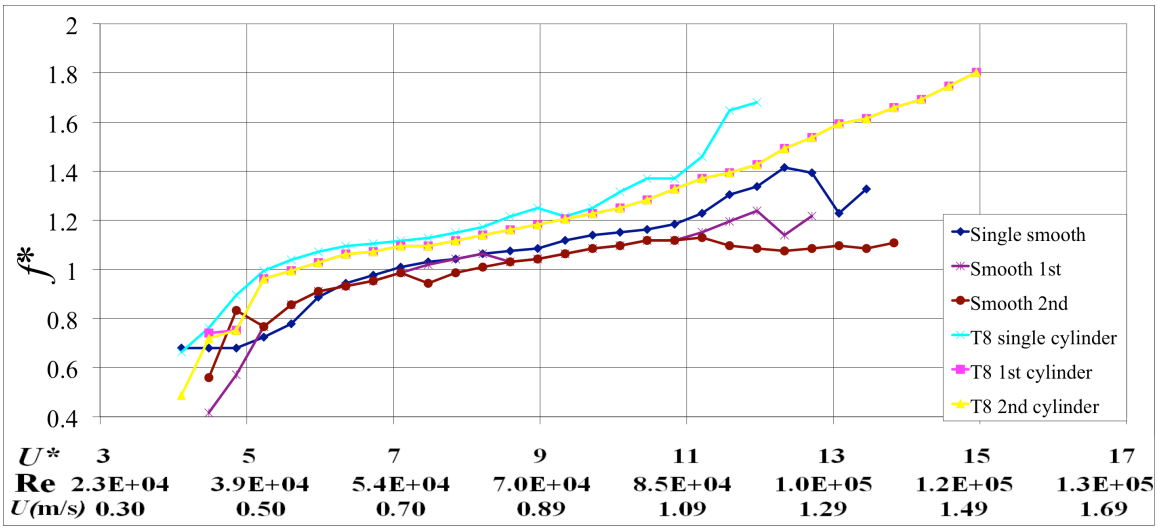

Fig. 9.28. Frequency response of two T8 cylinders in tandem arrangement at L'/D=2.5

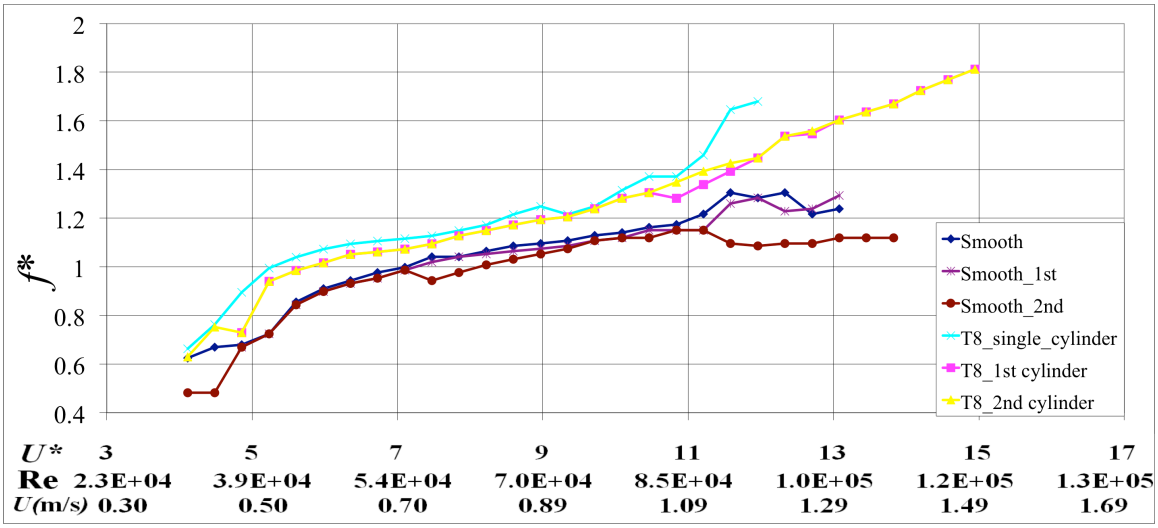

Fig. 9.29. Frequency response of two T8 cylinders in tandem arrangement at L'/D=3.0

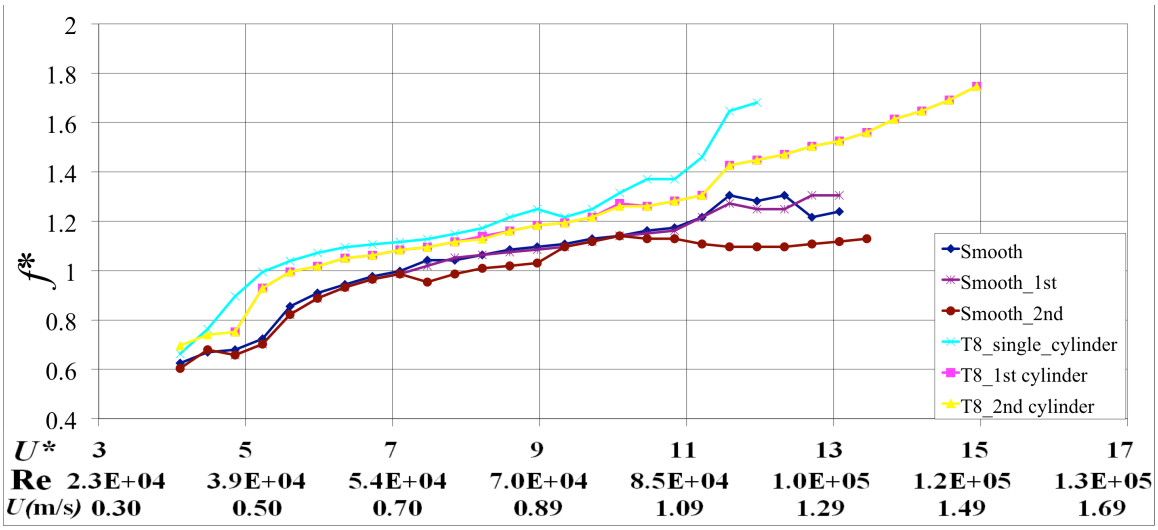

Fig. 9.30. Frequency response of two T8 in tandem arrangement at L'/D=3.5

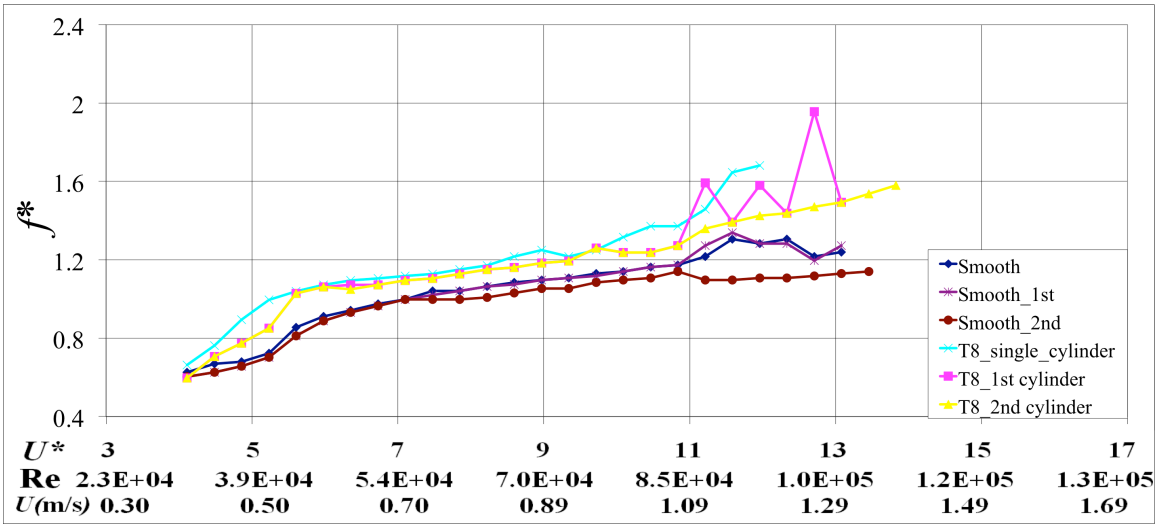

Fig. 9.31. Frequency response of two T8 cylinders in tandem arrangement at L'/D=4.0

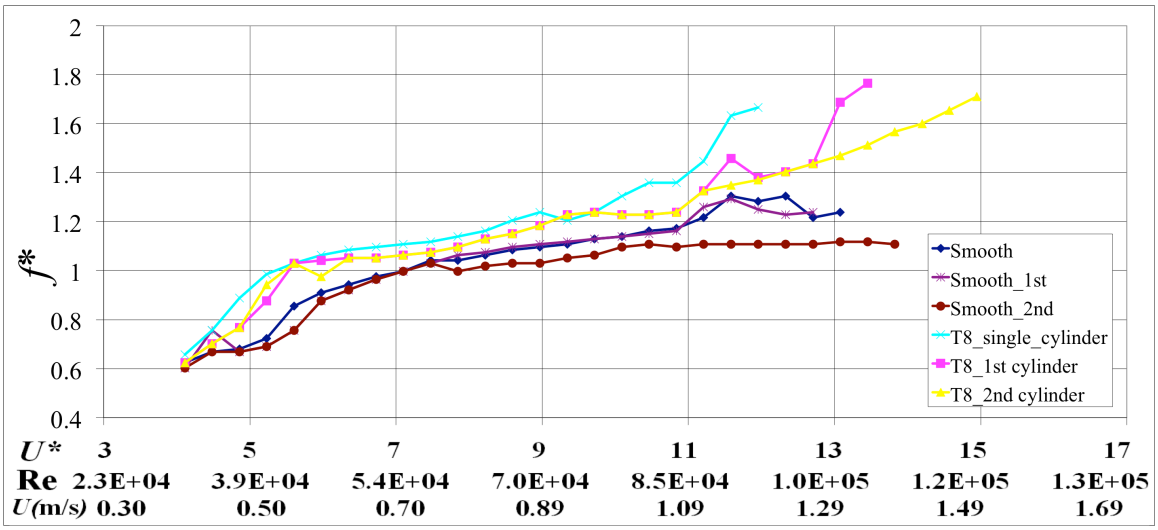

Fig. 9.32. Frequency response of two T8 in tandem arrangement at L'/D=4.5

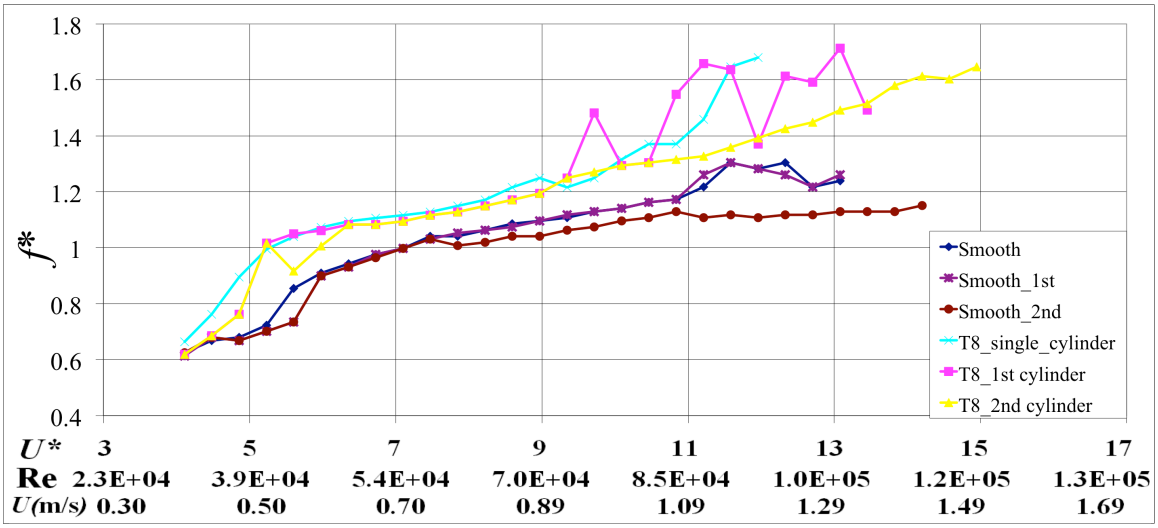

Fig. 9.33. Frequency response of two T8 cylinders in tandem arrangement at L'/D=5.0

9.2.2. Synchronization of oscillation frequency

As shown in the frequency response results, synchronization of the oscillation frequencies of two cylinders is observed in smooth cylinders and cylinders with PTC

suppression means. Fig. 9.34 shows the phase difference between displacements of the two smooth cylinders in a tandem configuration. For L'/D=2.5, three regions ($5 \le U^* \le 7$, $8.5 \le U^* \le 11$, and $13 \le U^* \le 14.5$) of synchronization are found. The phase difference between two smooth cylinders in first two regions is very small placing the two cylinders almost in phase. In the third region, the phase difference is around 90°. It should be noted that the two cylinders have different traveling distance (amplitude value) at the same U^* so that the phase angle cannot be exactly 0° or 180°. As L'/D increases from 2.5 to 3.0-3.5, the synchronization regions are decreased from three to two. For further increase of L'/D, the synchronization region is only observed at $4.5 \le U^* \le 7.5$. That is, as center-to-center distance is increased, interactions between the two cylinders are decreased. At $4.5 \le U^* \le 7.5$, as L'/D increases, the phase angle is changed from in-phase to out-of-phase.

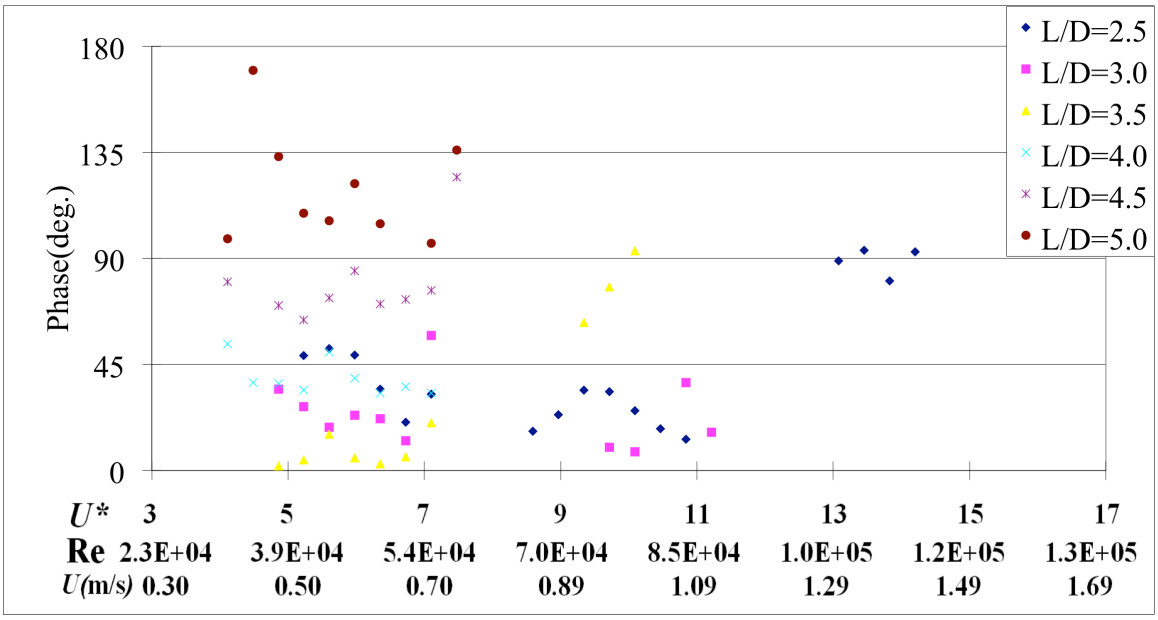

Fig. 9.34. Phase difference between time displacement histories of the two smooth cylinders

As shown in Fig. 9.35, for the T6 cylinders, frequency synchronization is obvious and broad range of frequency synchronization ($5.0 \leq U^* \leq 13.0$) is observed. As U^* is increased, the phase angle is shifted from in-phase to out-of-phase regardless of L'/D. In the initial branch, variation of phase angle is found and the reason is that the cylinder motion is not synchronized. At $9.0 \leq U^* \leq 13.0$, the closer the distance between the two cylinders (L'/D) is the more out-of-phase their motions are.

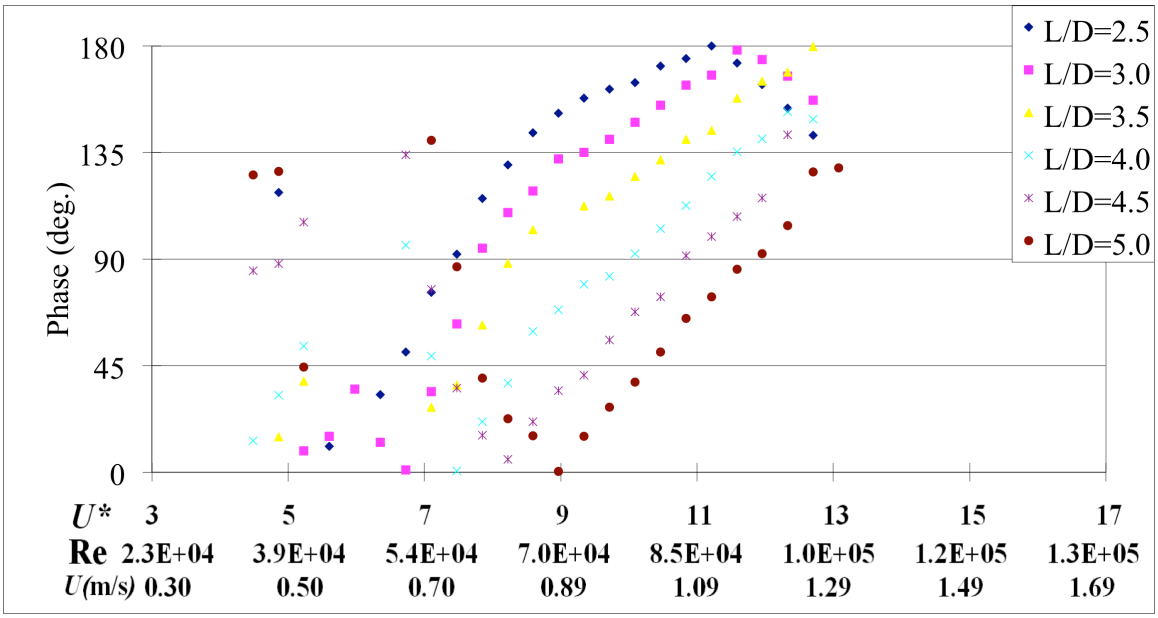

Fig. 9.35. Phase difference between time displacement histories of the two T6 cylinders

Similarly to the T6 cylinders, for the T8 cylinders, a broad range of frequency synchronization is found as seen in Fig. 9.36. Same as for the T6 cylinders, the phase of the T8 cylinders is changed from in-phase to out-of-phase as U^* increases. More variation in the phase angle is observed at $4 \leq U^* \leq 6$ for $L'/D=5$. Frequency synchronization is not observed at high reduced velocities for $L'/D=5$.

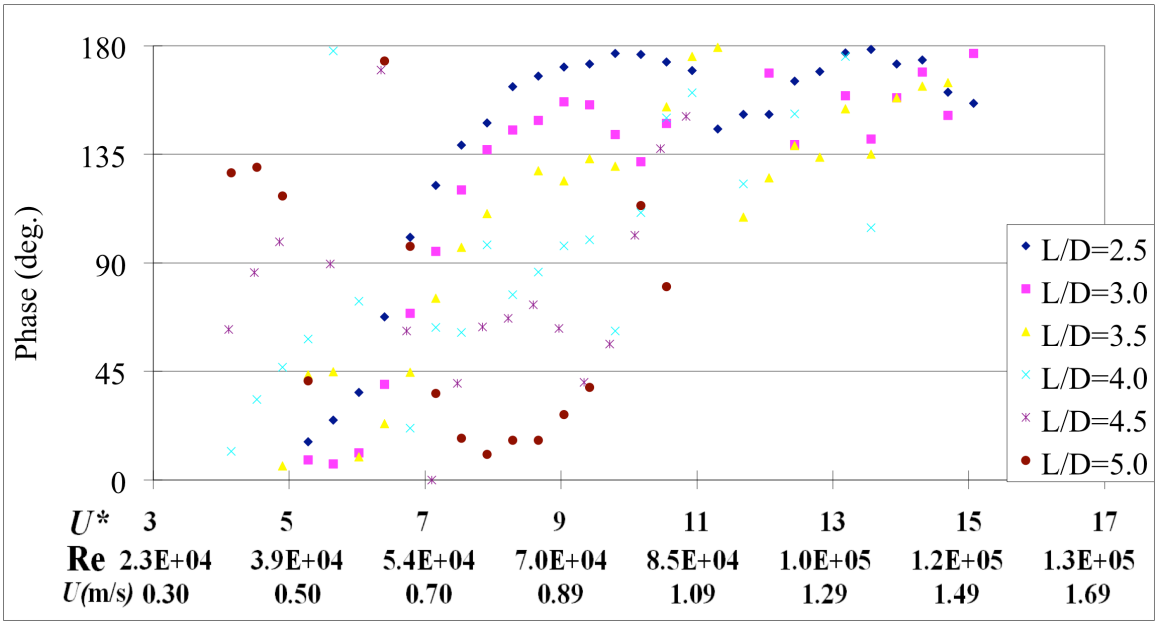

Fig. 9.36. Phase difference between time displacement histories of the two T8 cylinders

9.2.3. Displacement and power spectrum

In this section, time histories of displacement and power spectra are presented. As L'/D varies, the ranges of the initial, upper and lower branches change. The time histories of displacement and the power spectra within each branch change slightly. So only one L'/D is chosen as example for the smooth and suppression cylinders. Since two suppression models (T6 and T8) have similar results, only the T6 is selected as an example.

(i) Two smooth cylinders in a tandem arrangement

Time histories of displacement and power spectra for two smooth cylinders at L'/D=3.0 are presented in Fig. 9.37. At U^*=4.86 (Fig. 9.37(a)), both cylinders are in the initial branch. The amplitude of the two cylinders exhibits modulation and they are not fully synchronized. As shown in Fig. 9.37(a), the frequencies of the two smooth cylinders

are about equal. The two smooth cylinder oscillations become stable in the upper branch (Fig. 9.37(b)). For further increase of U^* in the upper branch (Fig. 9.37(c)), oscillation modulation is observed in the downstream cylinder. The modulation shows two different frequencies in the displacement plot with high and low amplitude groups. These two frequencies also appear in the power spectra. This modulation of downstream cylinder in the upper branch is observed at all L'/D values. As U^* is increased further in the upper branch (Fig. 9.37(d)), the modulation in the downstream cylinder decreases. As the upstream cylinder moves to the lower branch (Fig. 9.37(e)), oscillations in the upstream cylinder become less stable and the amplitude decreases. It is believed that this amplitude decrease in the upstream cylinder also reduces the amplitude of the downstream cylinder. As shown in Fig. 9.37(f), at desynchronization, the upstream cylinder has higher amplitude than that of the single smooth cylinder. This higher amplitude is due to proximity interference by the presence of the downstream cylinder. When both cylinders are at desynchronization (Fig. 9.37(g)), the upstream cylinder amplitude is negligible. The downstream cylinder amplitude is very small but higher than that of the single smooth cylinder at desynchronization because of the wake interference from the upstream cylinder.

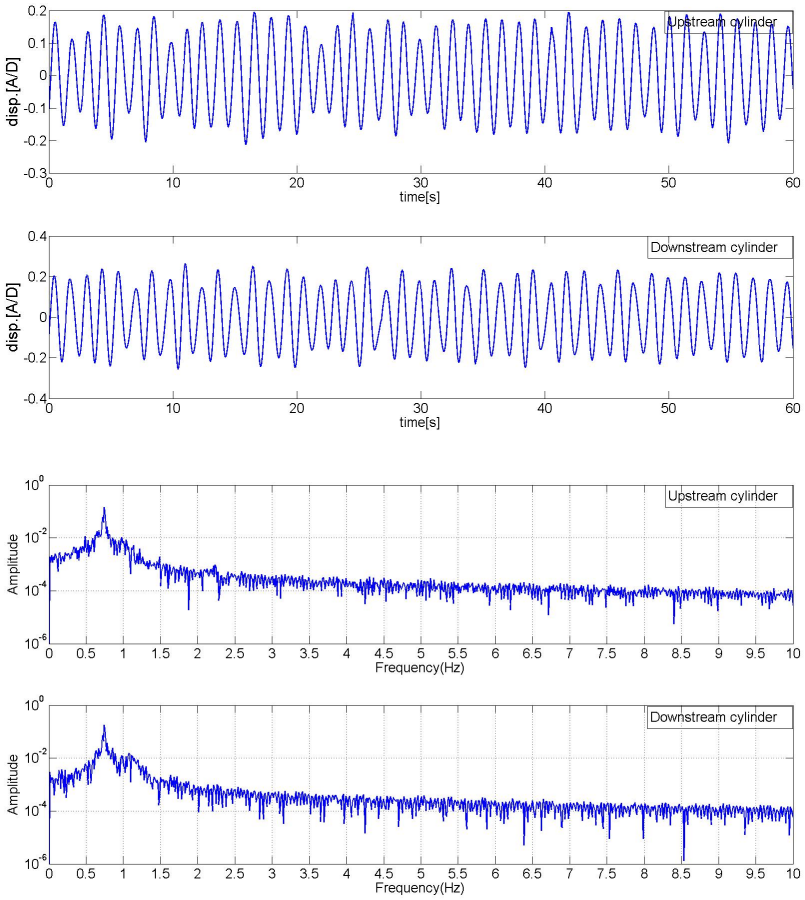

(a) U^*=4.86; initial branch

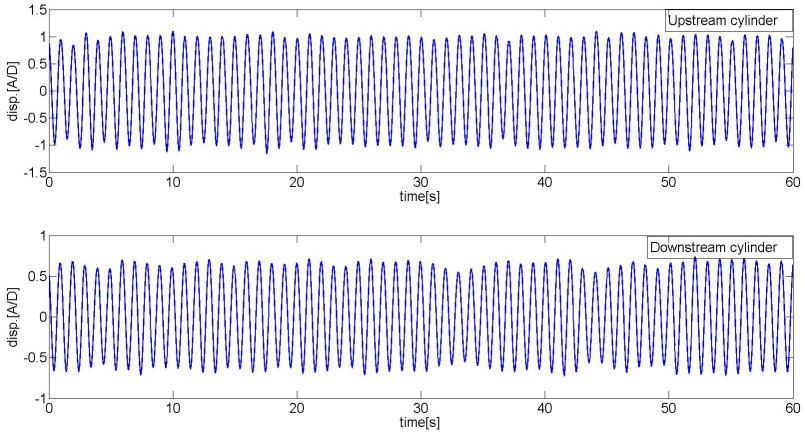

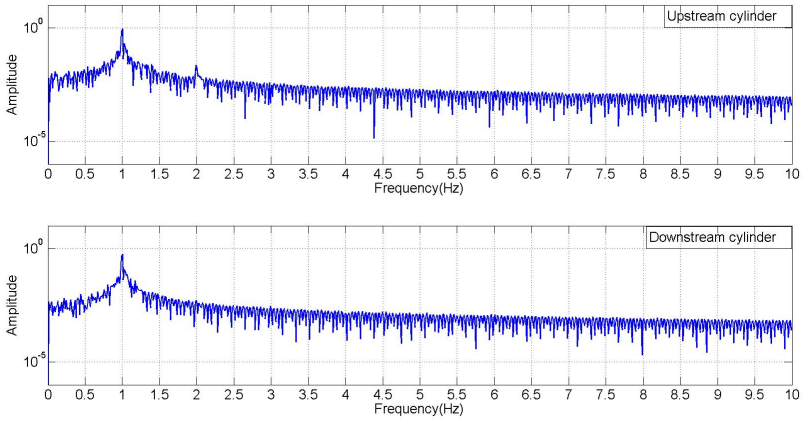

(b) U^*=5.98; upper branch

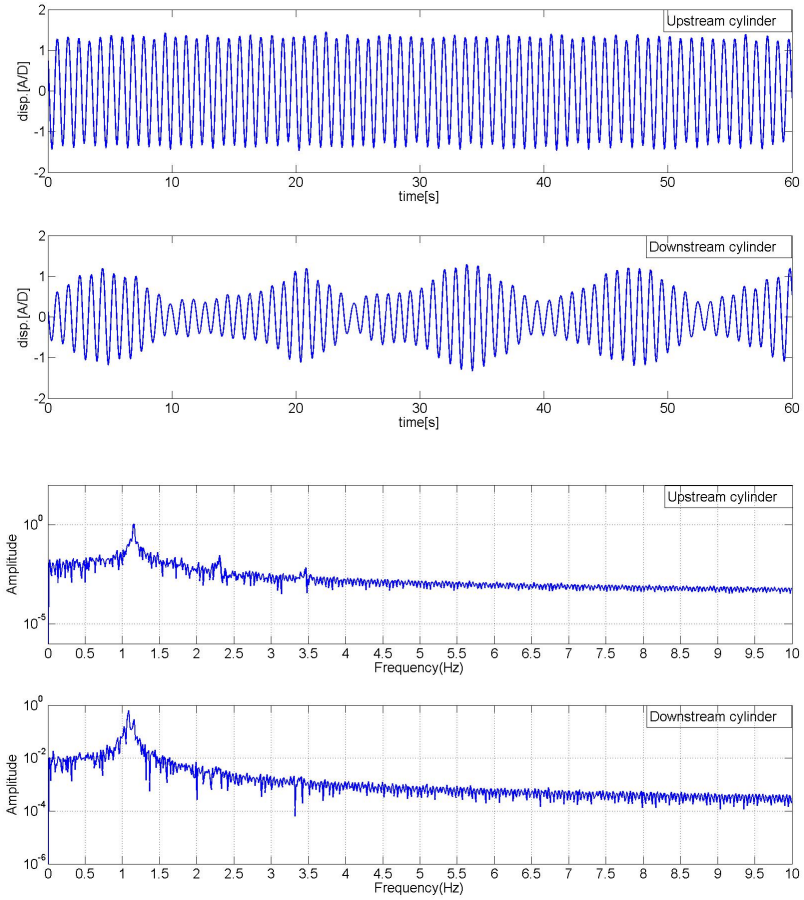

(c) U^*=7.85; upper branch

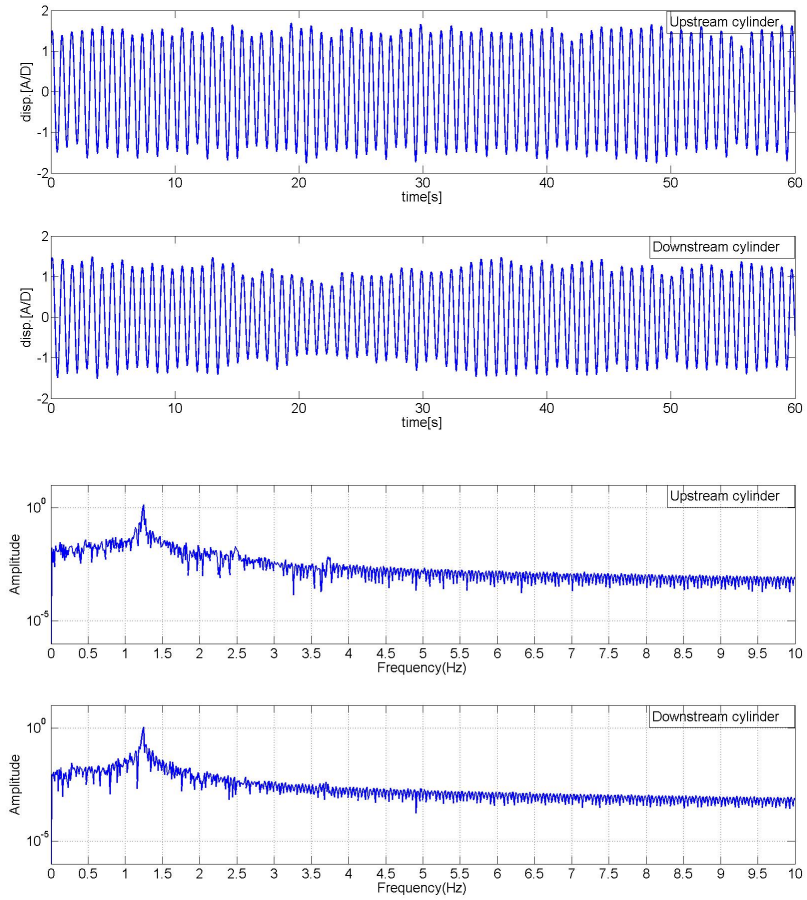

(d) U^*=10.09; upper branch

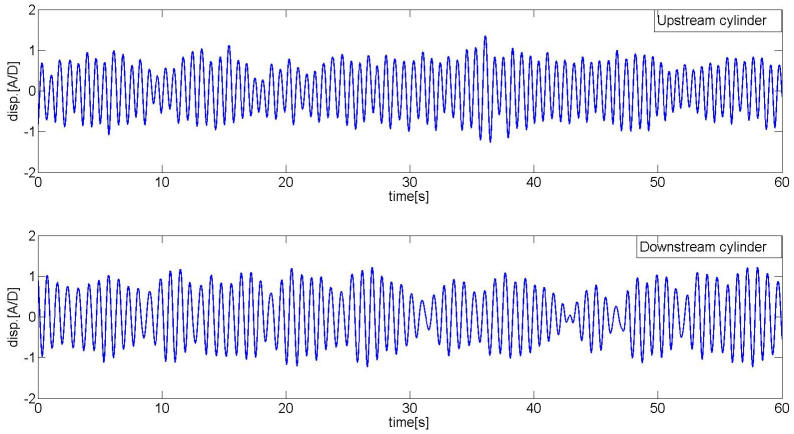

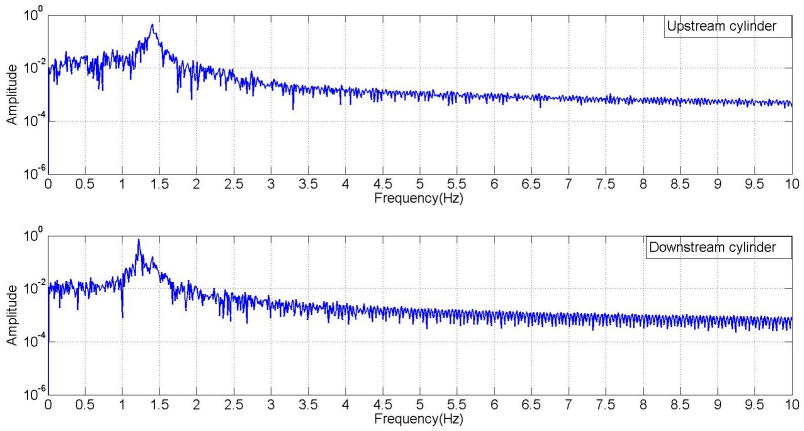

(e) U^*=11.58; upstream cylinder in lower branch and downstream cylinder in upper branch

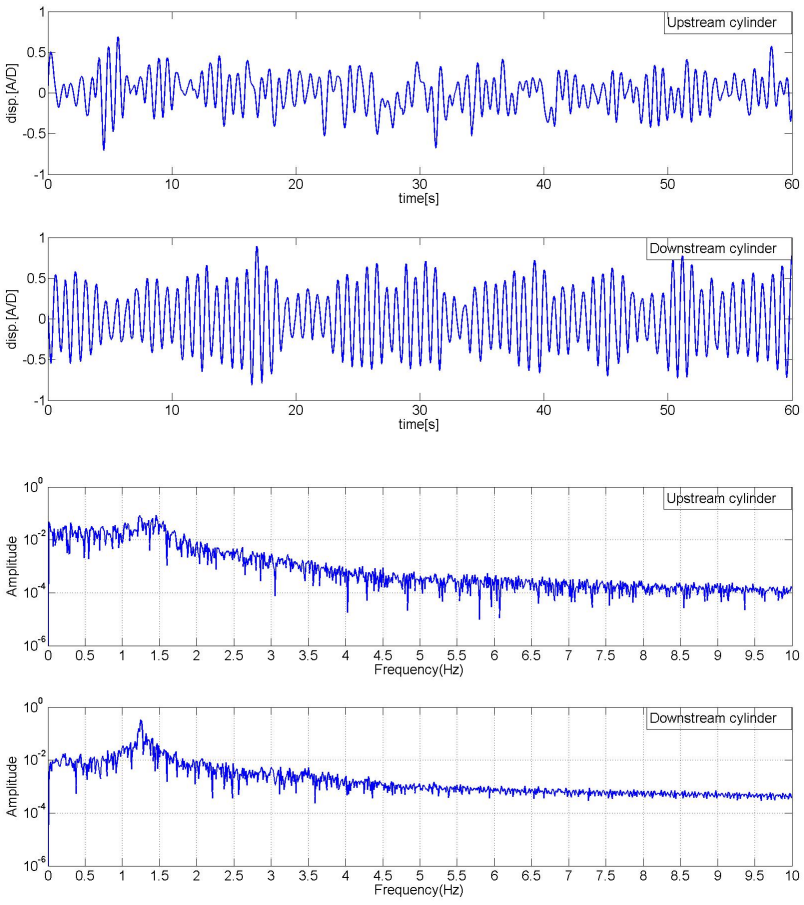

(f) U^*=13.82; upstream cylinder in desynchronization and downstream cylinder in lower branch

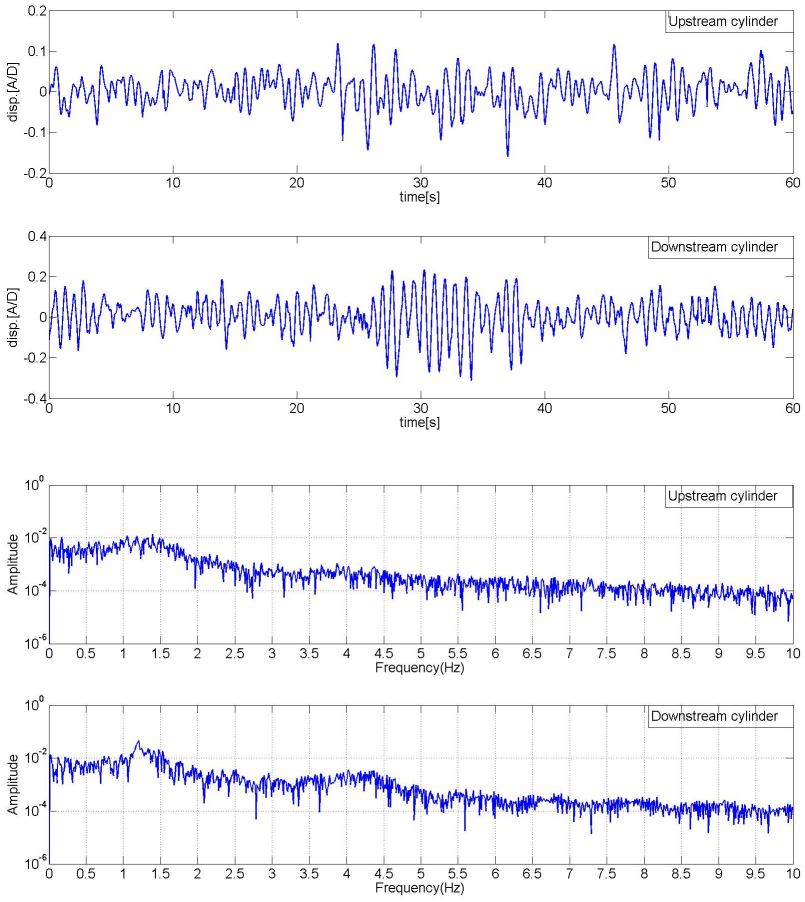

(g) U^*=14.57; desynchronization

Fig. 9.37. Time histories of displacement and power spectra for two smooth cylinders in tandem arrangement at L'/D=3.0

(ii) Two T6 cylinders in a tandem arrangement

As shown in Fig. 9.38, time histories of displacement and power spectra for the two T6 cylinders at L'/D=3.5 are presented. When both cylinders are at their initial branch (Fig. 9.38(a)), time histories of displacement show modulation and the downstream cylinder has higher amplitude than that of the upstream cylinder. Frequency synchronization is observed at the initial branch. At U^*=5.98 (Fig. 9.38(b)), where the upstream cylinder is in the upper branch and the downstream cylinder is in the initial

branch, the upstream cylinder has steady oscillation while the downstream cylinder exhibits modulation with groups of high and low amplitude. As U^* increases (Fig. 9.38(c)), steady and stable oscillations are observed for both cylinders in their upper branch. For further increase of U^* in the upper branch (Fig. 9.38(d)), amplitude modulation is not observed unlike the smooth cylinder downstream (Fig. 9.37(c)). At U^*=14.57 (Fig. 9.37(d)), the upstream cylinder is in the desynchronization and the amplitude is negligible. For the downstream cylinder, the amplitude response is in the lower branch and oscillation modulation increases.

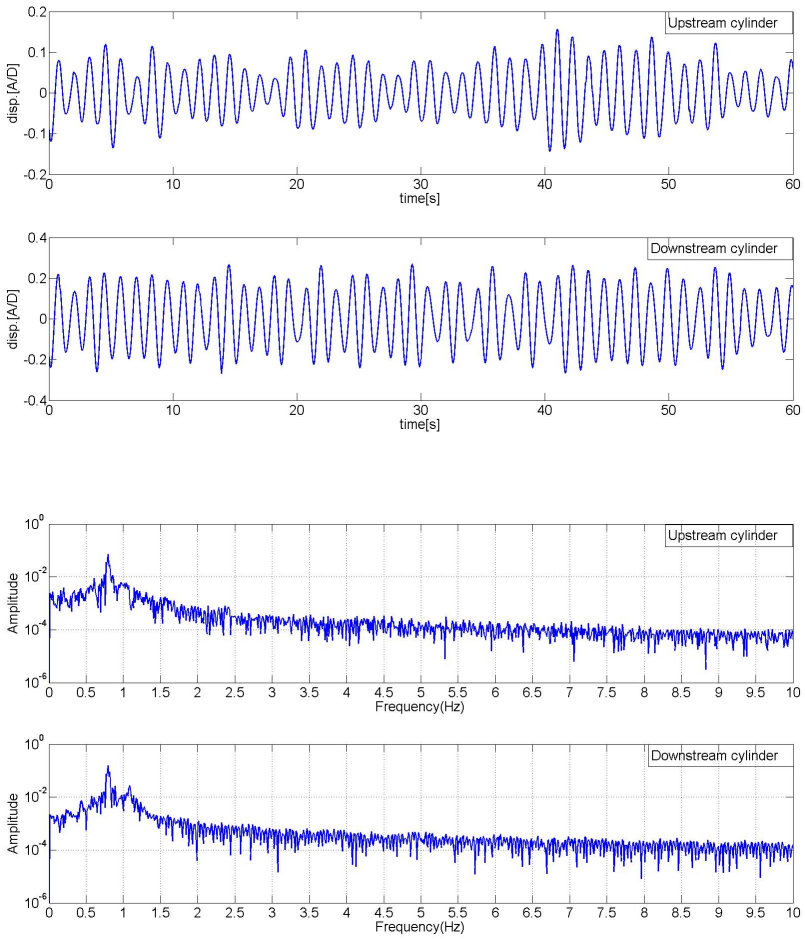

(a) U^*=4.86; initial branch

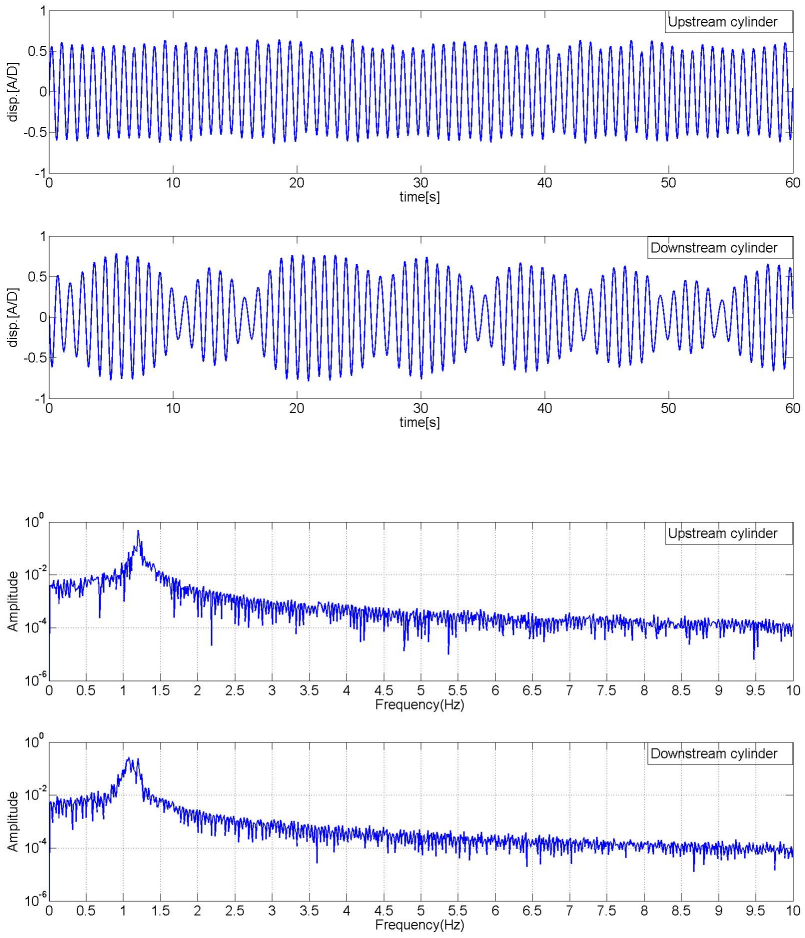

(b) U^*=5.98; upstream cylinder in upper branch and downstream cylinder in initial branch

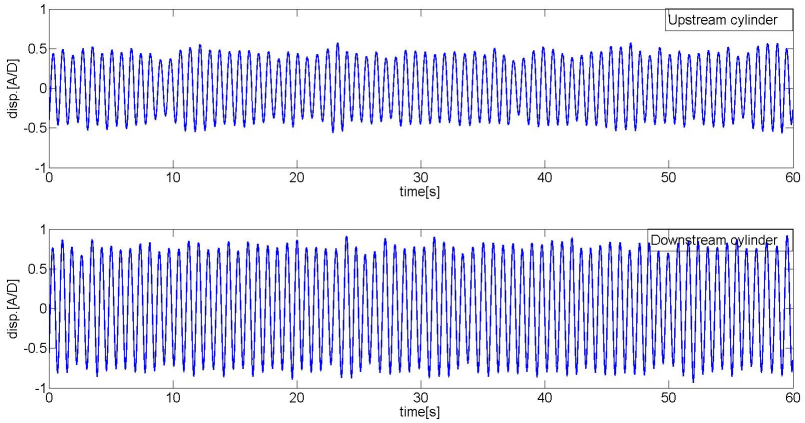

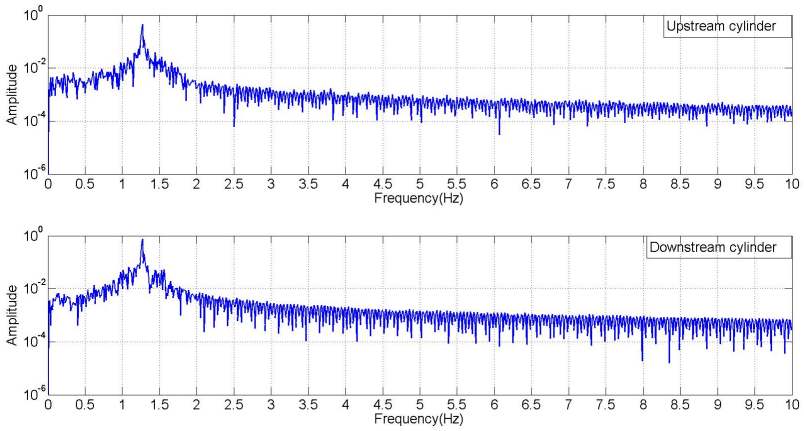

(c) U^*=7.47; upper branch

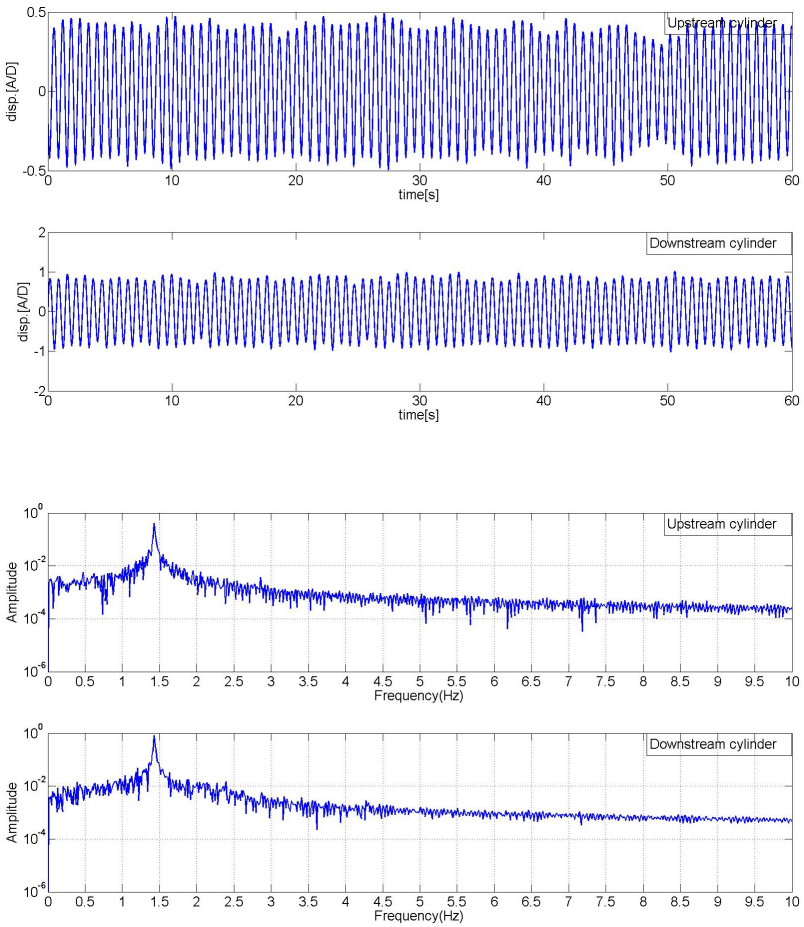

(d) U^*=11.58; upper branch

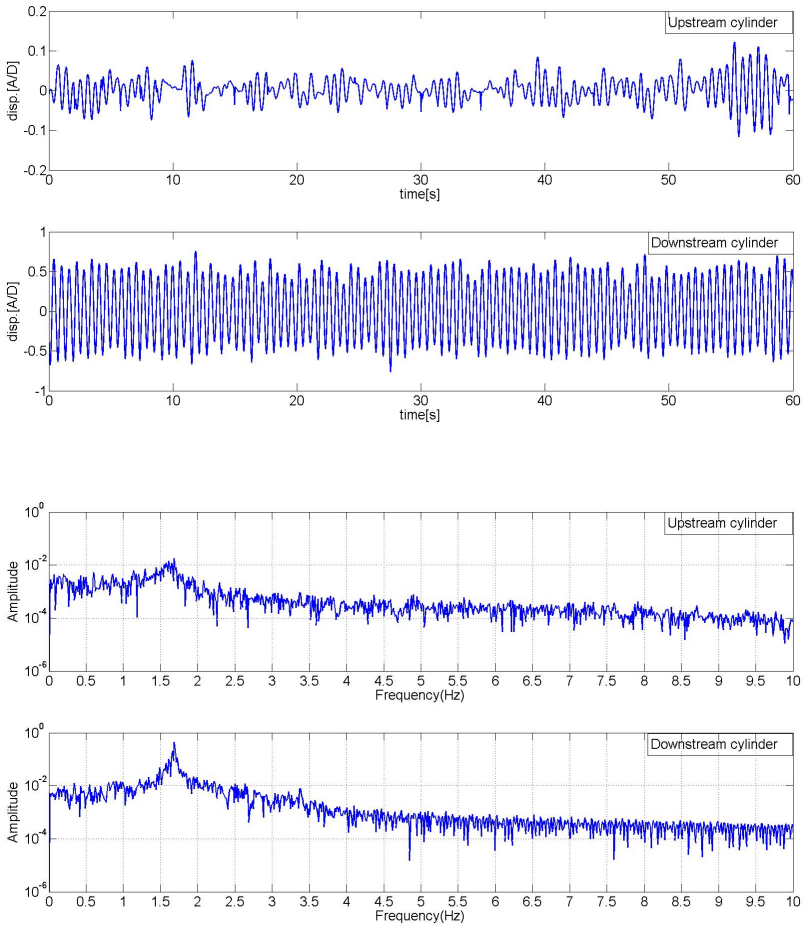

(e) U^*=14.57; upstream cylinder in desynchronization and downstream cylinder in lower branch

Fig. 9.38. Time histories of displacement and power spectra for two smooth cylinders in tandem arrangement at L'/D=3.5

To check wake interference and proximity interference, two simple tests were performed.

(i) As shown in Fig. 9.39, the upstream T6 cylinder was manually lifted for a while so that the downstream T6 cylinder was not exposed to the upstream cylinder wake. The cylinder amplitude in the downstream was almost suppressed.

(ii) The downstream cylinder was manually held for a while so that proximity interference was eliminated. As seen in Fig. 9.40, the upstream cylinder amplitude slightly decreased.

From these results, we may conclude that the wake interference influences more than proximity interference in the present study.

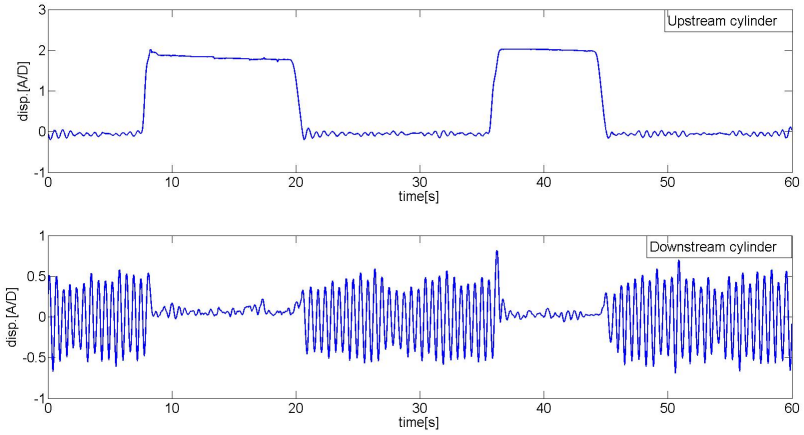

Fig. 9.39. Time history of displacement with manually lifting the upstream cylinder

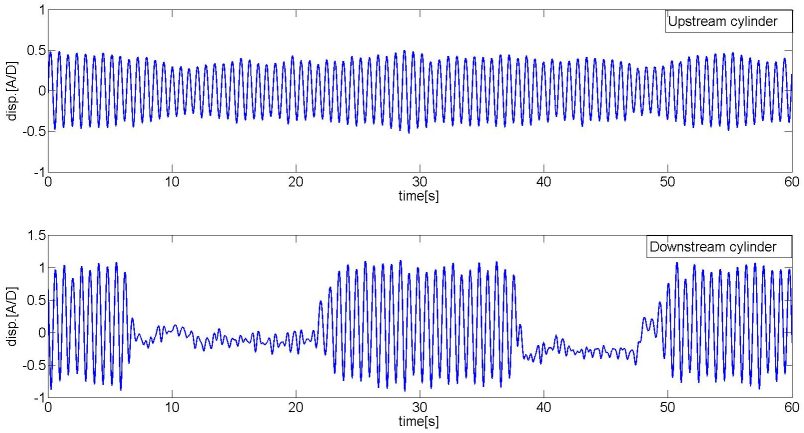

Fig. 9.40. Time history of displacement with manually holding the downstream cylinder

9.3. MAIN FINDINGS

(i) For the T6 and T8 cylinders, the upstream cylinder has higher amplitude and broader upper branch than that of the single suppression device. As L at L'/D increased, proximity interference decreased and the amplitude response of the upstream cylinder approached that of the single cylinder. The downstream cylinder has much broader upper branch than that of the single cylinder and the amplitude is not suppressed at U^*=15 (desynchronization region for the smooth cylinder).

(ii) For the T6 cylinder at all L'/D values tested, as the upstream cylinder reaches desynchronization, the amplitude response in the downstream cylinder goes into the lower branch. Hence, the response of the upstream cylinder can change the response region of the downstream cylinder.

(iii) The upstream cylinder with suppression means has longer wake region than that of the smooth cylinder. At high U^*, this longer wake interacts with the downstream cylinder and causes significantly higher amplitude than that of the smooth downstream cylinder. Hence, for suppression models T6 and T8, wake interference dominates the cylinder response over proximity interference.

(iv) For both smooth cylinders and cylinders with suppression means, the response of the downstream cylinder is affected by the upstream cylinder. Specifically, the galloping of the downstream cylinder decreased in amplitude.

(v) For the cylinders with PTC suppression means, synchronization of the two-body oscillating frequency is observed for a broad range of U^*. As U^* increases, the two oscillating cylinders move from in-phase to out-of-phase.

CHAPTER 10

CONCLUSIONS AND RECOMMENDATIONS FOR FUTURE WORK

The flow induced motions (FIM) of a single, rigid, circular cylinder on linear elastic springs with passive turbulence control (PTC) were studied experimentally at mass ratio m^*=1.725, mass-damping ratio $m^*\zeta$=0.0273, with high Reynolds numbers in the range $3\times10^4 \leq Re \leq 1.2\times10^5$ which primarily covers the TrSL3 high-lift regime. PTC consists of two roughness strips placed parallel to the cylinder axis and applied systematically at a varying circumferential location on the surface of the cylinder. From the PTC study, the ***"Map of PTC-to-FIM"*** was developed. The *Map of PTC-to-FIM* provides the information needed to design VIV suppression devices or ways to enhance FIM. Suppression devices effective regardless of the flow direction were studied in a two-cylinder tandem arrangement. The present study on the amplitude, frequency, and near-wake vortex-structures of the cylinder led to several conclusions and observations reported at the end of each chapter. The major conclusions are summarized in Section 10.1 and recommendations for future work are stated in Section 10.2.

10.1. CONCLUSIONS

1. *PTC-to-FIM Map:* The presence of PTC alters the FIM of the cylinder. FIM was found to depend strongly on the circumferential location of the roughness strips constituting the PTC. Each type of FIM was found to occur over a range of the circumferential angle of placement of the PTC defining an FIM zone. Two types of commercial sandpaper were used to set the PTC, a smooth one P180 and a rough one P60, exhibiting minor variations in the zonal ranges between the two resulting maps. Response features within each zone are nearly independent of the height of the roughness element. These measurements led to the development of the *PTC-to-FIM Map* in Figure 27.

Flow induced motions: The following FIM zones were established as a function of the starting point of the PTC location angle in clock-wise order from the forward stagnation point: Weak suppression WS1, hard galloping HG1, soft galloping SG, hard galloping HG2, weak suppression WS2, and strong suppression SS. It should be noted that for any location of the PTC - based on the *PTC-to-FIM Map* - the cylinder response changes with Reynolds number Re and reduced velocity U^* exhibiting different response from a smooth cylinder such as longer or shorter VIV branches, possibly transition from VIV to galloping, and galloping.

PTC can act as an FIM amplifier or FIM suppressor: This satisfies the intended goal of the present research. As the *PTC-to-FIM Map* shows, PTC acts as an FIM amplifier in the HG1, SG, and HG2 zones over a circumferential range of about 58° for P180 and 60° for P60 at higher reduced velocities $U^*>12.0$. PTC acts as an FIM suppressor in the SS

zone for a circumferential range of about 46° for P180 and 44° for P60 over a broad range of U^*.

2. *Smooth Cylinder Baseline:* Tests were conducted using a smooth circular cylinder with the same m^* and Reynolds number range to establish a baseline for comparison with the PTC cylinder. The results are in agreement with the original tests performed by Bernitsas et al. (2008, 2009). The upper branch is strong with oscillation amplitudes exceeding $1.5 \bullet D$ and overtaking the lower branch. The latter is weak and has characteristics of desynchronization. That is, non-steady oscillations are observed unlike stable and steady oscillations reported in the literature for $\mathrm{Re} \leq 10^4$. In the present study, stable and steady oscillations are observed in the upper branch while in the initial branch oscillations are steady with modulated amplitude.

3. *Weak Suppression:* Response features in the weak suppression zones (WS1 and WS2) are closely similar to those of the smooth cylinder but exhibit smaller amplitudes. The onset of the initial and upper branches in the weak suppression zones are identical to those of the smooth cylinder. The frequency ratio f^* is higher in the WS1 zone and lower in the WS2 zone with respect to f^* in the upper branch of the smooth cylinder.

4. *Hard Galloping:* In the HG1 and HG2 zones, galloping is initiated at high reduced velocities by applying manually an initial threshold static displacement of $1 \bullet D$. In the HG1 zone, the amplitude response exhibits a broader VIV upper branch and higher amplitude at galloping than the corresponding values in the HG2 zone. In HG2, the VIV and galloping regions are separated by almost complete suppression. Thus, prior to the onset of hard galloping at high reduced velocities, there is small amplitude motion in HG1 while the cylinder remains nearly stationary in HG2. Prior to the onset of hard

galloping, the frequency ratio f^* in HG2 cases is generally higher than that of HG1 and both exhibit higher f^* than that of the smooth cylinder.

5. *Soft Galloping:* There is one broad soft galloping zone. For any point of PTC location in that zone, the PTC cylinder response is divided into three major regions; VIV, transition from VIV to galloping, and galloping. In the VIV synchronization range, amplitude is partially suppressed. In transition from VIV to galloping, the oscillation frequency value starts to decline. In the galloping region, the cylinder amplitude reaches the limit of the experimental facility at $A^* \cong 2.9$. It should be noted that for high damping used in energy harnessing, the VIV and the galloping regions can be separated and reconnected by increasing the spring stiffness (Chang et al 2012).

For strip placement angles <40°, the larger the angle is, the earlier (at lower reduced velocities) the initiation and full development of galloping occurs. For strip placement angles ≥40°, the larger the roughness location angle (closer to the strong suppression zone) is, the later the initiation of galloping occurs, and the less the amplitude in VIV and the galloping region is.

For both hard galloping and soft galloping, the closer to the front stagnation point the PTC is located, the higher is the response amplitude in the VIV upper branch. When galloping is initiated, frequency ratio (f^*) approaches unity and higher harmonics are present.

6. *Strong Suppression:* Strong suppression (SS) was defined arbitrarily as at least 25% reduction in amplitude compared to the smooth cylinder response at the same m^* and Reynolds number Re. At the beginning of the SS zone (α<80°), a single dominant frequency is observed only in the narrow region $5.5 \leq U^* \leq 7.8$ closely related to the natural

frequency of the system in still water. The corresponding amplitude is about half that of the smooth cylinder. Away from that U^* range, amplitude is nearly suppressed. Near the end of the SS zone ($\alpha \geq 80°$) as we approach the WS2 zone, amplitude is about 50%-60% of the smooth cylinder response over the entire range of U^*.

7. *Zone Robustness:* Results with different strip widths showed that the strip area coverage does not significantly influence the amplitude and frequency response of the cylinder if the roughness strip is located inside any specific zone as defined by the *PTC-to-FIM Map*. Response is primarily zone-dependent, i.e., dependent on the circumferential location of the strip. Tests with staggered roughness configurations also led to the same conclusion. These results clearly indicate that correlation of vortex shedding is not a significant factor deciding the VIV or galloping oscillations.

When PTC is located on the boundary of two zones including the strong suppression zone (SS), amplitude of hard or soft galloping is significantly reduced. By removing the PTC segment in the SS zone, galloping amplitude is recovered. PTC should be applied very carefully around zone boundaries.

8. *Wake Structures:*

Smooth cylinder: For a smooth cylinder at these high Reynolds numbers, vortex structures were found to be a function of the ratio f_{osc}/f_s besides U^* and Reynolds number. Investigating wake vortex structures at the same Reynolds number $Re \cong 4.33 \times 10^4$ and U^* but at different values of f_{osc}/f_s due to different spring stiffness, the vortex structures vary from shedding of 3 individual vortices per cycle at $f_{osc}/f_s=0.64$ to 7 at $f_{osc}/f_s=0.74$ confirming previous investigations at lower Reynolds numbers that acceleration is an

important factor in formation of wake structures (Honji & Taneda 1969; Williamson & Roshko 1988).

In the present study for a smooth cylinder, vortex structures assumed conventional patterns 2P+S and 2S, and other non-conventional patterns as follows: At the onset of the initial branch, 2S is observed while at the upper end of the initial branch 3 individual vortices are shed per oscillatory cycle. In the upper branch, the 2P+S pattern is observed. In the lower branch, 6-7 vortices are shed per cycle with notable cycle-to-cycle variation in the near-wake structures. Vortices are much weaker (less circulation) and smaller (in core size) than those shed in the initial and upper branches.

Weak suppression: Flow visualization indicates that the vortex formation length is longer than that of the smooth cylinder though the vortex structures are quite similar but vortices are weaker (less circulation) and smaller (in core size) at identical reduced velocity values. However, the cause of longer vortex formation length would be different for WS1 and WS2. In WS1 cases, the flow separated at the upstream edge of the strip reattaches and the boundary layer is more diffused (thicker) due to interaction with the roughness elements. For WS2, the roll up of shear layers is adversely affected when PTC is located further downstream of the cylinder and leads to the formation of weaker (less circulation) and disorganized vortices. Diffusion of boundary layer and improper shear layer roll up cause drop in amplitude.

Galloping: Once the cylinder is excited to galloping oscillations, the wake structures over a cycle assume nearly the same pattern regardless of the type of galloping, i.e., SG, HG1 or HG2. At the same time, galloping wake structures are markedly different from the conventional vortex shedding modes in VIV with much higher number of vortices

shed per cycle (up to 10). Galloping is due to the effect of angle of incidence brought about by the asymmetry in geometry of the section.

Strong suppression: For U^*>7.5, two new wake structures are observed supporting the lift reduction. The first wake structure shows two weaker (less circulation) vortices shedding almost simultaneously rather than alternating periodically resulting in total circulation reduction. According to the Kutta-Joukowski theorem, this total circulation reduction results in proportional drop in the lift force. The second wake structure shows the cylinder near-wake confined between two flow lines forming a foil-like hydrodynamic tail with small eddies escaping into a narrow wake.

9. Map Robustness:

Response of cylinders with PTC configuration T7 show the effect of roughness height, location, and strip orientation. Even though there are minor changes in the response, the response zones of the Map of PTC-to-FIM are impervious to such changes.

10. *Multi-zone effect:*

From the progressive zone coverage and un-coverage, two designs are effective in VIV suppression. (a) Covering strong suppression zone: Strong suppression zone has the most influence among the zones. When the SS zone is included, strong suppression is always observed. (b) Covering all zones with specific PTC patterns: When all zones are covered with helically applied or staggered PTC, the least maximum amplitude is observed but amplitude at high reduced velocity is not fully suppressed unlike covering only the SS zone.

11. Two-cylinder FIM:

For two cylinders in a tandem configuration, longer wake region from the upstream cylinder with PTC suppression causes significant amplitude of the downstream cylinder at high reduced velocity. The suppression device in the upstream cylinder may not be good for amplitude suppression of the downstream cylinder. In the present study, wake interference has more influence than proximity interference.

For two cylinders in a tandem configuration, synchronization of two-body oscillating frequency is observed for the smooth and PTC cylinders. For PTC cylinders, synchronization is observed over a broad range of U^*. The two cylinders oscillate in-phase for small U^* and out-of-phase for higher U^* values for all tested spacing between the two cylinders.

10.2. RECOMMENDATIONS FOR FUTURE WORK

The following studies should be undertaken in future research:

1. *PTC* definitely affects the boundary layer, the separation point, and the shedding process. By measuring forces, we can find out: (a) How PTC changes lift and drag forces on a cylinder depending on PTC location. (b) Which flow region is triggered (subsritical, critical, super-critical, trans-critical). (c) What is the exact reason for the existence and robustness of the map of PTC-to-FIM. (d) By comparing the two end-forces on the cylinder, correlation of forces can be studied in enhancement and suppression of motions. Furthermore, for suppression devices, measuring the drag force is necessary to identify the drag penalty for any PTC suppression device.

2. *Bifurcation* is usually derived from the equation of motion. The reverse way should work for mathematical modeling of hard galloping and strong suppression. For strong

suppression, bifurcation was found in Chapter 5. From this bifurcation, we can derive the equation of motion. This will provide data on how to model the force terms in galloping and strong suppression.

3. *For hard galloping*, as the cylinder amplitude jumps from almost full suppression to $A^* \cong 3$, vortex structures change from small eddies to 10 vortices per cycle. By taking shots using a high-speed camera, the vortex transition can be studied. This study will help the understanding of the two equilibrium positions.

4. *The map of PTC-to-FIM* provides ideas on how to control the cylinder motions. In towing tank tests at MHL (Marine Hydrodynamic Laboratory), enhancement of the cylinder motion was successful for larger scale of the circular cylinder with PTC. More scales of application are needed to verify the effectiveness of map in enhancement and suppression of motions.

5. *The PTC-to-FIM map can be extended to multiple cylinders*. By applying PTC on the cylinder surface of two cylinders in a tandem arrangement, the motion of each cylinder can be studied.

6. *Calculate lift force on a single cylinder*. Based on the developed mathematical model in Chapter 3, reconstruct the lift force and phase lag based on the displacement time histories. Use this information to compare the relative magnitude of forces between the various branches of VIV and galloping.

7. *Two-cylinder synchronization:* From the time histories of displacement and our observations of synchronization of the oscillation frequency of the two cylinders - even though their natural frequencies differ by about 7% - the possibility of common flow patterns was identified. Flow patterns around oscillating cylinders have not been studied

so far and flow visualization is needed to understand interaction of the cylinder free shear layers, vortex formation and shedding process, and interactions between the vortex streets of the two cylinders.

8. *Two-cylinder mathematical modeling:* From the synchronization of the two oscillating frequencies, the mathematical modeling of the coupled motions of the two cylinders can be derived. The coupled equations of motion for two pendulums resulting in synchronization of the two pendulum oscillation frequencies are available in the literature. Similar equations for the frequency synchronization between two cylinders can be derived based on the data generated in this thesis.

REFERENCES

1. Achenbach, E. 1968, Distribution of local pressure and skin friction around a circular cylinder in cross-flow up to Re=5×10^6, Journal of Fluid Mechanics, 34, 625-639.

2. Achenbach, E. 1971 Influence of surface roughness on the cross-flow around a circular cylinder. *Journal of Fluid Mechanics* **46**, 321-335.

3. Achenbach, E. 1977 The effect of surface roughness on the heat transfer from a circular cylinder to the cross flow of air. *Int. J. Heat Mass Transfer.* **20,** 359.

4. Achenbach, E. & Heinecke, E. 1981 On vortex shedding from smooth and rough cylinders in the range of Reynolds numbers $6x10^3$ to $5x10^6$. *Journal of Fluid Mechanics* **109**, 239-251.

5. Alam, M.M., Sakamoto, H., & Moriya, M. 2003 Reduction of fluid forces acting on a single circular cylinder and two circular cylinders by using tripping rods. *Journal of Fluids and Structures* **18 (3-4),** 347-366.

6. Allen, D., & Henning, D.L. 2001 Surface roughness effects on vortex-induced vibration at critical and super-Critical Reynolds numbers. *Offshore Technology Conference* Paper No. OTC 13302.

7. Alonso, G., Valero, E., & Meseguer, J. 2009 An analysis on the dependence on cross section geometry of galloping instability of two-dimensional bodies having either biconvex or rhomboidal cross sections. *European Journal of Mechanics-B/Fluids* **28**, 328-334.

8. Assi, G. R. S. 2009 Mechanisms for Flow-Induced Vibration of interfering bluff bodies. PhD thesis, Imperial College, London.

9. Assi, G. R. S., Bearman, P. W., & Meneghini, J. R. 2010 On the wake-induced vibration of tandem circular cylinders: the vortex interaction excitation mechanism. *Journal of Fluid Mechanics* **661,** 365-401.

10. Baz, A., & Ro, J. 1991 Active control of flow-induced vibrations of a flexible cylinder using direct velocity feedback. *Journal of Sound and Vibration* **146(1),** 33-45.

11. Blekhman, I. I. 1988 Experimental and theoretical studies of Huygens apparatus are discussed in this textbook. *Synchronization in Science and Technology* ASME Press, New

York.

12. Benett, B., Schatz, M. F., Rockwood, H., & Wisenfeld, K. 2001 Recent study of a version of Huygens apparatus using pendulum clocks mounted on a heavy, wheeled cart. Huygens' clocks Proc. Roy. Soc.

13. Bearman, P. W. 1984 Vortex shedding from oscillating bluff bodies. *Annual Review of Fluid Mechanics* **16**, 195-222.

14. Bearman, P. W. 2011 Circular cylinder wakes and vortex-induced vibrations. *Journal of Fluids and Structures* **27,** 648-658.

15. Bearman, P., & Brankovic, M. 2004 Experimental studies of passive control of vortex-induced vibration. *European Journal of Mechanics* **23-1,** 9-15.

16. Bernitsas M. M., Raghavan K., Ben-Simon Y., & Garcia E. M. H. 2006a VIVACE (Vortex Induced Vibration Aquatic Clean Energy): A new concept in generation of clean and renewable energy from fluid flow. In 26th *Conference on Ocean, Offshore, and Artic Engineering*, Hamburg, Germany, June 2006; also *ASME Journal of Offshore Mechanics and Arctic Engineering* 2008, **130-4**, 041101-15.

17. Bernitsas M. M., Ben-Simon Y., Raghavan K., & Garcia E. M. H. 2006b The VIVACE converter: Model tests at Reynolds numbers around 10^5. In 26th *Conference on Ocean, Offshore, and Artic Engineering*, Hamburg, Germany, June 2006; also *ASME Journal of Offshore Mechanics and Arctic Engineering* 2009, **131-1,** 1-13.

18. Bernitsas, M. M. & Raghavan, K. 2007 Reduction/suppression of vortex induced forces & motion through surface roughness control**,** U.S. Provisional Patent Application, US2009/0114002 A1, May 25, 2007.

19. Bernitsas, M. M., & Raghavan, K. 2008 Reduction/suppression of VIV of circular cylinders through roughness distribution at $8\times10^3<Re<1.5\times10^5$. *Proceedings of the 27th Conference on Ocean, Offshore, and Artic Engineering*, Estoril, Portugal, June 15-20, 2008.

20. Bernitsas, M. M., & Raghavan, K. 2009 Converter of current, tide, or wave energy. United States Patent and Trademark Office Patent# 7,493,759 B2 issued on Feb. 24. 2009.

21. Bernitsas, M. M. & Raghavan, K. 2011 Enhancement of vortex induced forces & motion through surface roughness control. United States Patent and Trademark Office, Patent# 8,042,232 November 1, 2011.

22. Bishop, R.E.d., & Hassan, A.Y. 1963 The lift and drag forces on a circular cylinder oscillating in a flowing fluid. *Processing of the Royal Society (London), Series A* **277,** 51-75.

23. Bishop, R.E.d., & Hassan, A.Y. 1964 The lift and drag forces on a circular cylinder in a flowing fluid. *Processing of the Royal Society (London), Series A* **277,** 32-50.

24. Blackburn, H.M. & Henderson, R.D. 1999 A study of two-dimensional flow past an oscillating cylinder. *Journal of Fluids Mechanics* **385,** 255–286.

25. Blevins, R. D. 1990 Flow-induced vibration, First ed. Van Nostrand Reinhold, New York.

26. Blevin, R. D. & Coughran, C. S. 2009 Experimental investigation of Vortex-Induced Vibration in one and two dimensions with variable mass, damping, and Reynolds number. *Journal of Fluids Engineering* **131,** 101202.

27. Bokaian, A., & Geoola, F. 1984a Proximity induced galloping of two interfering circular cylinders. *Journal of Fluid Mechanics* **146,** 417-449.

28. Bokaian, A., & Geoola, F. 1984b Wake induced galloping of two interfering circular cylinders. *Journal of Fluid Mechanics* **146,** 383-415.

29. Bokaian, A. R, & Geoola, F. 1984 Hydroelastic instabilities of square cylinders. *Journal of Sound Vibration* **92,** 117-141.

30. Carberry, J., & Sheridan, J. 2001 Vortex forces on an oscillating cylinder. *Melbourne Graduate Fluids Conference.*

31. Carberry, J., Sheridan, J., & Rockwell, D. 2001 Forces and wake modes of an oscillating cylinder. *Journal of Fluids and Structures* **15,** 523-532.

32. Chang, S.I. 2004 Bifurcation analysis of a non-linear hysteretic oscillator under harmonic excitation. *Jounral of Sound and Vibration* **276,** 215-225.

33. Chang, C.C.(Jim) 2010 Hydrokinetic energy harnessing by enhancement of flow induced motion using passive turbulence control, Dissertation, University of Michigan.

34. Chang, C. C., & Bernitsas M. M. 2011 Hydrokinetic energy harnessing using the VIVACE converter with passive turbulence control. *Proceedings of the 30th Conference on Ocean, Offshore, and Artic Engineering* 2011, Rotterdam, The Netherlands, June 19-24, 2011; also, *ASME Journal of Offshore Mechanics and Arctic Engineering* in press.

35. Chang, C. C., Kumar, R. A. & Bernitsas M. M. 2011 VIV and galloping of single circular cylinder with surface roughness at $3.0\times10^4 \leq Re \leq 1.2\times10^5$. *Ocean Engineering* **38-16,** 1713-1732.

36. Chen, S. S. 1987 In: Flow-induced vibration of circular cylindrical structures. Hemisphere Publishing Corporation, Washington, DC, USA.

37. Corless, R. M. & Parkinson, G. V. 1988 A model of the combined effects of vortex-induced oscillation and galloping. *Journal of Fluids and Structures* **2,** 203-220.

38. Dahl,J.M., Hover, F.S., & Triantafyllou M.S. 2010 Dual resonance in vortex-induced vibrations at subcritical and supercritical Reynolds numbers. *Journal of Fluid Mechanics* **643,** 395-424

39. Dalton, C. 2010 A review of vortex-induced vibrations. *Proceeding of Conference on American Society of Civil Engineering* 2010 **366,** 198.

40. Den Hartog, J. P. 1956 Mechnaical vibrations. 4th ed. McGraw Hill.

41. Every, M. J., King, R., & Weaver, D. S. 1982 Vortex-excited vibrations of cylinders and cables and their suppression. *Ocean Engineering* **9,** 135-157.

42. Fage, A. & Warsap, J. H. 1930 The effect of turbulence and surface roughness on the drag of a circular cylinder. *Aero. Res. Counc. Lond. R. & M.* **no. 1283.**

43. Farell, C. 1981 Flow around fixed circular cylinders: fluctuating loads. *Jounral of the Engineering Mechanics Division*, *ASCE* **107,** 565-587.

44. Farell, C. & Arroyave, J. 1990 On uniform flow around rough circular cylinders at critical Reynolds numbers. *Journal of Wind Engineering and Industrial Aerodynamics* **36,** 621-631.

45. Farell, C., & Fedeniuk, S.K. 1988 Effect of end plates on the flow around rough cylinders. *Journal of Wind Engineering and Industrial Aerodynamics* **28,** 219-230.

46. Fathi N. M. 2009 Beating phenomenon of multi-harmonics defect frequencies in a rolling element bearing: Case study from water pumping station. *World Academy of Science, Engineering and Technology* **57,** 327-331.

47. Feng, C.C. 1968 The measurement of vortex-induced effects on flow past stationary and oscillating circular and D-section cylinders. M.Sc. Thesis The University of British Columbia.

48. Fox,T.A. & West, G.S. 1990 On the use of end plates with circular cylinders. *Exp. Fluids* **9,** 237-239.

49. Gabbai, R. D., & Benaroya, H. 2005 An overview of modeling and experiments of vortex-induced vibration of circular cylinders. *Journal of Sound and Vibration* **282,** 575-616.

50. Gartshore, I. S., Khanna, J., & Laccinole, S. 1978 The effectiveness of vortex spoilers on a circular cylinder in smooth and turbulent flow. *Proceeding 5th International Conference on Wind Engineering* Fort Collins, CO.

51. Gerrard, J. H. 1961 An experimental investigation of the oscillating lift and drag of a circular cylinder shedding turbulent vortices. *Journal of Fluid Mechanics* **11-2,** 244-256.

52. Gerrard, J. H. 1966 The mechanics of the formation region of vortices behind bluff bodies. *Journal of Fluid Mechanics* **25,** 401-413.

53. Gharib, M. R., Leonard, A., Gharib, M. & Roshko, A. 1998 The absence of lock-in and the role of mass ratio. In Paper Proceedings Conference on Bluff Body Wakes and Vortex-Induced Vibrations Washington DC, 21-23 June 1998. (eds P.W. Bearman & Williamson C.H.K.), Paper Number 24; also Paper FEDSM98-5312 in CD-ROM from ASME.

54. Govardhan, R., & Williamson, C. H. K. 2000 Modes of vortex formation and frequency response of a freely vibrating cylinder. *Journal of Fluid Mechanics* **420,** 85–130.

55. Govardhan, R., & Williamson, C. H. K. 2006 Defining the modified Griffin plot in vortex-induced vibration: revealing the effect of Reynolds number using controlled. *Journal of Fluid Mechanics* **561,** 147-180.

56. Gu, W., Chyu, C. & Rockwell, D. 1994 Timing of vortex formation from an oscillating cylinder. *Physics of Fluids* **6,** 3677-3682.

57. Gu, Z. F., & Sun, T. F. 1999 On interference between two circular cylinders in staggered arrangement at high subcritical Reynolds numbers. *Journal of Wind Engineering and Industrial Aerodynamics* **80,** 287-309.

58. Güven, O., Farell, C., & Patel, V.C. 1980 Surface-roughness effects on the mean flow past circular cylinders. *Journal of Fluid Mechanics* **98,** 673-701.

59. Higuchi, H., Kim, H. J., & Farell, C. 1989 On flow separation and reattachment around a circular cylinder at critical Reynolds numbers. *Journal of Fluid Mechanics* **200,** 149-171.

60. Honji, H., & Taneda, S. 1969 Time dependent flow around a circular cylinder accelerated uniformly from one speed to another. Report of the Research Institute of Applied Mechanics (Kyushu University, Japan) **17,** 187-193.

61. Hover, F.S., Techet, A. H. & Triantafyllou, M. S. 1998 Forces on oscillating uniform and tapered cylinders in crossflow. *Journal of Fluid Mechanics* **363,** 97-114.

62. Hover, F. S., Tvedt, H., & Triantafyllou, M. S. 2001 Vortex-induced vibrations of a cylinder with tripping wires. *Journal of Fluid Mechanics* **448,** 175-195.

63. Hover, F. S., & Triantafyllou, M. S. 2001 Galloping response of a cylinder with upstream wake interference. *Journal of Fluids and Structures* **15,** 503-512.

64. Igarashi, T. 1981 Characteristics of a flow around two circular cylinders arranged in tandem (1st report). *Bulletin of the JSME* **24,** 323-331.

65. Igarashi, T. 1986 Effects of tripping wires on the flow around a circular cylinder normal to an airstream. *Bull. Japan. Soc. Mech. Engng* **29,** 2917-2924.

66. Ishigai, S., Nishikawa, E., Nishimura, K., & Cho, K. 1972 Experimental study of structure of gas flow in tube banks with tube axes normal to flow (Part I, Karman vortex flow from two tubes at various spacings). *Bulletin of the JSME* **15,** 949-956.

67. Jauvtis N., & Williamson, C.H.K. 2004 The effect of two degrees of freedom in vortex-induced vibration of low mass and damping. *Journal of Fluid Mechanics* **509,** 23-62.

68. Khalak, A., & Williamson, C.H.K. 1997a Fluid forces and dynamics of a hydroelastic structure with very low mass and damping. *Journal of Fluids Structure* **11,** 973-82.

69. Khalak, A., & Williamson, C.H.K. 1997b Investigation of the relative effects of mass and damping in vortex-induced vibration of a circular cylinder. *Journal of Wind Engineering Industry Aerodynamics* **69-71,** 341-50.

70. Khalak, A., & Williamson, C.H.K. 1999 Motions forces and mode transitions in vortex-induced vibrations at low mass-damping. *Journal of Fluids and Structures* **13,** 813-851.

71. Kim S., Alam M. M., Sakamoto, H. & Zhou, Y. 2009 Flow-induced vibration of two circular cylinders in tandem arrangement. Part 2: Suppression of vibrations. *Journal of Wind Engineering and Industrial Aerodynamics* **97,** 312-319.

72. Kim E. S., Bernitsas M. M., & Kumar, A. R. 2011 Multi-cylinder flow induced motions: Enhancement by passive turbulence control at 28,000<Re<120,000. *Proceedings of the 30th Conference on Ocean, Offshore, and Artic Engineering* 2011, Rotterdam, The Netherlands, June 19-24, 2011; also, *ASME Journal of Offshore Mechanics and Arctic Engineering* in press.

73. Kiu, K.Y., Stappenbelt B., and Thiagarajan, K. P. 2011 Effects of uniform surface roughness on vortex-induced vibration of towed vertical cylinders. *Journal of Sound and Vibration* **330,** 4753-4763.

74. Korkischko, I., & Meneghini, J. R. 2010 Experimental investigation of flow-induced vibration on isolated and tandem circular cylinders fitted with strakes. *Journal of Fluids and Structures* **26,** 611-625.

75. Kubo, Y., Yasuda, H., & Kotsubo, C. 1993 Active control of super-tall structures under wind action by a boundary layer control method. *Journal of Wind Engineering and Industrial Engineering* **50,** 361-372.

76. Kumar, A. R., Sohn, C. H., & Lakshmana Gowda, B. H. L. 2008 Passive control of vortex-induced vibrations: An overview. *Recent Patents on Mechanical Engineering* **1,** 1-11.

77. Kumar, A. R., Sohn, C. H., & Lakshmana Gowda, B. H. L. 2009 Influence of corner radius on the near wake structure of a transversely oscillating square cylinder. *Journal of Mechanical Science of Technology* **23-9,** 2390-2416.

78. Landl, R. 1975 A mathematical model for vortex-excited vibrations of bluff bodies. *Journal of Sound and Vibration* **42,** 219-234.

79. Lee, J. H. 2010 Hydrokinetic power harnessing utilizing vortex induced vibrations through a virtual c-k VIVACE model, Dissertation, University of Michigan.

80. Lee, S. J., & Kim, H. B. 1997 The effect of surface protrusions on the near wake of a circular cylinder. *Journal of Wind Engineering and Industrial Aerodynamics* **69-71**, 351-361.

81. Lee J. H. & Bernitsas M. M. 2011 High-damping, high-Reynolds VIV tests for energy harnessing using the VIVACE converter. *Ocean Engineering* **38, #16,** 1697-1712.

82. Lee J. H., Xiros N., & Bernitsas M. M. 2011 Virtual damper-spring system for VIV experiments and hydrokinetic energy conversion. *Ocean Engineering* **38, #5-6,** 732-747.

83. Lighthill, J. 1986 Fundamentals concerning wave loading on offshore structures. *Journal of Fluid Mechanics* **173,** 667-81.

84. Ljungkrona, L. 1992 Characteristics of mean and fluctuating surface pressure distributions on tubes in tandem arrangement and in-ine tube bundles. Ph.D. Thesis, Department of Thermodynamics and Fluid Dynamics, Chalmers University of Technology, Göteborg, Sweden.

85. Ljungkrona, L. & Sundén, B. 1993 Flow visualization and surface pressure measurement on two tubes in an inline arrangement. *Experimental Thermal and Fluid Science* **6,** 15-27.

86. Ljungkrona, L., Norberg, C., & Sundén, B. 1991 Free-stream turbulence and tube spacing effects on surface pressure fluctuations for two tubes in an in-line arrangement. *Journal of Fluids and Structures* **5,** 701-727.

87. Lu, X-Y., & Dalton, C. 1996 Calculation of the timing of vortex formation from an oscillating cylinder. *Journal of Fluids and Structures* **10,** 527-541.

88. Lubbad, R. K., Løset, S., Gudmestad, O. T., Torum, A., & Moe, G. 2007 Vortex induced vibrations of slender marine risers-effects of rounded-sectioned helical strakes. In *the17th International Offshore and Polar Engineering Conference*, Lisbon, Portugal, July 1-6.

89. Lubbad, R. K., Løset, S., & Moe, G. 2011 Experimental investigations of the efficiency of round-sectioned helical strakes in suppressing vortex induced vibrations. *Journal of Offshore Mechanics and Arctic Engineering*. **133-4,** 041102.

90. Meneghini, J.R., & Bearman, P. W. 1995 Numerical simulation of high amplitude oscillatory flow about a circular cylinder. *Journal of Fluids and Structures* **9,** 435-455.

91. Mercier, J. 1973 Large amplitude oscillations of a circular cylinder in a low-speed stream. PhD thesis Stevens Institute of Technology.

92. Morsbach, M. 1967 Über die Bedingungen für eine Wirbelstraβenbildung hinter Kreiszylindern. Diss RWTH Aachen.

93. Moe, G., & Wu, Z-J. 1990 The lift force on a cylinder vibrating in a current. *ASME Journal of Offshore Mechanics and Arctic Engineering* **112,** 297-303.

94. Muddada, S., & Patnaik, B. S. V. 2010 An active flow control strategy for the suppression of vortex structures behind a circular cylinder. *European Journal of Mechanics-B/Fluids* **29,** 93-104.

95. Nakamura, Y., & Tomonari, Y., 1982 The effects of surface roughness on the flow past circular cylinder at high Reynolds numbers. *Journal of Fluid Mechanics* **123,** 363-378.

96. Nakamura, Y., Hirata, K., & Urabe, T. 1991 Galloping of rectangular cylinders in the presence of a splitter plate. *Journal of Fluids and Structures* **5,** 521-549.

97. Nakamura, Y., & Hirata, K. 1994 The aerodynamic mechanism of galloping. *Trans. Japan Soc. Aero. Space Sci* **36, No 114,** 257-269.

98. Nebres, J., & Batill, S. 1993 Flow about a circular cylinder with a single large-scale surface perturbation. *Experiments in fluids* **15,** 369-379.

99. Niemann & Hölscher 1990 A review of recent experiments on the flow past circular cylinders. *Journal of Wind Engineering and Industrial Aerodynamics* **33,** 197-209.

100. Nishimura, T. 1986 Flow across tube banks. In: Cheremisionoff, N.P. (Ed.), Encyclopedia of Fluid Mechanics – Flow Phenomena and Measurement, vol. 1. Gulf Publishing Company, Houston, USA, pp. 763-785.

101. Ongoren, A., & Rockwell, D. 1988 Flow structure from an oscillating cylinder Part 1: Mechanisms of phase shift and recovery in the near wake. *Journal of Fluid Mechanics* **191,** 197-223.

102. Owen, J.C., Bearman, P.W., & Szewczyk, A.A. 2001 Passive control of VIV with drag reduction. *Journal of Fluids Structures* **15,** 597-605.

103. Park H., Bernitsas, M. M., & Kumar, A. R. 2011 Using the map of passive turbulence control to flow induced motions to suppress circular cylinder motion at 31,000<Re<120,000. *Proceedings of the 30th Conference on Ocean, Offshore, and Artic Engineering* 2011, Rotterdam, The Netherlands, June 19-24, 2011; also, *ASME Journal of Offshore Mechanics and Arctic Engineering* in press.

104. Park H., Kumar, A. R. & Bernitsas, M. M. 2012 Map of passive turbulence control to flow induced motions of circular cylinder on springs at $3\times10^4 \leq Re \leq 1.2\times10^5$. *Submitted Journal of Fluids and Structures.*

105. Parkinson, G. V. 1971 Wind-induced instability of structures. *Philosophical Transaction of the Royal Society Lond. A* **269,** 395-409.

106. Parkinson, G. V., & Sullivan, P.P. 1979 Galloping response of towers. *Journal of Wind Engineering and Industrial Aerodynamics* **4,** 253-260.

107. Parkinson, G. V. 1989 Phenomena and modeling of flow-induced vibrations of bluff bodies. *Progress in Aerospace Science* **26,** 169-224.

108. Raghavan, K., Bernitsas, M. M., & Maroulis, D. 2007a Effect of Reynolds number on vortex induced vibrations. *IUTAM Symposium*, Hamburg, Germany, July 2007.

109. Raghavan, K., Bernitsas, M. M., & Maroulis, D. 2007b Effect of bottom boundary on VIV for energy harnessing at $8\times10^3<Re<1.5\times10^5$. *Proceedings of the 26th Conference on Ocean, Offshore, and Artic Engineering*, San Diego, California, USA June 10-15, 2007; also, 2009 *ASME Journal of Offshore Mechanics and Arctic Engineering* **131-3,** 031102.

110. Raghavan, K., & Bernitsas, M. M. 2011 Experimental investigation of Reynolds number effect on vortex induced vibration of rigid cylinder on elastic supports. *Ocean Engineering* **38, #5-6**, 719-731.

111. Ribeiro, J.L.D. 1992 Fluctuating lift and its spanwise correlation on a circular cylinder in a smooth and in a turbulent flow: a critical review. *Journal of Wind Engineering and Industrial Aerodynamics* **40,** 179-198.

112. Roshko, A. 1961 Experiments on the flow past a circular cylinder at very high Reynolds number. *Jounral of Fluid Mechanics.* **10,** 345.

113. Roshko, A. 1970 On the aerodynamic drag of cylinders at high Reynolds numbers. In Proceeding U.S.-Japan Research Seminar on Wind Loads on Structures, Honolulu, p87. University of Hawaii.

114. Sarpkaya, T. 1978 Fluid forces on oscillating cylinders. *ASCE Jounral of Waterway, Port, Coaastal, and Ocean Division* **104,** 275-290.

115. Sarpkaya, T. 1979 Vortex-induced oscillations – a selective review. *Journal of Applied Mechanics* **46,** 241-258.

116. Sarpkaya, T. 1995 Hydrodynamic damping, flow-induced oscillations, and biharmonic response. *ASME Jounral of Offshore Mechanics and Arctic Engineering* **117,** 232-238.

117. Sarpkaya, T. 2004 A critical review of intrinsic nature of vortex-induced vibrations. *Journal of Fluids and Structures* **19,** 389-447.

118. Schaudt, K. J., Wajnikonis, C., Spencer, D., Xu, J., Leverette, S., & Masters, R., 2008 Bench marking of VIV suppression systems. *Proceedings of the 27th Conference on Ocean, Offshore, and Artic Engineering*, Estoril, Portugal, 2008.

119. Schewe, G. 1983 On the force fluctuations acting on a circular cylinder in cross flow from subcritical up to transcritical Reynolds numbers. *Journal of Fluid Mechanics* **133,** 265-285.

120. Strogatz, S. H., 2001, Nonlinear dynamics and chaos, Westview press.

121. Sumer, M and Fredsøe, J., Hydrodynamics around cylindrical structures, World Scientific, Singapore, 1997.

122. Sumner, D. 2010 Two circular cylinders in cross-flow: A review. *Journal of Fluids and Structures* **26,** 849-899.

123. Sumner, D., Richards, M. D., & Akosile, O. O. 2005 Two staggered circular cylinders of equal diameter in cross-flow. *Journal of Fluids and Structures* **13,** 309-338.

124. Szechenyi, E. 1975 Supercritical Reynolds number simulation for two-dimensional flow over circular cylinders. *Journal of Fluid Mechanics* **70,** 529.

125. Teverovskii, B.M. 1968 Effect of surface roughness on the vibration of a cylinder in hydrodynamic conditions. *Russian Engineering Journal* **XLVIII,** No.12.

126. Tombazis, N. & Bearman, P. W. 1997 A study of three-dimensional aspects of vortex shedding from a bluff body with a mild geometric disturbance. *Journal of Fluid Mechanics* **330,** 85-112.

127. Vickery, B.J. & Watkins, R.D. 1964 Flow induced vibrations of cylindrical structures. *Proc. 1st Aust. Conf. on Hydraulics and Fluid Mechanics, Pergamon,* pp.213-241.

128. Vikestad, K., Vandiver, J. K., & Larsen, C. M. 2000 Added mass and oscillation frequency for a circular cylinder subjected to vortex-induced vibrations and external disturbance. *Journal of Fluids and Structures* **14,** 1071-1088.

129. Walker, D. T., Lyzenga, D. R., Ericson, E. A., & Lund, D. E. 1996 Radar backscatter and surface roughness measurements for stationary breaking waves. *Proceedings of the Royal Society Lond. A* **452-1952,** 1953-1984.

130. Williamson, C. H. K., & Roshko, A. 1988 Vortex formation in the wake of an oscillating cylinder. *Journal of Fluids and Structures* **2,** 355-381.

131. Williamson, C. H. K., & Govardhan, G. 2004 Vortex-induced vibrations. *Annual Review of Fluid Mechanics* **36,** 413-455.

132. Wong, H. Y., & Kokkalis, A. 1982 A comparative study of three aerodynamic devices for suppressing vortex-induced oscillation. *Journal of Wind Engineering and Industrial Aerodynamics* **10,** 21-29.

133. Wu, J.C. 1981 Theory for aerodynamic force and moment in viscous flows. *AIAA Jounral* **19-4,** 432-441.

134. Wu W., Bernitsas M. M., & Maki, K. J. RANS 2011 simulation vs. experimental measurements of flow induced motion of circular cylinder with passive turbulence control at 30,000<Re<120,000. *Proceedings of the 30th Conference on Ocean, Offshore, and Artic Engineering* 2011, Rotterdam, The Netherlands, June 19-24, 2011; also, *ASME Journal of Offshore Mechanics and Arctic Engineering* in press.

135. Zdravkovich, M. M. 1977 Review of flow interference between two circular cylinders; series of unexpected discontinuities. *Journal of Industrial Aerodynamics* **2,** 255-270.

136. Zdravkovich, M. M. 1981 Review and classification of various aerodynamic and hydrodynamic means for suppressing vortex shedding. *Journal of Wind Engineering and Industrial Aerodynamics* **7,** 145-189.

137. Zdravkovich, M. M. 1982 Modification of vortex shedding in the synchronization range. *Trans. ASME: Journal of Fluids Engineering* **104,** 513-517.

138. Zdravkovich, M. M. 1985 Flow induced oscillations of two interfering circular cylinders in cross flow. *Journal of Sound and Vibration* **101,** 511-521.

139. Zdravkovich, M. M. 1987 The effects of interference between circular cylinders in cross flow. *Journal of Fluids and Structures* **1,** 239-261.

140. Zdravkovich, M. M. 1988 Review of interference-induced oscillations in flow past two parallel circular cylinders in various arrangements. *Journal of Wind Engineering and Industrial Aerodynamics* **28,** 183-200.

141. Zdravkovich, M. M. 1990 Conceptual overview of laminar and turbulent flows past smooth and rough circular cylinders. *Jounral of Wind Engineering and Industrial Aerodynamics* **33,** 53-62.

142. Zdravkovich, M. M. 1993 Interstitial flow field and fluid forces. In Au-Yang, M. K. (Ed.), Technology for the 90s: A Decade of Progress. ASME, New York, USA, pp. 594-658.

143. Zdravkovich, M. M. 1997 Flow around circular cylinders Volume 1: Fundamentals. Oxford University Press, England.

144. Zdravkovich, M. M. 2003 Flow around circular cylinders Volume 2: Applications. Oxford University Press, England.

145. Zhou, Y., & Yiu, M.W. 2006 Flow structure, momentum and heat transport in a two-tandem-cylinder wake. *Journal of Fluid Mechanics* **548,** 17-48.